BOILING WATER HEAT TRANSFER DURING QUENCHING OF STEEL PLATES AND TUBES

By

Dianfeng Li

B. Eng. (Nonferrous Metallurgical Eng.), Northeastern University, China, 1988
M.A. Sc. (Nonferrous Metallurgical Eng.), Northeastern University, China, 1994
M.A. Sc. (Metals & Materials Eng.), The University of British Columbia, 1999

A THESIS SUBMITTED IN PARTIAL FULFILLMENT OF
THE REQUIREMENTS FOR THE DEGREE OF
DOCTOR OF PHILOSOPHY

in

THE FACULTY OF GRADUATE STUDIES
DEPARTMENT OF METALS AND MATERIALS ENGINEERING

We accept this thesis as conforming
to the required standard

THE UNIVERSITY OF BRITISH COLUMBIA

July 2003

ABSTRACT

The design, analysis and control of many metallurgical and materials operations hinges, in part, on being able to quantify the heat transfer occurring at the boundary of the components being processed. Critical to the accurate determination of the surface heat flux is a precise inverse heat conduction model as well as correct temperature measurement during the quench test. This research has explored the factors that can affect the accuracy of a boiling curve prediction including parameters related to both the inverse heat conduction model as well as the temperature measurement technique.

During the research, extensive analysis as well as some experiments were done to determine a "best practices method" to measure the temperature-history experienced by the sample during a quench operation. Specifically, two different temperature measurement techniques including surface, where the thermocouple is located on the quench surface, and sub-surface, where the thermocouple is located at an interior position, were analyzed in detail to identify and quantify errors that can be induced in the measured data. Results from the research have highlighted the need to include the thermocouple hole in cases where the thermocouples are instrumented at 90° and a severe water quench occurs at the surface of the sample. Although the work in this study has been conducted on steel alloys, the analysis has been extended to other material and quench conditions and has identified, in a very simple manner using the Biot number, under which quench conditions the thermocouple hole needs to be included in the Inverse Heat Conduction (IHC) analysis.

The optimized IHC model and measurement techniques were then used to assess the influence of material start temperature and sample thickness during a water quench test on samples of AISI 316 stainless steel plate. Start temperature is an important parameter during transient quench conditions as it can influence the overall shape and magnitude of the boiling curve. It was determined that, unlike steady state boiling conditions, under transient boiling conditions, a unique boiling curve does not exist for the different quench conditions. Instead the boiling curve becomes a function of the thermal history experienced by the material during the quench and can vary both in magnitude and shape.

The work has also identified a new region in boiling water heat transfer during transient quench conditions that identifies the initial interaction of the water and the hot surface and has been called the initial cooling region. In cases where the start temperature of the sample is above the Leidenfrost point, after the initial cooling region is complete, the sample will experience the full boiling curve including, film boiling, transition boiling, nucleate boiling and convective cooling. However if the sample start temperature is below the Leidenfrost point, after the initial cooling region, the sample will only experience nucleate boiling and convective cooling.

The work has proposed a relatively simple method to incorporate the influence of sample start temperature during transient quench conditions on the boiling curve and the method involves knowing what the full boiling curve is for the quench condition being studied as well as the change in the heat flux as a function of surface temperature during the initial boiling region.

TABLE OF CONTENTS

LIST OF FIGURES

LIST OF TABLES

NOMENCLATURE

A	Area, m^2
A_m	Koistinen and Marburger coefficient
Bi	Biot number
C_p	Specific heat, J/Kg°C
$[C]$	Heat capacity matrix
d	Distance, m
D	Diameter, m
d_r	Prior austenite grain size, m
g_x	Gravitational acceleration, m/s^2
ΔH_i	Enthalpy of transformation, J/kg
h	Heat transfer coefficient, W/m^2s
h	Height of tube, m
k	Thermal conductivity, W/m°C
$[K]$	Heat conduction matrix
L	Characteristic dimension of the material, m
m	Empirically determined constant for Avrami equation
M_f	Martensitic transformation finish temperature, °C
M_s	Martensitic transformation start temperature, °C
N_i	shape function
Nu	Nusselt number
n, b	Constants in the JMAK equation
P	Perimeter of the T/C wire, m
Pr	Prandtl number
q	Heat flux, W/m^2
Q	Heat generated by phase transformation, W
$\dot{Q}$	Heat flow, W
$\dot{Q}$	Heat generation rate, W/m^3
Ra	Rayleigh number
R	Relaxation coefficient

R	Residual function
r	Radius, m
t	Time, s
T	Temperature, °C, °K
T_w	Tube surface temperature, °K
T_∞	Air temperature, K
$\bar{T}$	Approximate temperature, °C, °K
ΔT	Temperature difference, °C, °K
Δt	Time incremental, s
V	Volume, m^3
X	Fraction transformed
w_i	Weighted function
α	Thermal diffusivity, m^2/s
β	Coefficient of thermal expansion, 1/K
ν	Kinematic viscosity, m^2/s
ε_{tube}	Emisivity of the tube
τ^+	Thermocouple time constant, s
ξ_i	Volume of phase i, m^3
ρ	Density, Kg/m^3
σ	Stephan Boltzman constant (5.676×10^{-8} $W/(m^2K^4)$)
θ	Angle, °
θ	Crank Nicolson parameters

1.0 INTRODUCTION

Increasingly, computational modeling of industrial metallurgical and materials manufacturing processes is becoming an integral part of enhancing final product quality. The modeling, design and control of many of these operations hinges, in part, on being able to accurately quantify the heat transfer occurring at the boundary of the products being processed. In many cases, water is used as the medium to cool these components to the desired temperatures before further processing occurs. Often the associated heat transfer experienced by the sample is characterized using a boiling water heat transfer curve that represents the relationship between heat flux or heat transfer coefficient and surface temperature. Quantification of the heat transfer boundary conditions in these situations can be quite challenging, especially as rapid non-linear changes in the heat flux or heat transfer coefficient occur with the variation of the component surface temperature. Moreover, the boundary condition can also change dramatically depending on the properties of the water, the conditions under which the water is applied to the surface of the component and the interaction of the water with the surface of the component. Further complicating factors are the variation in the material thermal diffusivity with temperature in the component as well as the latent heat that may evolve due to phase transformations. Although much boiling water heat transfer work has already been done, most of it has focused on steady-state conditions, whereas in many industrial operations, the boiling water heat transfer experienced by the component being produced is under transient conditions.

In conjunction with this, as manufacturers gain knowledge regarding the interaction between deformation, temperature and microstructure evolution, they are taking advantage of Controlled Thermo-Mechanical Processing (CTMP) to enhance final product quality and properties in hot rolled products [1-5].

An example of this is Timken, a bearing steel company located in Canton, Ohio, who proposed a five-year program to develop and demonstrate controlled thermo-mechanical processing technology for tubes and pipes [6]. The objective of this program is to deliver a final product with an enhanced microstructure and properties while reducing the required processing and energy costs. The methodology being employed for the project includes the development of a mathematical model, referred to as the Hot Tube Mill Model (HTMM) and its use to develop a "virtual tube mill" to efficiently process a variety of tube products. The HTMM model will then be used to simulate the evolution of temperature, stress/strain and microstructure that occurs during each of the stages of the tube-making process.

As shown in Figure 1.1, the process proposed by Timken to produce tubes for the oil industry and bearings involves the following process steps:

1) heating in a rotary hearth furnace,

2) piercing,

3) deformation in an elongation mill,

4) temperature control using either induction heating or quenching,

5) deformation in a reducing mill,

6) deformation in a sizing mill, and

7) final microstructure control using a slow cool bed.

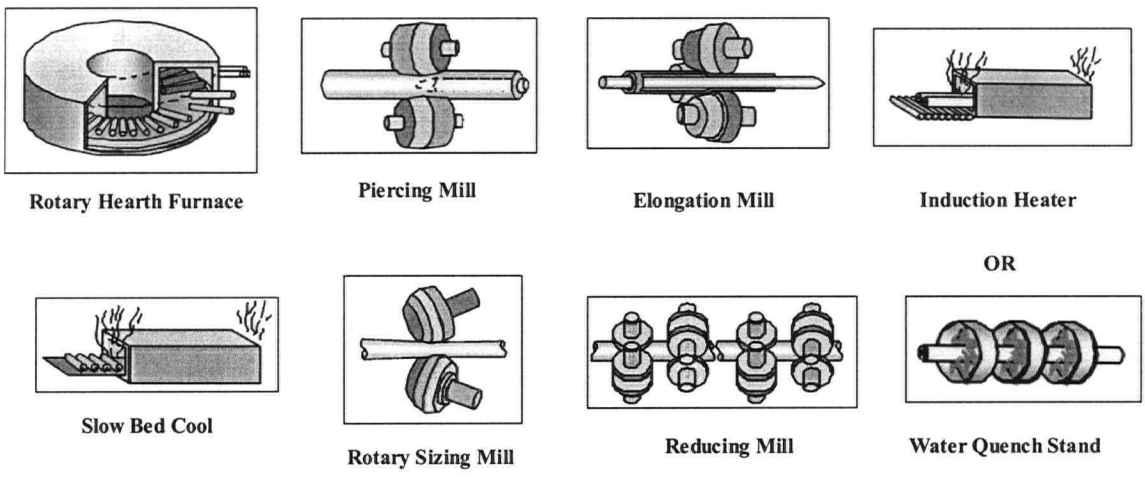

Figure 1.1 – Schematic of the Timken tube making process.

One of the key components of Timken's proposed CTMP process will be an in-line quench which will quench the tube down to a certain temperature and restrict austenite grain growth so that optimized final microstructures can be obtained.

In order to develop an accurate model of the tube-making process, it is critical to quantify boundary conditions accurately at each stage of the process. For the in-line quench part of the tube-making process, this involves quantifying the boiling water heat transfer that the tube is exposed to during the quench process. A further complicating factor is that during the in-line quench, transformation of the steel from austenite to non-

equilibrium (i.e. bainite or martensite) or equilibrium (i.e., ferrite and pearlite) products can occur and evolve heat during the transformation.

In light of the need for quantification of the boiling water heat transfer during the quench process and the challenges associated with this, researchers are increasingly turning to Inverse Heat Conduction (IHC) methods to quantify surface heat fluxes based on experimental data. In these methods, the boundary heat flux is not initially known but is calculated based on accurate knowledge of the temperature-time history experienced at a known location in the material during the cooling process.

The application of inverse methodologies to the quantification of heat transfer in industrial processes that involve boiling water heat transfer is not trivial. Critical to accurate quantification of the heat transfer boundary condition using this method, is the need for a robust inverse heat conduction technique as well as accurate temperature-time data measured during the cooling process. As a result, the objectives of this research include: 1) the development of a robust IHC model that can be used to analyze measured temperature-time data during water quenching of both tubes and plates under water quench conditions, 2) the identification of a "best practices" method to measure the thermal history during a water quench operation to ensure that the temperature-time data input to the IHC model is correct, and 3) the quantification of the influence of sample start temperature and thickness on boiling heat transfer during water quenching.

Although boiling water curves have been quantified for a number of different water spray conditions, part of the uniqueness of this study lies in its focus on transient boiling heat transfer and the influence of sample start temperature and thickness on the

resulting boiling curve. In addition, no other research has been found where the influence of the temperature measurement technique used during a water quench operation, and its associated errors, were identified and quantified.

2.0 LITERATURE REVIEW

Boiling water heat transfer is a complicated subject that has been studied extensively. As a result, there is a vast amount of literature available that covers a number of different aspects of this research topic including: the effect of quench and sample parameters on boiling water heat transfer and inverse heat conduction techniques to quantify the boiling water heat transfer. Initially the main goal of this research was to determine the boiling water heat transfer during quenching of steel plates and tubes. Since this is a transient quench process, the first part of the literature review is focused primarily on transient boiling water heat transfer and includes a general description of boiling water heat transfer as well as the influence of different factors on the resulting boiling curve. The work also involved developing an Inverse Heat Conduction (IHC) model to quantify the boiling water heat transfer based on measured temperature-time data during a quenching operation. Hence, the second part of the literature review describes the various numerical techniques that have been used in IHC models. One of the materials being studied in this research, AISI 52100, undergoes a solid-state phase transformation during the quenching operation that evolves latent heat. Since this evolution in heat will impact on the thermal field in the sample during the quenching operation, it is necessary to integrate the phase transformation kinetics into the IHC model. Thus, the third part of the literature review explores the techniques available to model the decomposition of austenite to both equilibrium and non-equilibrium products and their associated latent heats.

2.1 Boiling Water Heat Transfer

Water is used widely to cool product surfaces down to a prescribed temperature in a number of different industrial metals and materials operations, ranging from casting, to forming to heat treatment. Although much research has been devoted to modeling the evolution of temperature in metallurgical products during quench processing [7-11], the complexity of the boiling water heat transfer requires that the heat transfer is characterized in each situation, owing to the wide range of parameters that can influence the rate of heat transfer.

The Generic Boiling Curve

In the vast majority of metallurgical operations, the water quenching process involves boiling heat transfer, since the work piece surface temperature is usually much higher than the boiling point of water. A typical steady state boiling curve is shown in Figure 2.1 [12], which illustrates the relationship of heat flux to wall surface superheat. Wall surface superheat is the temperature difference between the surface temperature of the component being quenched, T, and the water saturation temperature, T_{sat}, i.e. $\Delta T = (T - T_{sat})$. Historically, steady state boiling curves were obtained using a horizontal nichrom wire, submerged in a water pool. The heat flux was then determined based on the power input necessary to maintain the wire at the temperature of interest [12].

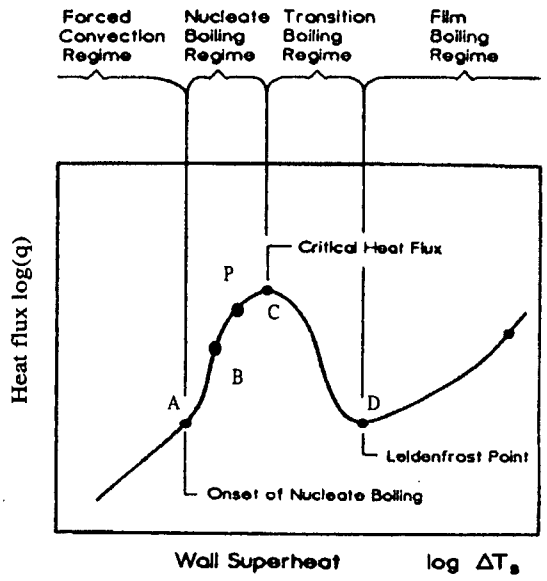

Figure 2.1 – Typical steady state boiling curve used to represent the relationship between the heat flux and wall surface superheat during boiling heat transfer [12].

As shown in Figure 2.1, the steady state boiling curve can be divided into a number of different regimes of behavior. At relatively low temperatures, $\Delta T < \Delta T_A$, free convection cooling exists. In this regime water completely wets the surface and classical convection heat transfer correlations can be used to estimate heat transfer coefficients and heat transfer rates.

Nucleate boiling exists in the range $\Delta T_A < \Delta T < \Delta T_C$. In this region, two different flow regimes may be distinguished. In region A-B, isolated bubbles form at nucleation sites and separate from the surface. This separation induces considerable fluid mixing near the surface, substantially increasing the heat transfer coefficient and the heat flux. As ΔT is increased beyond ΔT_B (region *B*-*C*), more nucleation sites become active and

increased bubble formation causes bubble interference and coalescence. Interference between the densely populated bubbles inhibits the motion of liquid near the surface resulting in a decrease in the rate of increase of the heat flux. Point *P* corresponds to an inflection point in the boiling curve at which the heat transfer coefficient, *h,* is a maximum. However, since the heat flux, *q*, is a function of both heat transfer coefficient, *h,* and temperature difference, ΔT, (i.e. $q=h\times\Delta T$), the heat flux will still increase beyond point *P* and achieve a maximum value at point *C* which is usually termed the critical heat flux (CHF) or peak heat flux.

The region corresponding to $\Delta T_C < \Delta T < \Delta T_D$ is termed transition boiling, unstable film boiling, or partial film boiling. Bubble formation is now so rapid that a vapor film or blanket begins to form on the surface. At any point on the surface, conditions may oscillate between film and nucleate boiling, but the fraction of the total surface covered by the film increases with increasing ΔT. Because the thermal conductivity of the vapor is much less than that of the liquid, the heat flux decreases with increasing ΔT.

At point *D* on the boiling curve, referred to as the Leidenfrost temperature, the heat flux is a minimum and the surface is completely covered by a vapor blanket. Heat transfer from the surface to the liquid occurs by conduction through the vapor. As the surface temperature is increased beyond the Leidenfrost temperature, radiation through the vapor film becomes significant and the heat flux increases with increasing ΔT.

2.1.1 Factors that influence boiling water heat transfer

Steady-state boiling heat transfer is a very complicated process, which has been studied for many years by numerous researchers, and is a subject that has received some good review papers [13-15]. Many factors have been found to influence steady-state boiling water heat transfer and include: water properties (e.g., temperature, quality), material surface conditions (e.g., morphology, surface tension) and the interaction between the water and the surface of the product being cooled (e.g., water flow rate, water pressure, nozzle distance from surface). In reality, however, many industrial practices involve transient boiling heat transfer and hence the relationships based on steady-state boiling are not appropriate. As a result, the remaining literature review on boiling water heat transfer has focused primarily on transient conditions.

Many of the recent studies have focused on doing experimental measurements under laboratory or industrial conditions and analyzing the temperature-time data using an inverse conduction technique to calculate the boiling curve for a given set of quenching conditions. This work has been done under a wide variety of quench set-ups that encompass typical unsteady state conditions used for both industrial casting [15-19] and hot deformation [20,21] processes.

Much of the work to date on boiling water heat transfer in the ferrous industry, has focused on the development of correlations for run-out table cooling in hot strip mills [22,23]. The investigations have looked at the influence of factors such as: water pressure, nozzle type, and stationary versus moving samples. Unfortunately, since most of the hot strip mills use very different run out table cooling systems, each study has

focused on measuring the heat transfer for a specific mill configuration. A further complicating factor during run-out table cooling, is that the water stays on top of the strip and pool boiling can start to occur after the initial water spray has hit the sample. However, at the bottom of the strip, the water will fall away from the sample almost immediately.

Nozzle type

Many studies have been done to investigate the influence of nozzle type on boiling water heat transfer of steel rolling products [24-26]. The nozzle types include spray nozzles [27,28], circular jets [29,30], planar jets [31,32] and air-mist jets (atomized water and air) [33]. The studies found that it is difficult to develop a universal formula relating heat transfer rate to spray characteristics. Hence it is recommended that for each specific nozzle, product geometry and quench condition being used, independent measurements of the boiling water heat transfer are made.

Stationary versus moving sample

Although many studies have been done using stationary samples, the effect of surface motion on heat transfer has only recently been studied. Some examples include rotating cylindrical surfaces [34,35] and planar moving surfaces [24,32,36,37]. Limited information on jet-impingement heat transfer on moving surfaces makes it difficult to design a proper cooling strategy under different operating conditions.

Spatial variation in heat flux

Most of the studies on boiling heat transfer have paid attention to only the area near the impingement region. In reality, heat transfer will change away from the impingement point where the flow characteristics of the water on the sample are quite different. From a modeling perspective, it is critical to accurately determine the spatial dependence of the heat flux, so that precise temperature profiles of the sample can be developed. A few studies have been done to quantitatively assess the spatial dependence of the heat flux away from the jet impingement point [22,38-40]. The temperature at which film boiling occurred decreased away from the primary impingement point of the spray, indicating that for a given spray configuration, a different boiling curve exists at different locations under the spray as shown in Figure 2.2. The Leidenfrost temperature also showed a strong dependence on the location relative to the impingement point. Some empirical correlations have been developed to describe the change in heat transfer coefficient based on the spatial position away from the impingement point but these are very dependent on the nozzle being used and the interaction between the quench water and the component being cooled.

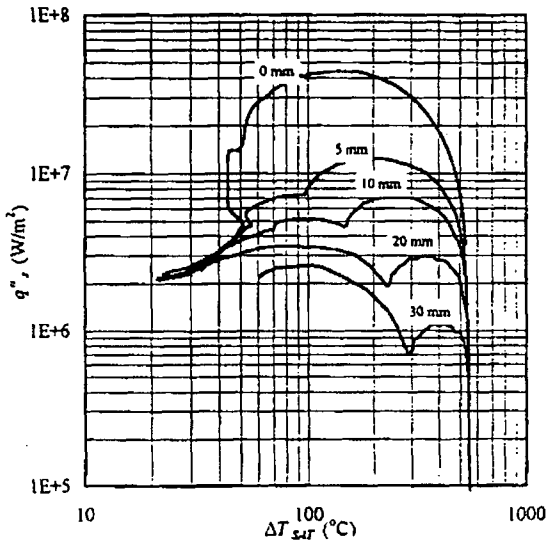

Figure 2.2 - Calculated boiling curves for various positions away from the water impingement point [38].

Liu [41] studied quenching of steel plates in a laboratory under conditions intended to simulate run-out table cooling during hot rolling of steel. In Liu's study, the effect of the interaction of neighboring water jets was examined. Liu observed that there was a strong interaction when the flow from two adjacent nozzles collided. The cooling intensity of the water was reduced in the area of interaction due to stagnation of water flow.

Overall, almost all studies show that the heat transfer coefficient will decrease with increasing distance away from the impingement point and may also be influenced by interaction of the flow streams between adjacent nozzles.

Water temperature

Another important parameter that has been studied and can have an influence on the heat flux during water quenching is water temperature. Many studies [39,42,43] have looked at this parameter with water temperatures ranging from 10°C to 100°C.

Langlais et al. [44] and Ho [45] found that the quenchability of water is strongly affected by temperature when the water temperature is high (over 30°C). But when the water temperature is low (below 20°C), the change in water temperature will have very little effect on the water quenchability. Another phenomenon that was observed to occur was that the Leidenfrost temperature decreased and the heat flux decreased as the water temperature increased.

Liu [41] studied the effect of water temperature (13°C and 30°C) on the boiling heat transfer during quenching of steel plates. The results showed that the cooler water caused the test sample temperature to drop more quickly and thus had a higher heat transfer capacity. Heat fluxes calculated from the measured cooling curves however did not show any effect of water temperature.

Jet velocity, water flow rate and water pressure

One of the most important parameters in terms of heat extraction to the quench water is the momentum of the water stream as it contacts the component surface. For a given nozzle configuration, the specification of either the water pressure or water flow rate will determine the jet velocity and its momentum. Many studies [11,38-40,43,44,46-49] have examined the effect of these parameters on boiling water heat transfer.

Increasing the jet velocity, through either an increase in water flow rate or water pressure, usually results in an increase in the boiling heat transfer and also an increase in the Leidenfrost temperature. However, if the impinging pressure or velocity is too high, it may cause the water spray to bounce from the surface and, consequently, diminish the heat transfer [41,50,51].

Water quality

Results from Stewart et al. [25] show that contamination in water can reduce the heat flux significantly. This is important from an industrial perspective as often the cooling water is recycled and its composition can change over time.

In 1985 Yu [45], used a hot aluminum block dropped into water to show that various additives affect the boiling heat transfer. The results show that dissolved air, surfactant, cationic poly-electrolyte and dissolved castor oil were all found to reduce the boiling heat transfer flux. Another study conducted by Langlais et al. [44] gave similar results.

Tests conducted by Grandfield [43] indicated that water quality had the largest effect on the peak heat flux, whereas the effect of water quality on the boiling water heat transfer in the convection and nucleate boiling regimes was relatively small.

Sample initial temperature

A few studies [17,18,48] have shown that the sample starting temperature can significantly impact the measured boiling curve. Specifically, the experiments conducted

by Miroslav et al. [48] showed that care must be taken when comparing the results obtained with different starting temperatures. For example, if the starting temperature is increased from 600 to 900°C for steel products, it can significantly influence the boiling curve. Li [17,18] also found that sample starting temperature had a dramatic impact on heat transfer to aluminum, with the effect being most pronounced in the transition and nucleate-boiling regimes when the sample starting temperature was below the Leidenfrost point.

Sample morphology

A few studies [17,18, 52-55] have examined the influence of the sample surface or morphology on the measured heat flux during water quenching. All of the studies found that surface morphology can have a significant effect on boiling water heat transfer. In general, as the surface becomes rougher, higher maximum heat fluxes were measured and higher Leidenfrost points.

Sample thermal conductivity

The influence of sample thermal conductivity on the resulting boiling curves has only been addressed in one study [56]. In this research, three aluminum alloys (AA5182, AA3004, AA1050), which have different thermal conductivities, were used to examine boiling water heat transfer in the impingement region during water cooling. It was found that thermal conductivity had a significant impact on the predicted variation in heat flux with temperature. The effect was most pronounced in the peak nucleate boiling regime, where the heat-transfer rate increased with increasing conductivity.

2.2 Inverse Heat Conduction Models

There are three possible ways to characterize the heat transfer boundary condition [57]:

a) Direct measurement of the surface heat flux.

b) Prediction of the surface heat flux.

c) Indirect measurement of the surface heat flux.

For direct measurement of surface heat flux, heat will be supplied at one side of sample by heating equipment such as an electric furnace, and will be extracted from the other side of sample by cooling water. A critical aspect of this measurement technique is maintaining the thermal balance across the sample. Bamberger and Prinze [58] have pointed out that the rapid change of heat flux with surface temperature in transition boiling makes it very difficult to attain thermal equilibrium and, therefore, precludes the direct measurement of heat flux during a quenching operation.

In order to predict the surface heat flux, relationships between heat flux and the factors which have an effect on heat flux, such as surface temperature, water flow rate, and water impingement velocity, have to be derived based on both theoretical and experimental analyses of the boiling process. However, this is not an easy task, as it involves a coupled heat and fluid flow analysis of the quenching process. Although many researchers [59-61] have done studies on boiling heat transfer based on theoretical predictions, the results usually do not match the experimental measurements well.

For indirect measurement of the surface heat flux, usually, thermocouples are embedded in the test sample and the temperature changes in the sample are recorded during the quenching process. These temperature-time histories are then used to estimate the surface heat flux or heat transfer coefficients using either analytical or numerical methods.

A heat conduction problem in a solid with the initial and boundary conditions completely specified is a well-posed problem that can be solved by various analytical and numerical methods. On the other hand, when the boundary condition is to be determined from measured temperature-time data inside the solid, the problem is ill-posed and known as an inverse heat conduction (IHC) problem [62]. Although an analytical solution for a one-dimensional IHC problem exists [63], a numerical method is generally preferable since it offers control over the accuracy and stability of the solution.

2.2.1. Analytical solution

Analytical solutions for IHC problems were proposed by many researchers [63-66]. Burgraf [63] presented an approximate solution for unsteady conduction with unknown surface boundary conditions. He approached the problem by assuming that both the temperature T(t) and heat flux q(t) were known functions of time at a single sensor location inside the medium. The temperature field was represented in terms of an infinite series of both T(t) and q(t) and their derivatives and the solution was found for some very simple geometries, such as a cylinder and sphere. In 1972, Imber and Khan [64] obtained an exact solution for the temperature field using Laplace transforms when the temperature was known at two distinct interior points in a one-dimensional problem.

The paper by Alam et al. [69] developed an analytical solution to the direct problem, which consists of determining the temperature in a one-dimensional plate for a given time-dependent heat flux. The heat flux input at the surface is assumed to be a polynomial function of time. The direct solution is determined by an approach based on separation of variables. To solve the inverse problem, the solution of the direct problem is combined with a least-squares method to minimize the difference between the analytical prediction and experimental temperature profiles. The surface heat flux determined by the inverse method is reasonably accurate only up to the time that the heat flux can diffuse to the temperature sensors in the experimental setup. Similarly, Taler [70] subdivided the problem he studied into two separate problems: a direct problem for the semi-infinite solid and an inverse problem for the flat plate. The heat flux at the location of the temperature sensor is determined from the solution of one-dimensional heat conduction using Duhamel's theorem. Knowing both the temperature and heat flux at a sensor location, the temperature and heat flux at the active surface are determined from the solution of the inverse heat conduction problem using the Stefan-Burggraf-Langford method.

Recently, with the development of computer technology, numerical methods have been used more frequently to solve IHC problems. The reasons for this include the fact that analytical solutions can only be used for simple geometries and linear problems, which represents only a small percentage of IHC problems.

2.2.2. Numerical method

The main advantage of using numerical methods to solve an IHC problem is that discrete methods based on finite differences or finite elements can be applied to any problem [71-74] and the phenomena, which evolve heat, such as phase transformations, which can occur during the quenching of steel products, can be included in the analysis. However, these numerical methods can induce numerical noise and oscillations due to the unstable nature of the inverse problem.

Numerical methods have been the focus of many recent studies in IHC problems [75-90]. The boundary element method (BEM) was used by Lesnic et al. [76] to determine the boundary conditions in a transient conduction problem where energies are specified in two areas of a one-dimensional slab. Applications of IHC problems to manufacturing processes are described by Tseng et al.[75], Hunag et al. [77], and Keanini [78]. In these studies, the finite element procedure was employed to analyze and solve the problem.

Numerical methods such as the finite difference method, finite element method and boundary element method are usually used to solve a direct heat conduction problem. However, for an inverse heat analysis, other techniques are required to estimate the boundary heat flux. Some of the well-known techniques to do this include: the space-marching technique [79], the frequency domain adjoin method [80], the mollification method [81], the iterative regulation method [82], the direct sensitivity coefficient method [83], and the sequential function specification method [78]. The aims of these

methods are to obtain a solution that is accurate and not very sensitive to changes in input temperature data.

The sequential function specification method developed by Beck was adopted in the studies by Ampere A. Tseng et al. [17, 18, 56, 75, 84], Hernandez-Morales et al. [85-87,8] and many other researchers [56,88,89]. The essence of this method is that a functional form for the unknown variation in the external heat flux is presumed; typically, a piecewise constant or linear variation is assumed. In this method, the heat flux is adjusted using sensitivity coefficients, which are the first derivative of temperature with respect to the boundary heat flux. Using these coefficients, the boundary heat flux can be easily estimated. The sensitivity coefficient can be solved directly at all times using the finite element method.

The time domain employed in the IHC analysis can be used to classify the method of solution. Three time domain approaches have been proposed: (1) one time step in the domain, (2) a few time steps in the domain or multiple future time step method, and (3) complete time domain or whole domain method. When the one time step method is used in the IHC analysis, the calculated results will become unstable if the time step is too small, and will produce a large error if the time step is too large. Conversely, the whole domain method is very powerful as a very small time step can be used to ensure accuracy of the solution however it is not computationally efficient and the calculated heat flux can be affected by the measured temperature data over the whole time domain. The multiple future time step method is a comprimise between these two methods and takes the advantage from the one time step and whole domain methods to do the calculation in a few future time steps.

2.2.3 Factors that affect results of IHC calculation

In addition, there are a number of factors that can influence the results of the inverse calculation, which are discussed in some detail below.

Time step

Calculations and experiments done by Hurpisz [91] and Archambault et al. [92] prove that the stability and accuracy of the IHC results are dependent on numerous parameters. In particular, the chosen time step is the most critical parameter. Usually the greater the error or noise in the measurement, the greater the time step which should be used. However, a larger time step can lead to an inaccurate approximation of the temperature history and inaccurate results, especially in cases where the Biot number is large.

Temperature noise

Another factor that can significantly affect the accuracy of the IHC model predictions is noise in the measured temperature-time data [93,94]. Research [93] indicates it is critical to smooth measured data so that noise is minimized yet the original trend in the data is preserved.

Thermocouple position

Maciag and Al-Khatib [95] conclude that in order to reduce the effect of the noise in the measured temperature for a fixed time step one should locate the thermocouple as close to the boundary as possible. Hurpisz [91] also concluded that the thermocouples

should be located as close to the boundary as possible to ensure accuracy and stability of the IHC solution.

Thermocouple dynamics

Although various types of temperature sensors may be employed to provide the internal temperature history of the body, the thermocouple is the most commonly used. When the heat flux is steady or varying only slowly in time, application of the IHC analysis yields accurate values for the unknown flux. However, if the heat flux is changing rapidly, even in a non-periodic manner, the effect of the inherent thermocouple sensor dynamics can have a major influence on the temperature history. If these data are then used to estimate the unknown surface heat flux, errors in both magnitude and timing of the heat flux history will result.

The thermocouple's ability to portray the transient temperature of its surroundings depends on two factors. First, as the temperature of the sample changes, there must be heat transfer between the sample and the temperature sensor. In order to achieve accurate readings, the contact resistance between the sample and the temperature sensor must be minimized. Secondly, the thermocouple junction inherently has a finite volume, and this volume's thermal mass must be as small as possible in order to have as fast a thermal response as possible to mirror the change in the temperature of the sample. Therefore, for a given thermocouple material, the mass of the junction should be minimized in order to attain a rapid thermocouple response. For example, Tseng [75] suggests that for typical heat transfer coefficients obtained during water cooling (i.e., in the order of 100

$kW/m^2°K$) the corresponding response time for the thermocouple used should be in the order of 1 ms.

In another study by Woodbury [96], the effect of thermocouple sensor dynamics was investigated in detail. In order to check the effect of thermocouple sensor dynamics, the two factors controlling the thermocouple's response may be combined into a single parameter, known as a time constant, shown in Equation 2-1:

$$\tau^+ = \frac{\rho C_p V}{hA} \qquad 2\text{-}1$$

where ρ is thermocouple bead density (kg/m^3), C_p is specific heat of thermocouple (J/kg/K), V is the volume of thermocouple (m^3), A is the contact area between thermocouple and surroundings (m^2), and h is the heat transfer rate between thermocouple and surroundings ($W/m^2/K$). As τ^+, the time constant, is increased, the sensor lags progressively behind the true temperature and results in increasing error in the estimated surface temperatures. The nature of this error is a combination of a progressive shift in the time of the response as well as a damping in its magnitude.

Usually it is extremely difficult to determine the time constant for a given thermocouple, as the contact resistance of the thermocouple is usually unknown. One way around this according to Woodbury [96] is to obtain data from a second sensor and by assuming that the two sensors have similar dynamics, then numerical methods can be used to predict both the unknown surface heat flux and the unknown value of τ^+.

2.3 Phase Transformations During the Quenching Process

During the quenching of materials, phase transformations can occur. In steel products, for example, phase transformations can occur as the steel is quenched from a high temperature where the structure is austenite, into equilibrium (ferrite/pearlite) or non-equilibrium (bainite/martensite) products depending on the cooling rate and composition of the steel. It is necessary to include these phase transformations in the inverse models as the evolved heat will influence the predicted boiling curve.

Early work done to predict boiling water heat transfer during quenching of steel products did not incorporate these phase transformations [97-101], however recently, some inverse models have incorporated phase transformations to predict the microstructure evolution during the cooling process [92,102-106].

The latent heat that evolves during one or more of the phase transformations is usually incorporated into the heat transfer equations by assuming a linear law of mixtures [107]. The volumetric heat generated per unit time during phase evolution is given by Equation 2-2:

$$\dot{Q} = \frac{\rho}{\Delta t}\sum_{i=1}^{4}\frac{\partial H_i}{\partial \xi_i}d\xi_i \qquad 2\text{-}2$$

where H_i is the enthalpy of transformation (J/kg), ξ_i is the volume of phase i (m^3) , ρ is the density of material (kg/m^3) and Δt is the time increment (s).

The increment in a particular phase i must be calculated from knowledge of the phase transformation kinetics. The prediction of microstructural evolution during non-

isothermal processing of steels is complicated by the variations in both the driving force for the transformation and the diffusivity of the rate-controlling species. Thus, nucleation and growth rates for the new phase are independent functions of temperature [108].

One of the most common equations which is used to characterize isothermal phase transformation kinetics in steels, is the classic equation proposed by Avrami [109] and shown in Equation 2-3:

$$X = 1 - \exp(-bt^n) \qquad 2\text{-}3$$

where X is the fraction transformed, t is the transformation time, and b and n are empirically determined constants. In general, b is a kinetic parameter that represents the combination of nucleation and growth rates, whereas n is related to the geometry of the growing phase and the conditions of nucleation. In addition to cooling rate and chemistry, the transformation kinetics is also influenced by the austentite grain size. In one approach, the Avrami equation was modified to account for grain size by Umemoto et al. [110] as shown in Equation 2-4:

$$X = 1 - \exp\left(\frac{-bt^n}{d_r^m}\right) \qquad 2\text{-}4$$

where m is an empirically determined constant and d_r is the prior austenite grain size.

Recognizing the limitations in applying the isothermal equations to non-isothermal events, the additivity principle has been proposed to enable the application of the Avrami equation over a range of temperatures. The principle of additivity states that a transformation occurring under continuous cooling can be considered as a series of

isothermal events, in which the phase transformation is treated as a function only of the fraction transformed and the temperature. Various criteria for the application of additivity to phase transformations in metals have been proposed [111-116] and application of the Avrami equation through the additivity principle for both the austenite-ferrite and austenite-pearlite transformations during non-isothermal treatment has met with success [110,117,118].

The kinetics of the austenite-to-martensite transformation has been described using the empirical equation proposed by Koistinen and Marburger [119] and shown in Equation 2-5:

$$X = 1 - \exp[-A_m(M_s - T)] \tag{2-5}$$

where A_m is the Koistinen and Marburger coefficient and M_s is the martensitic transformation start temperature (°C). This equation was used in the study by Archambault at al. [120]. The study by Hagasaka, et al., [11] also used this equation and specified the parameter A_m as shown in Equation 2-6.

$$X = 1 - \exp[-0.011(M_s - T)] \tag{2-6}$$

The martensite start temperature, M_s, is dependent on the concentration of the austenite-stabilizing alloying elements. Andrews has described the M_s with the quantitative formula [121]:

$$M_s(^\circ C) = 512 - 453C - 16.9Ni + 15Cr - 9.5Mo + 217C^2 - 71.5CMn - 67.6CCr \tag{2-7}$$

Where C, Ni, Cr, Mo, Mn should be the concentration of different elemental species in weight percentage. Although the trend among researchers is to use the Andrew's equation, the formula of Steven and Haynes [122] has also been used:

$$M_s(^\circ C) = 561 - 474C - 17Ni - 21Mo - 33Mn - 17Cr \quad (2\text{-}8)$$

2.4 Summary

1. Cooling and quenching by water play an important role in the metallurgical industry. Because of its importance and impact on product quality, a significant amount of research has been done to quantify heat transfer in the various industrial processes that use water as a quench medium. Owing to the high temperatures involved, the heat transfer typically can involve one or more of the following phenomena: convective heat transfer, nucleate boiling heat transfer, transition boiling heat transfer and film boiling heat transfer. Within these various regimes, the heat transfer flux can vary significantly.

2. There are many factors that can influence heat transfer from the product during the water quenching process. These include: spatial location relative to the impinging water, water temperature, jet velocity, water flow rate and water pressure, water quality, sample thermal properties, sample initial temperature, and sample surface condition. It is noteworthy that the factors influencing transient cooling have received comparatively little attention in the literature.

3. An inverse heat conduction (IHC) method is usually used for calculating the heat transfer coefficient or heat flux during cooling. This method uses the measured

temperature at a known interior point of the sample to indirectly calculate the heat flux at the surface or boundary of the component. Many factors can affect the results calculated using the IHC method. These include: data sampling frequency, data noise, thermocouple position, thermocouple response time and time step used for the calculations. It is critical to incorporate the latent heat when analyzing samples that are undergoing a phase transformation as this can significantly impact the calculated boiling curve.

3.0 SCOPE AND OBJECTIVES

3.1 Objectives

The overall objective of this work was to develop a quantitative understanding of the boiling water heat transfer that occurs during water spray quenching of some ferrous alloys. The work has focused on both high carbon steel (AISI 52100) tubes as well as AISI 316 stainless steel plate. The AISI 52100 material was chosen as this was the high carbon tube material produced by Timken, the industrial sponsor for the project, and both equilibrium (ferrite/pearlite) and non-equilibrium (bainite/martensite) phase transformations can occur during the quench operation. On the other hand, the AISI 316 stainless steel plate was used as no phase transformations occurred, a simplified geometry could be used (flat plate versus a tube) and little oxidation or scale formation occurred during the reheating process to the test temperature. Hence, the boiling water phenomena during a transient water quench could be more accurately assessed in the absence of these complicating factors.

Towards the overall goal of the project, the work has focused on the development of a 2-D axisymmetric inverse heat conduction (IHC) model capable of calculating the heat transfer boundary condition at the surface of the steel product based on the measured thermal history at the known locations in the quenched sample. The work has also investigated methods to accurately measure the thermal history in the sample during a water quench operation including both surface as well as sub-surface thermocouples.

Once developed and verified, the IHC model was used to quantify the influence of sample start temperature and thickness on the resulting boiling curves for an AISI 316 stainless steel. Using these data, quantitative correlations to predict the boiling curves as a function of sample start temperature were developed.

Specifically, the objectives for this research work include the following:

- To develop a 2-D axisymmetric inverse heat conduction (IHC) model capable of accurately quantifying the heat transfer boundary condition during water quenching for a variety of geometries ranging from solid cylinders, tubes, and flat circular plates.

- To analyze the sensitivity of the IHC model predictions to material properties such as thermal conductivity, volumetric specific heat and latent heat evolution associated with phase transformations as well as IHC model parameters such as time step and thermocouple location.

- To identify a "best practices" method for sample thermal history measurement during water quenching. This was done by analyzing the influence of thermocouple installation techniques (i.e., sub-surface and surface) on the resulting thermal field in the sample during cooling and quantifying the error in the predicted boiling curves as a result of the perturbation of the thermal field in the sample due to the presence of the thermocouple.

- To study the effect of sample thickness, and sample start temperature in an AISI 316 stainless steel plate on the resulting boiling curves during the quench process and determine a method to model this effect.

3.2 Methodology

Figure 3-1 schematically shows the methodology adopted for the work. As can be seen, the project was divided into two major activities: 1) development of a 2-D IHC model which can be used to calculate the boiling curve based on measured temperature data and 2) experimental measurements to support some of the analysis as well as provide temperature-time data for input to the IHC model.

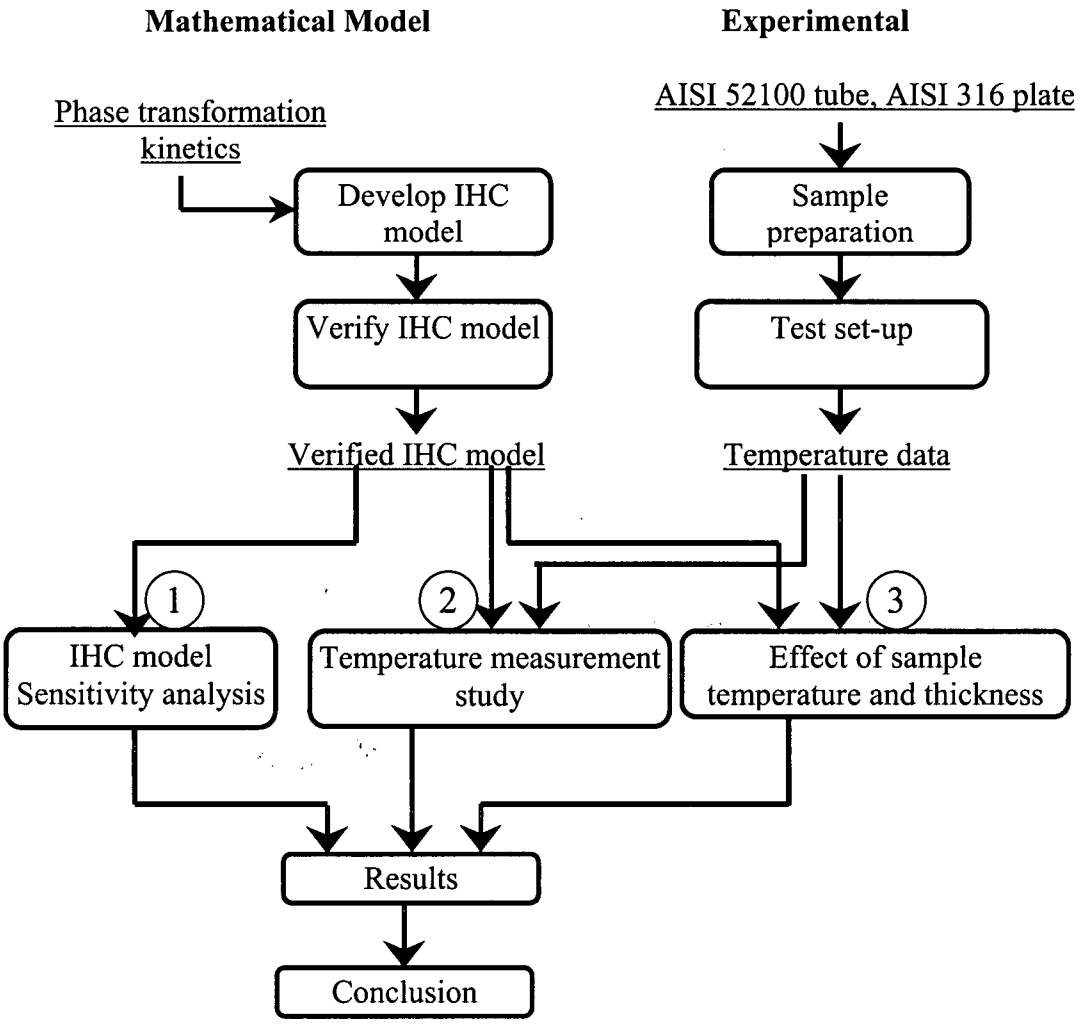

Figure 3-1. Methodology used for this research.

The IHC model used for this research was based on the future time step technique and employs a 2-D finite element based conduction model. Both the conduction and inverse components of the model were validated using analytical solutions as well as using the commercial Finite Element (FE) package ABAQUS^{TM}.

The experimental part of the program was performed using a quench unit designed and built at the University of British Columbia (UBC).

4.0 EXPERIMENTAL

A wide variety of tests were performed using the experimental apparatus built at UBC. This apparatus was quite versatile and could be used to do a variety of cooling tests ranging from four water spray nozzles which could be placed around the periphery of a tube sample, to a single water spray nozzle placed directly above the sample, to a simple air cooling test. Data generated from the experimental part of the program were used for the following purposes: 1) to validate the IHC model, 2) to test different thermocouple measurement techniques and 3) to generate data on the influence of sample start temperature and thickness on boiling water heat transfer.

As mentioned previously, different materials were investigated during the study and included AISI 52100 high carbon steel tubes as well as AISI 316 stainless steel plates. An important aspect of the experiments was the methodology used to install thermocouples in the tubes and plates.

Initially, the method chosen to instrument the samples was to use sub-surface T/Cs. For the tube specimens, this involved cutting a tube in half axially, drilling holes from the back of the cut specimen towards the surface of the tube so that the T/C's could be installed and then welding the two halves of the tube back together – this then created a full tube for testing purpose. In other cases, to reduce sample preparation, only half tubes were examined. In this case, instead of welding the tubes back together, insulation and a backing were put on the back of half tube after the thermocouple instrumentation was complete. For the flat plate tests, instrumentation was relatively easy and involved drilling a series of holes from the back of the sample along its diameter. In the majority of the cases, the sub-surface thermocouples were installed 90° to the quench surface,

however in one case a half tube was instrumented with T/C's at 45° to the quench surface to evaluate the influence of the T/C hole on the thermal field in the sample. After the tests were completed, the tubes and plates were sectioned to determine the exact location of the thermocouples.

Table 4.1 outlines the different types of tests that were run in the experimental program, the material used as well as the purpose of each test. Results from these tests will be presented in the temperature measurement and results and discussion sections.

Table 4.1 – Summary of tests run using the experimental quench rig at UBC.

Test	Material	Geometry	Test conditions	No. of tests run	Purpose
IHC model - validation of phase transformations	AISI 52100	Full tube (OD = 80 mm; ID = 58 mm)	Air cool	2	To validate microstructure evolution (latent heat) in IHC model
Temperature measurement techniques	AISI 52100	Half tube (OD = 80 mm; ID = 58 mm)	Water quench; water flow rate (1.262 l/s)	1	To determine influence of sub-surface T/C installation (i.e., 45° or 90°) on predicted boiling curve
	AISI 316	Flat plate (Radius = 13.97 cm, thickness = 12.7 mm)	Water quench; water flow rate (1.262 l/s)	2	To compare data from sub-surface and surface T/C's on the predicted boiling curve
Boiling water heat transfer	AISI 316	Flat plate (Radius = 13.97 cm, thickness = 12.7 mm)	Water quench; water flow rate (1.262 l/s)	7	To quantify the influence of sample start temperature on boiling heat transfer
	AISI 316	Flat plate (Radius = 13.97 cm, thickness = 6.4 mm, 12.7 mm and 19.1 mm)	Water quench; water flow rate (1.262 l/s)	3	To quantify the influence of sample thickness on boiling heat transfer

4.1 Quench Rig and Test Procedure

The experimental program for this research was performed using a custom-built quench unit at the University of British Columbia (UBC). The experimental setup included: an electric furnace to heat the samples to the desired temperature, a spray chamber to quench the sample and a water supply system (water tank and water pump) to supply cooling water to the quench chamber as shown in Figure 4.1. Also included in the set-up was a data acquisition system that was used to record the temperature change in the sample. The spray chamber could be adjusted to accommodate either one circular cone nozzle (for plate or half tube samples) as shown in Figure 4.2 or four circular cone nozzles (for full tube samples). Each of the nozzles had a diameter of 12.7 mm. In addition, for one test which was used to investigate phase transformation kinetics in AISI 52100 steel, no spray nozzles were used in the test chamber and the sample was allowed to cool in air under natural convection and radiation conditions. With this experimental set-up, a wide variety of cooling tests ranging from water quenching to natural convection could be done on a variety of sample geometries ranging from a flat plate to either full or half tubes.

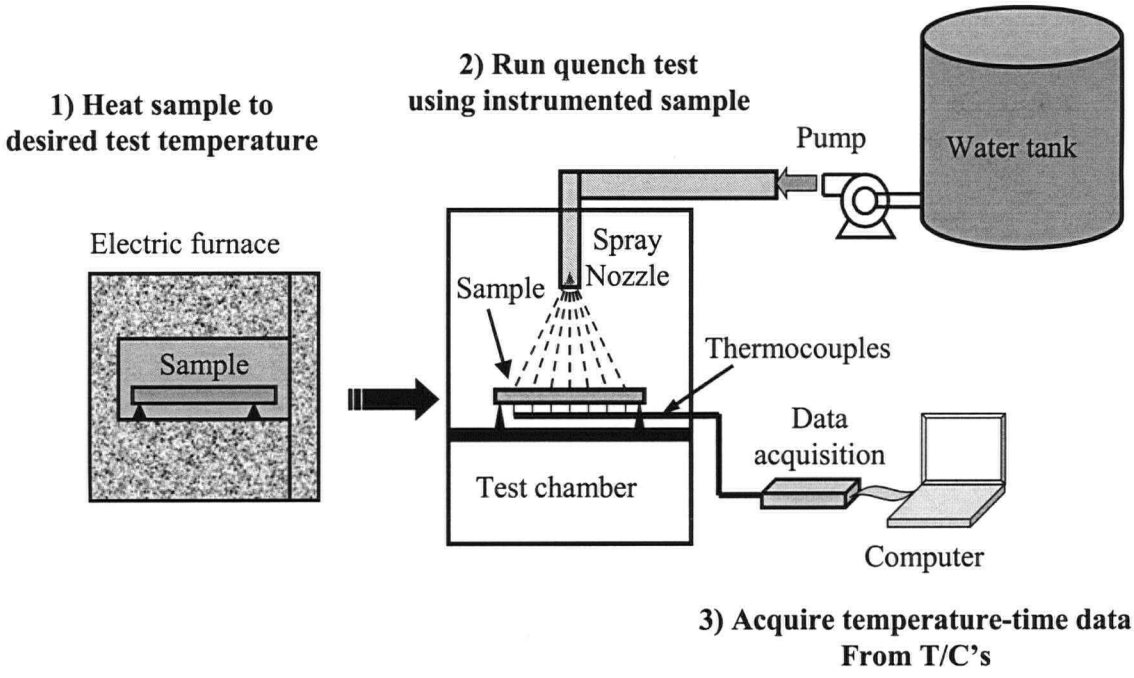

Figure 4.1 - Schematic of experimental setup.

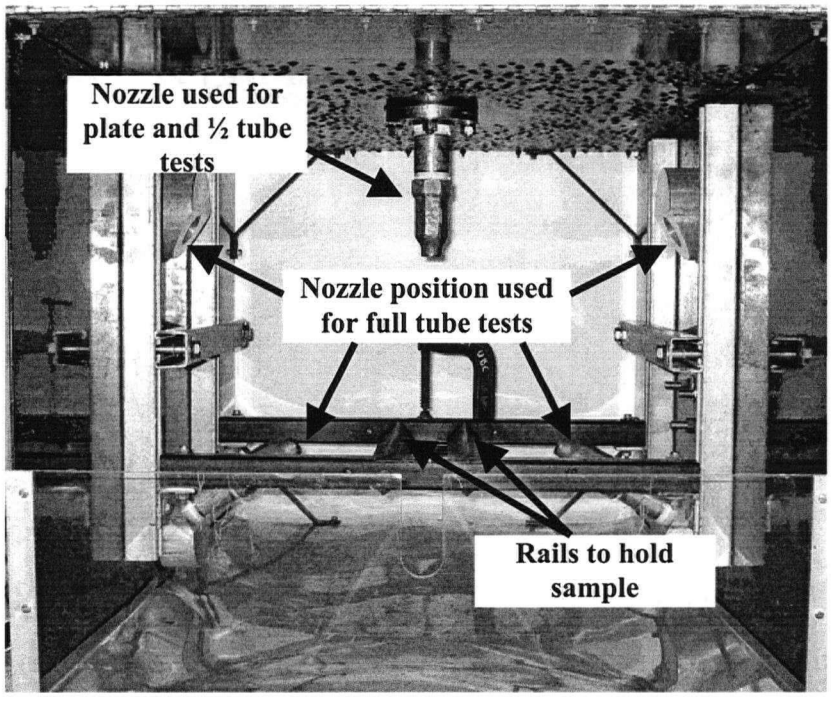

Figure 4.2 - Photo of quench chamber showing nozzle configuration and rail system to hold samples.

For each test, the sample was put into the furnace and heated to the desired temperature. Depending on the sample size and desired test temperature, the time for heating the test samples varied from 0.5 hour (400°C, plate sample) to 5 hours (1000°C, tube sample). After being heated to the desired temperature, the instrumented sample was held for approximately 30 minutes at the test temperature to ensure a uniform sample temperature. The sample was then taken out the furnace and placed in the quench chamber such that the center of the sample was directly under the water nozzle. Accurate positioning of the sample in the test chamber was done by attaching two steel notches at the back of the sample which could sit on two rails in the quench chamber. When the hot sample was put into the quench chamber, the position of the sample along the rails was adjusted until it hit the stopper at the back of the quench chamber. The stand off distance from the nozzle to the surface of the sample could also be adjusted by moving the rail system up or down.

For the water spray tests, the water, which had a temperature of 15 °C, was turned on to the desired flow rate and the sample was quenched. To ensure there was no transient in the water flow rate at the beginning of the quenching process, a thin metal sheet was put right below the nozzle before the water was turned on to shield the sample from the water. Once the desired flow rate was reached (usually within a few seconds) the shield was removed and the sample was quenched. During cooling of the sample, a data acquisition system recorded the temperature-time history as experienced by the thermocouples at a frequency of 1000 Hz.

4.2 Test Samples

Both AISI 316 stainless steel plate and AISI 52100 high carbon steel tubes were used during the quench tests. The reason both these ferrous alloys were chosen was that the AISI 52100 high carbon steel tube was material that had been supplied by Timken, the industrial sponsor of the research, for evaluation and would experience a phase transformation during cooling. In contrast, the AISI 316 stainless steel plate was chosen to simplify the experimental procedure as well as the data analysis. For example, the AISI 316 plate did not undergo phase transformations during the quench, would not oxidize or generate much scale during the reheating process to the test temperature and had a simplified geometry as compared to the tube sample. In addition, AISI 316 stainless steel could be supplied in plate form in a variety of thickness including: 6.3, 12.7 and 19.1 mm (¼, ½, ¾ inch), so that the influence of sample thickness on boiling water heat transfer could be assessed. To avoid edge effects in the plate samples, all of the stainless steel samples were cut out as circles with a diameter of 279.4 mm with the center of the circle positioned directly under the spray nozzle during a test. Each sample was instrumented with seven thermocouples which were installed from the back surface to measure the temperature history in the sample across its diameter during a quench test.

For the AISI 52100 steel tube samples, all the samples had a length of 406 mm, an outer diameters of 80mm and inner diameters of 58 mm. As described earlier, since the full tubes were extremely difficult to instrument with thermocouples without cutting and rejoining them, most of these samples were used in the ½ tube configuration and

instrumented from the back with three thermocouples at different axial locations along the tube length as shown in Figure 4.3.

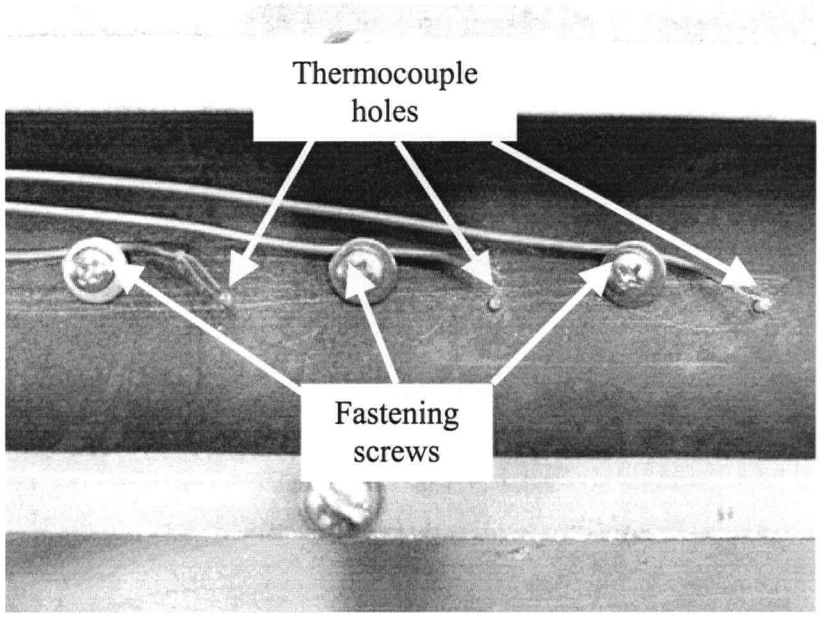

Figure 4.3 - Photo showing the back of an instrumented tube with three thermocouples and fastening screws.

The chemical compositions of the samples used in this investigation are shown in Table 4.2.

Table 4.2 – Nominal chemical composition of the samples used in this study in wt %.

Sample	% C	% Mn	% Ni	% Cr	%Si	% S	% P	% Fe
52100	0.98-1.01	0.25-0.45	-	1.3-1.6	0.15-0.30	0.025 Max	0.025 Max	Bal.
316	0.06	2.5	12	17	-	-	-	Bal.

4.3 Temperature Measurement

4.3.1 Instrumentation using sub-surface thermocouples

In order to get accurate temperature data, thermocouple (T/C) holes with a diameter of 1.6 mm were drilled into each sample from the back surface such that the bottom of the holes were within ~1 mm of the quenched surface. The holes were drilled as close as possible to the quenched surface so that the thermocouple could capture the detailed change in the temperature of the material during the quench process. A critical aspect of being able to record precise thermal histories for each sample during a quench was to ensure that the thermocouple made good contact with the sample and had a fast response time. As a result, electric spark welding was used to attach the two 0.26 mm T/C wires to the bottom of the thermocouple holes. Mullite ceramic with two fine holes was used to insulate the wires from each other in the hole. The T/C wires were fastened to the back of the sample using a fastening screw to ensure they remained securely in place. Figure 4.4 shows a detailed schematic of the T/C instrumentation for each test. Instrumenting the sample in this fashion ensured that there was no thermal contact resistance between the tip of the thermocouple where the measurement took place and the sample. In all of the tests type-K thermocouples were used and hence the two wires were made from chromel and alumel. After the quench tests were complete, the sample was sectioned to determine the exact position of the tip of the T/C in relation to the quenched surface. Figure 4.5 shows a typical photo of a cut sample showing the thermocouple hole and mullite ceramic.

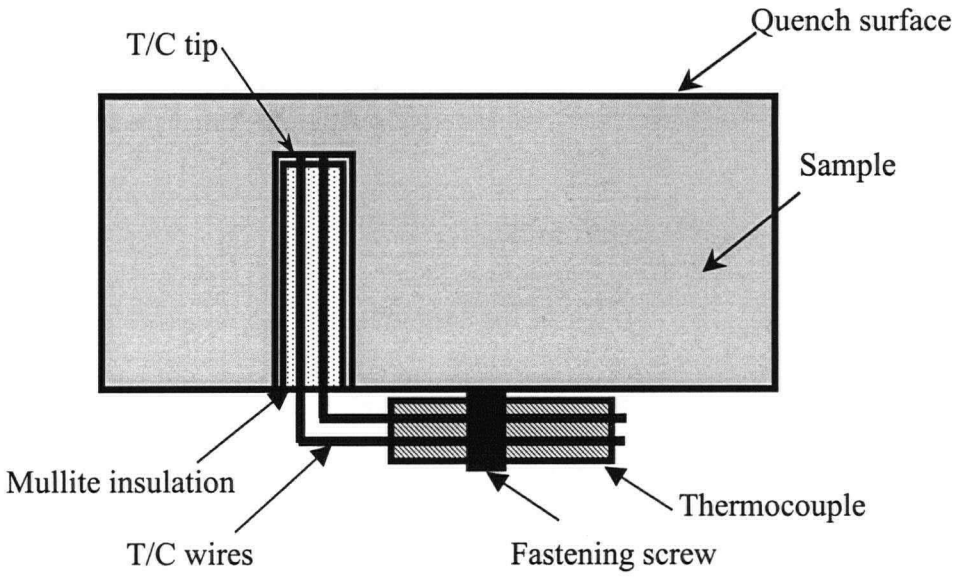

Figure 4.4 - Schematic of sub-surface thermocouple installation during a quench test.

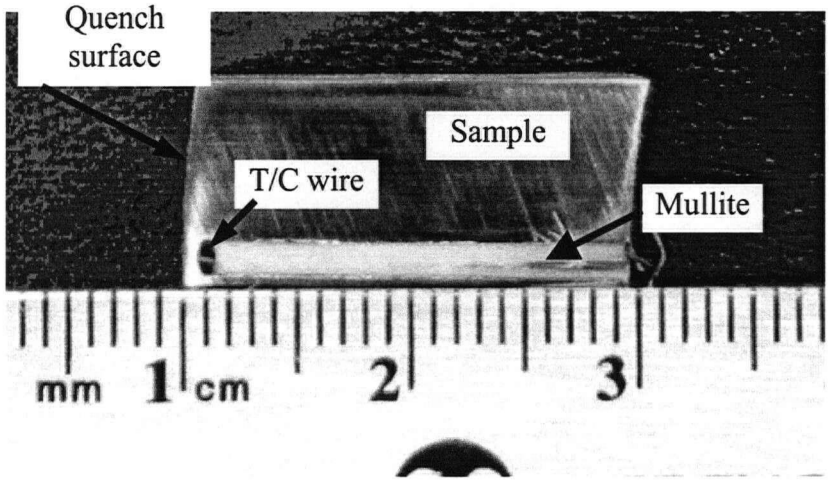

Figure 4.5 – Photo of a cut sample after quenching, showing the mullite and sub-surface T/C in the sample.

4.3.2 Instrumentation using surface thermocouples

An alternate temperature measurement technique was investigated which involved measuring the temperature at the surface of the sample directly. To install the surface thermocouple, a through hole of 1.6 mm diameter was drilled through the thickness of sample, and the thermocouple was put through the hole from the back such that ~30 mm of the T/C was on the quenched surface of the sample. The T/C wires were then stripped to expose the bare alumel and chromel wires each with a diameter of 0.26 mm and the wires were cut to a length of ~15 mm so that the T/C tips could be welded away from the T/C hole. Each of the thermocouple wires was attached to the surface of the sample using electric spark welding. Figure 4.6 shown a schematic of how the instrumentation of the surface T/C's was done.

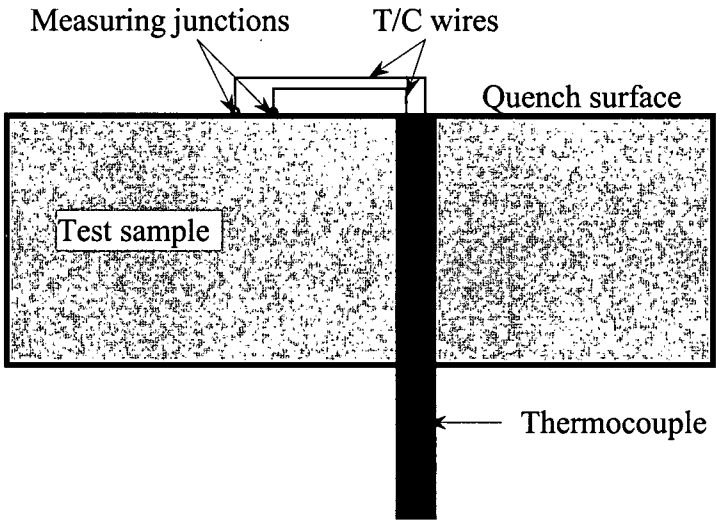

Figure 4.6 – Schematic of the method used to attach the surface T/C to the quenched sample.

4.4 Water Flow Distribution on the Quenched Surface

4.4.1 Flat plate tests

For each of the quench tests done using a flat plate, one circular cone nozzle was used to spray the water onto the sample surface as shown in Figure 4.7. During each test, the nozzle maintained a stand-off distance of 150 mm from the quenched sample surface. It was evident that two regions could be identified on the plate surface namely: 1) an area where the water impinged directly on the sample surface and 2) an area around the periphery of the nozzle where the water did not directly impinge but flowed horizontally as it was pushed away from the center of the sample due to the force of the spray.

A set of copper tubes was used to quantitatively determine the spatial variation in the water flux across the surface of the sample. The water flux at the locations consistent with each tube was calculated based on the volume of water in each tube and water spray exposure time. The water flux pattern was measured at 150 mm from the spray nozzle at flow rates of 1.14 l/s (18 gallon/min) and 2.21 l/s (35 gallon/min). The data from these experiments are shown in Table 4.3 and Figure 4.8. From these results, it can be seen that the spatial distribution of the water flow rate from the nozzle in the direct spray or impingement zone is quite uniform. One thing that should be pointed out is that the measured water distribution is a kind of incidence distribution. During quenching tests, the water sprayed in the center zone will flow out to the edge of the sample through the outer zone, so the real water distribution will be little different from these test results.

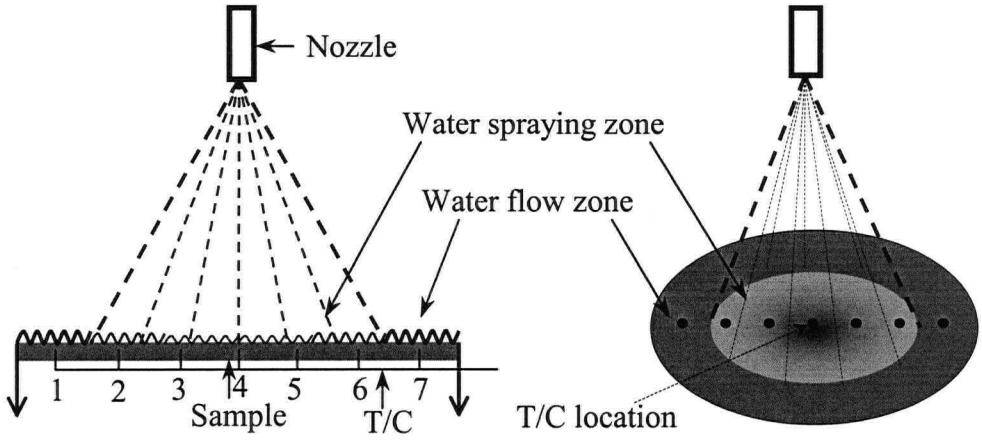

Figure 4.7 - Cooling water spray pattern on sample surface.

Table 4.3 - Spatial distribution of the water flow rate (in l/s/m^2) across the surface of the sample at a stand-off distance of 150 mm.

Distance from sample center (cm)	Nozzle water flow rate 1.14 l/s (18 gallon/min)		Nozzle water flow rate 2.21 l/s (35 gallon/min)	
	Test 1	Test 2	Test 1	Test 2
1.0	71.92	71.16	147.61	132.85
4.0	60.56	62.45	130.58	135.88
8.0	65.48	65.10	124.53	124.15
10	64.345	63.97	124.90	129.45
12	22.16	23.00	55.48	67.73
14	22.16	23.00	55.48	67.73

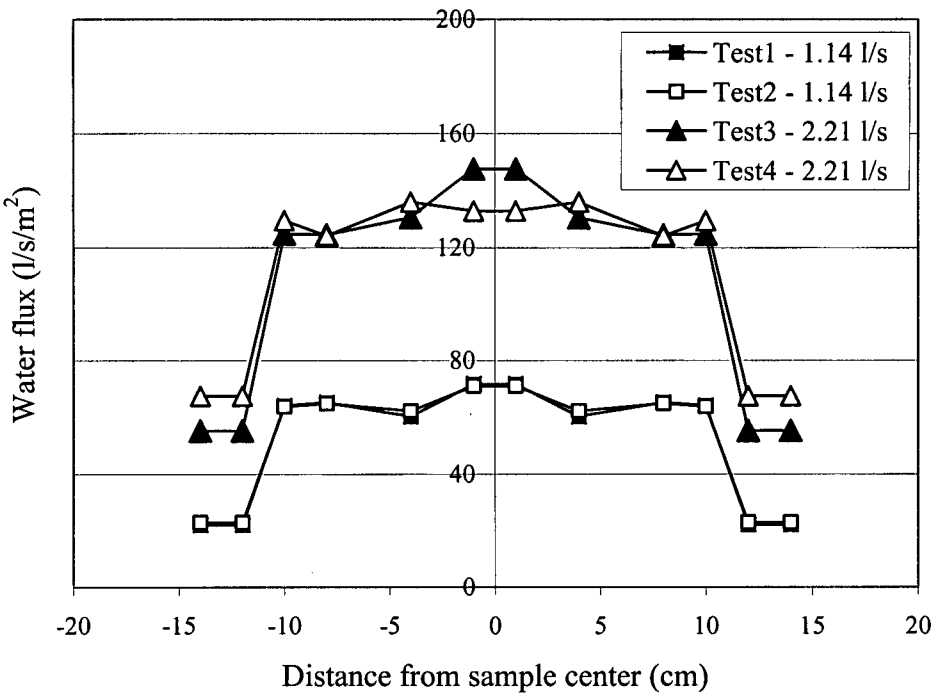

Figure 4.8 – Spatial variation in the water flow rate along the surface of the sample.

5.0 MODEL DEVELOPMENT

In order to calculate the associated boiling curves for each test condition performed using the test rig, it was necessary to develop a mathematical model, which is a two-dimensional Finite Element (FE) model in this study, capable of solving the governing heat conduction equation associated with an inverse heat transfer analysis. In this study, a two-dimensional Finite Element (FE) axisymmetric model was developed. The model consists of a conduction component to calculate the temperature at any location in the sample at a given time as well as an inverse component, to identify the heat flux at the boundary. For the inverse part of the model, an initial heat flux at the surface of the sample is assumed and then a comparison of the predicted and measured temperature distribution within the sample is made. The heat fluxes are then adjusted and the analysis run again to determine the new temperature profile. This process is performed iteratively until the difference between the predicted and measured temperatures meet the accuracy requirement (~ 0.2 °C).

5.1 Formulation of the Inverse Problem

Prediction of the boiling curves during water spray quenching of hot steel samples requires solving an inverse heat transfer problem as the surface heat flux is predicted based on the temperature history experienced by the sample at a known interior location. The inverse heat conduction (IHC) problem is much more difficult to solve than a direct heat conduction problem. One of the reasons for this is that this type of problem is

extremely sensitive to measurement errors, and the use of small time steps frequently introduces instabilities in the solution of the IHC problem unless restrictions are employed. In order to overcome these difficulties, thermocouples should be put as close to the quenched surface as possible and the frequency that the temperature data is captured during a test should be as high as possible. Key to the solution of the inverse problem is a conduction model which is used to calculate the temperature history at various points in the domain based on the heat flux applied at the surface of the sample. This calculated temperature history is then compared to the measured one and the heat flux is adjusted accordingly to minimize the difference between the predicted and measured temperature histories at the known locations in the sample. This procedure is continued until an acceptable difference between the measured and predicted temperature profiles, i.e., convergence is obtained.

In this research, the sequential function specification method was used. The sequential method calculates the heat flux in sequence over the cooling period for a given time interval. This reduces the effect of the heat flux at later quenching times on the calculated heat flux at the current time step typical of the whole domain method. In order to overcome the problem of divergence when a small time step is used, the multiple future time step method was employed. Whereby a small time step in used in the conduction model and a large time step in the inverse model. In terms of the conduction model, the Finite Element Method (FEM) was used to determine the thermal field in the quenched sample. Figure 5.1 shows a flowchart for the IHC model developed and used during this research. At the beginning of the IHC calculation, material data such as thermal conductivity, specific heat, density, and the measured temperature data from test

will be input to the model. At the start of the calculation an assumed surface heat flux is used and using this heat flux, the FE conduction model calculates the sample temperature distribution at time, t_1. This is then compared with the measured temperature from the test. If the calculated temperature matches (i.e., within 0.2°C) the measured temperature, the assumed heat flux will be adopted as the right one and will be used as the assumed heat flux for the next time step, t_2. Otherwise, the heat flux at the surface will be adjusted to a higher or lower value consistent with the calculated temperature being either too high or too low compared to the measured temperature. This adjusted heat flux will then be used in the conduction model and again a comparison will be made between the predicted and measured temperatures. This process will be repeated until an acceptable difference between the measured and calculated temperatures is achieved. The model will then move on to the next time step and repeat the process.

In the inverse model, the heat flux is adjusted using a relaxation coefficient, R, according to the formulation shown in Equation 5-1

$$q_i = q_i + R \times \rho \times Cp \times \Delta T_i \qquad (5\text{-}1)$$

where ΔT_i is the difference between the calculated and measured temperature, R is the relaxation coefficient (or correction coefficient), q_i is the heat flux applied on the boundary during the calculation of FE conduction model, ρ is material density, Cp is material specific heat. If the calculated temperature is lower than the measured temperature, ΔT_i will be negative, indicating that the heat flux applied on the boundary is larger than the real one, hence the adjusted heat flux will be lower than its previous value. Whereas, if the calculated temperature is higher than the measured temperature, ΔT_i will

be positive, which means the heat flux applied on the boundary during calculation is lower than the real one, hence the adjusted heat flux will be higher than its previous value.

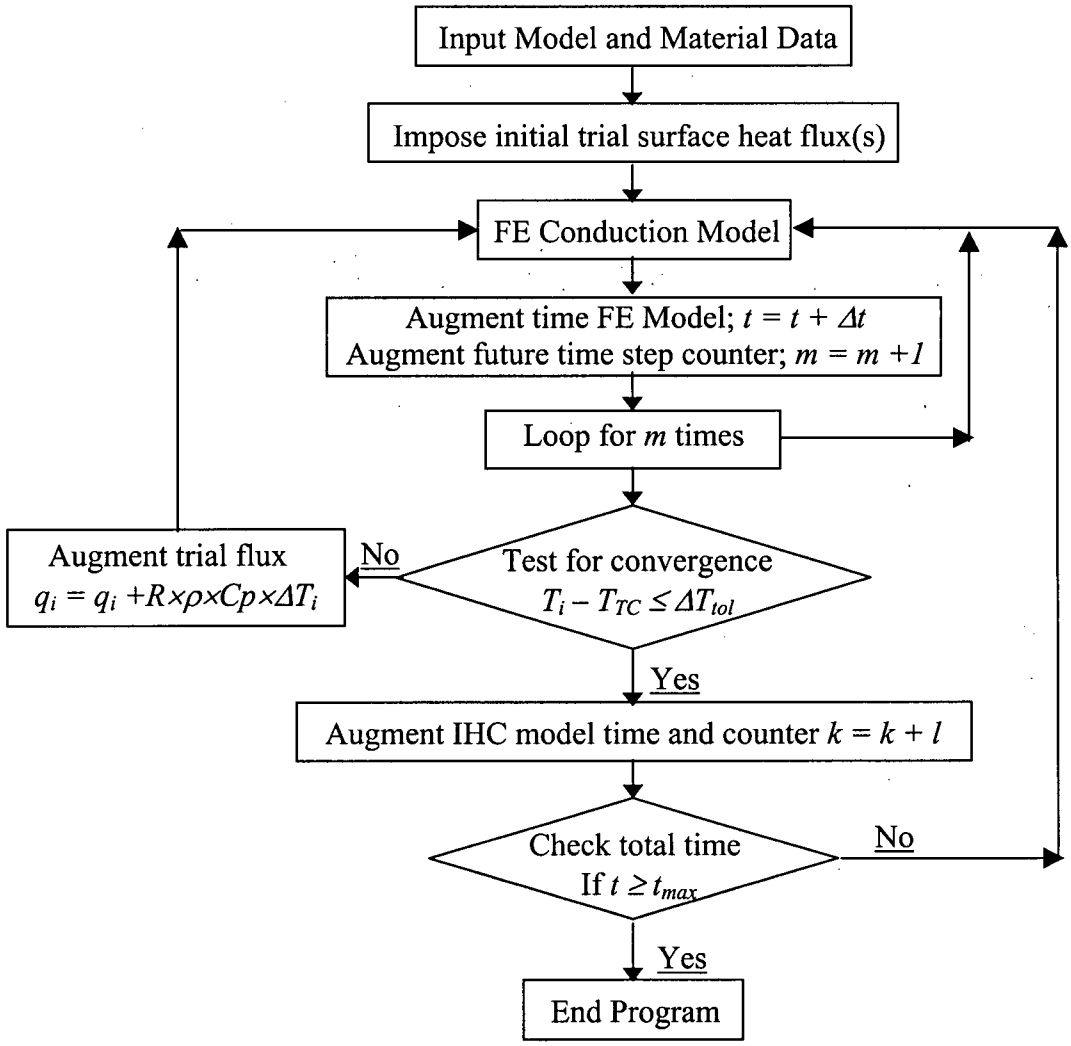

Figure 5.1 - Flowchart for the IHC model.

An important aspect in the numerical procedure is the selection of the relaxation coefficient R, if the value of R is too large, convergence problems can be encountered as the model will oscillate between a heat flux which produces a positive ΔT_i and one which

produces a negative ΔT_i. From this point of view, a small R should be used in the heat flux correction procedure, but a very small R will exert only a small modification on the corrected heat flux and little change on the calculated temperature difference ΔT_i after the next iteration of the IHC model's calculation. Hence, the computational time (number of iterations required to reach convergence for the IHC model) can be quite high. The selection of R depends on many factors such as material properties, thermocouple location, time step, and the FE mesh of sample geometry, and there is no simple way to tell what value it should be. During this study, the value of R was chosen by trial and error, different values of R were determined for different IHC calculations, and a fixed value of R was used for one IHC calculation. The values of R ranged between 0.001 to 5.

5.2 2-D FEM thermal conduction model

As can be seen in Figure 5.1, an important aspect of the 2-D IHC model is a 2-D thermal conduction model that is used to calculate the sample thermal field during cooling. The next section describes the development of the 2-D FE thermal conduction model that was used in conjunction with the IHC model.

5.2.1 Basic heat transfer

Referring to Figure 5.2, a general 2-D axisymmetric heat conduction model based on the FE method was developed to describe heat transfer in a tube. The model was formulated in a general manner so that it could also encompass and be used for the wide variety of geometries used in this study as shown in Figure 5.3, ranging from industrial tubes ($R_i > 0$, $R_o > R_i$), solid cylinders ($R_i = 0$, $R_o > 0$), flat circular plates ($R_i = 0$, R_o is

much larger than h), and flat circular plates with thermocouple holes (R_i varies from 0 to T/C hole radius) such that the influence of thermocouple installation on the local thermal field in the sample could be assessed. As can be seen in Figure 5.2, heat transfer in the tube was assumed to occur in the radial or r-direction to both the outer diameter (OD) as well as the inner diameter (ID) of the tube as well as the axial or z-direction towards the ends of the tube. Heat transfer in the θ-direction was assumed to be equal to zero. Hence, this model is applicable in cases where there is little or no circumferential variation in heat transfer.

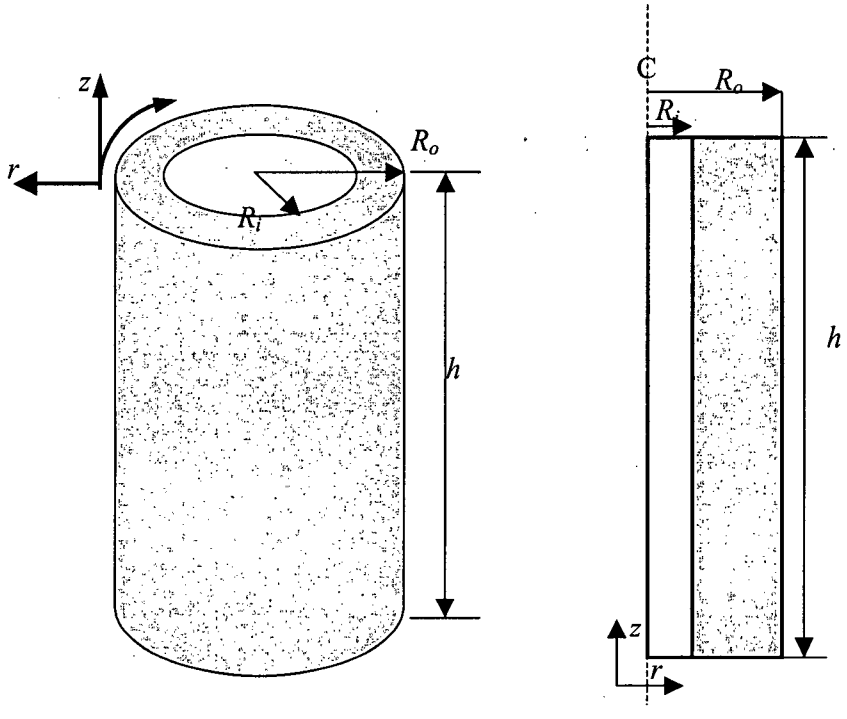

Figure 5.2 – Schematic of the geometry used for the 2-D heat conduction model.

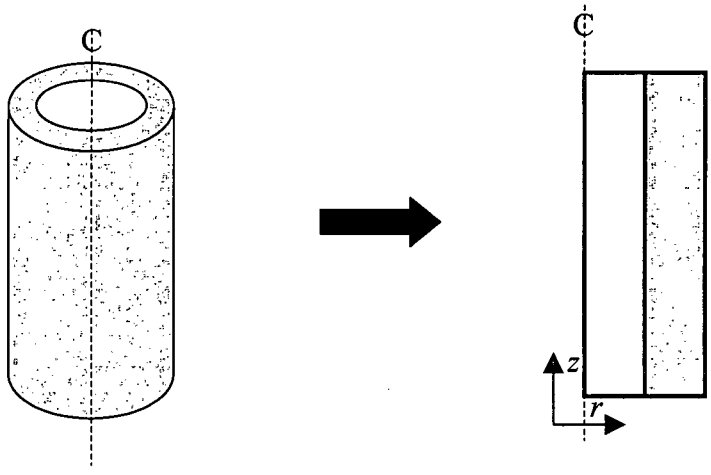

a) tube

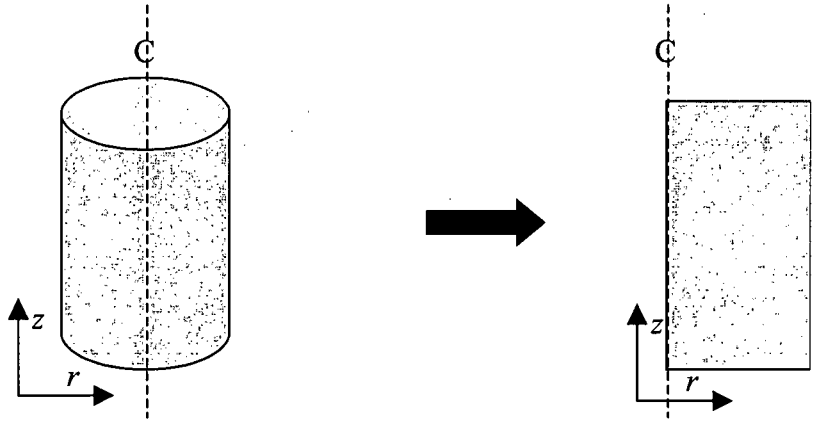

b) solid cylinder

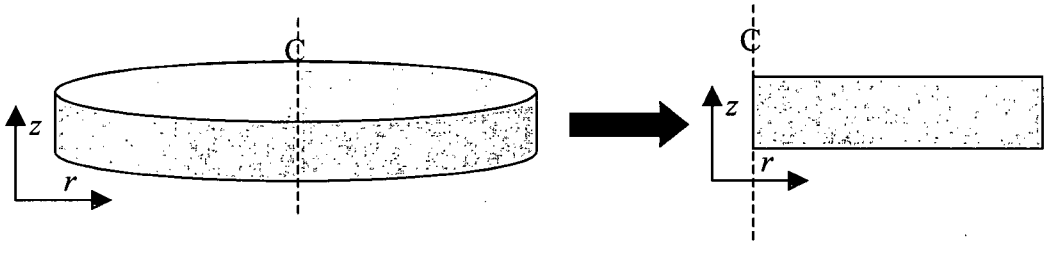

c) flat plate

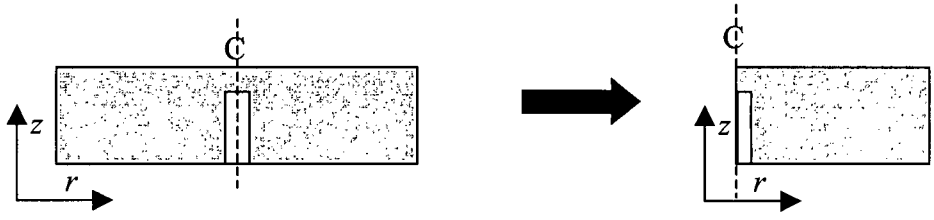

d) flat plate with T/C hole

Figure 5.3 – Schematic of the geometries that can also be solved by the developed 2-D axisymmetric model showing: a) tube, b) solid cylinder, c) flat plate and d) flat plate with T/C hole.

In view of the above assumptions, the flow of heat in the sample can be described as follows:

$$\frac{1}{r}\frac{\partial}{\partial r}\left(kr\frac{\partial T}{\partial r}\right)+\frac{\partial}{\partial z}\left(k\frac{\partial T}{\partial z}\right)+\dot{Q}=\rho C_p\frac{\partial T}{\partial t} \tag{5-2}$$

where $\dot{Q}$ is the heat generation rate in the domain, for example in steels, it can be associated with phase transformations that occur in the steel during quenching.

The applicable boundary conditions and initial conditions for the model are defined as follows:

1) At the outside of the tube, r = R_o, at times greater than 0 (i.e., t>0);

$$-k\frac{\partial T}{\partial r}\bigg|_{r=R_o}=h_1(T-T_c)=q_1 \tag{5-3}$$

2) At the inner diameter of the tube, $r = R_i$ and times greater than 0 (i.e., t > 0);

$$-k\frac{\partial T}{\partial r}\bigg|_{r=R_i} = h_2(T - T_c) = q_2 \tag{5-4}$$

3) At the upper end of the tube, $z = h$ and times greater than 0 (i.e., t>0);

$$-k\frac{\partial T}{\partial z}\bigg|_{z=h} = h_3(T - T_c) = q_3 \tag{5-5}$$

4) At the lower end of the tube, $z = 0$ and times greater than 0 (i.e., t>0);

$$-k\frac{\partial T}{\partial z}\bigg|_{z=0} = h_4(T - T_c) = q_4 \tag{5-6}$$

5) The initial condition is given by:

$$T(r,z)\big|_{t=0} = T_i(r,z) \tag{5-7}$$

5.2.2 FE method algorithm

The finite element solution to the partial differential heat conduction equation given in Equation 5-2 is based on the method of weighted residuals. This is a general method for deriving an approximate solution to both linear and non-linear partial differential equations (PDE's). For the FE model, 2-D, 4-node, linear temperature elements were used. Details of this technique are given in Appendix A.

5.2.3 Verification of the 2-D FE thermal conduction model

Verification of the 2-D FE thermal conduction model developed and used in this research was done in two ways, namely by comparing the numerical solution with one

obtained analytically and with the solution obtained from a well-known commercial FE software package, ABAQUS™.

Verification against analytical solution:

In order to analytically verify the 2-D FE thermal conduction code, a solid cylinder, which had a length of 0.1 m and a diameter of 0.02 m, was used as the calculation domain as shown in Figure 5.4. For this problem, the FE mesh was made up of 100 elements in the *z*-direction and 40 elements in the *r*-direction. The number of elements in the z-direction can be reduced to just one element in the case of uniform cooling on the quenched surface and adiabatic boundaries are assumed on the two ends of the cylinder. The total number of elements used was 4000 and the total number of nodes was 4141. The material thermal properties were assumed to be independent of temperature and are shown in Table 5.1

Table 5.1 – Material thermal physical properties used for verification purposes.

Thermal conductivity, k (W/m/K)	Specific Heat, C_p (J/kg/K)	Density, ρ (kg/m^3)	Thermal diffusion coefficient, α (m^2/s)
30	470	7800	8.18×10^{-6}

™ABAQUS is a trademark of Hibbitt, Karlsson, and Sorensen

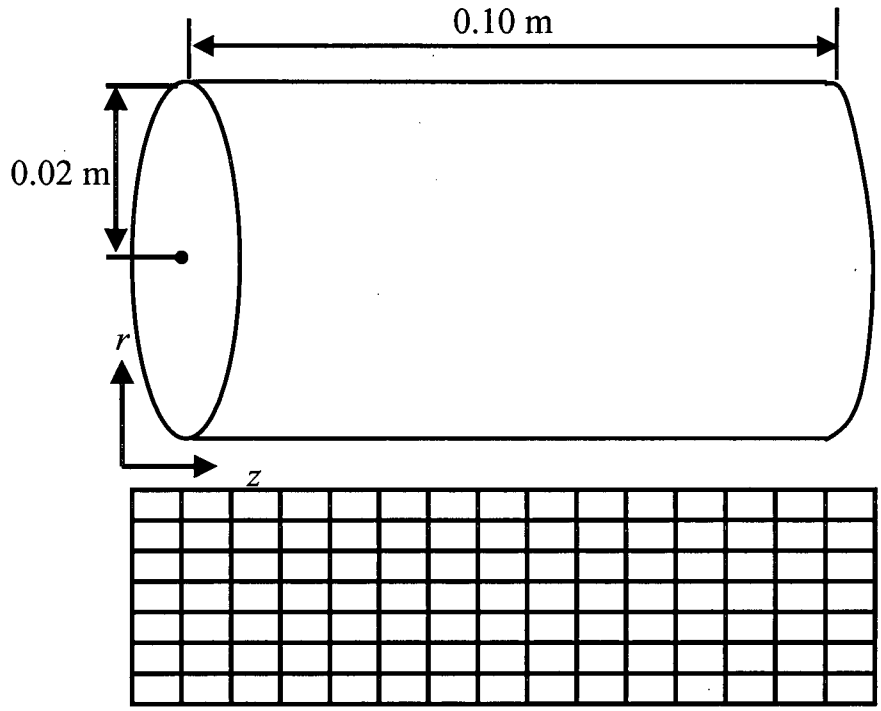

Figure 5.4 - Geometry used to verify 2-D thermal conduction model against an analytical solution as well as the commercial FE code ABAQUS™.

The sample was assumed to start with a uniform initial temperature of 900°C. At the surface of the cylinder, convection heat transfer, with a fixed heat transfer coefficient of 3000 $W/m^2/K$, was applied. The two ends of the cylinder were assumed to be adiabatic. The analytic solution for this problem can be solved using Heisler charts for a system with finite internal and surface resistances [125]. The calculated temperature profiles at different locations from the centre (i.e., radius=0.0, 0.016, 0.02 m) are shown in Figure 5.5. Because the solution from the Heisler charts [125] will produce an error when the cooling time is short, only the results of cooling times $t > 10$ s are presented. As can be seen good agreement between the model-predicted and analytical solution is obtained.

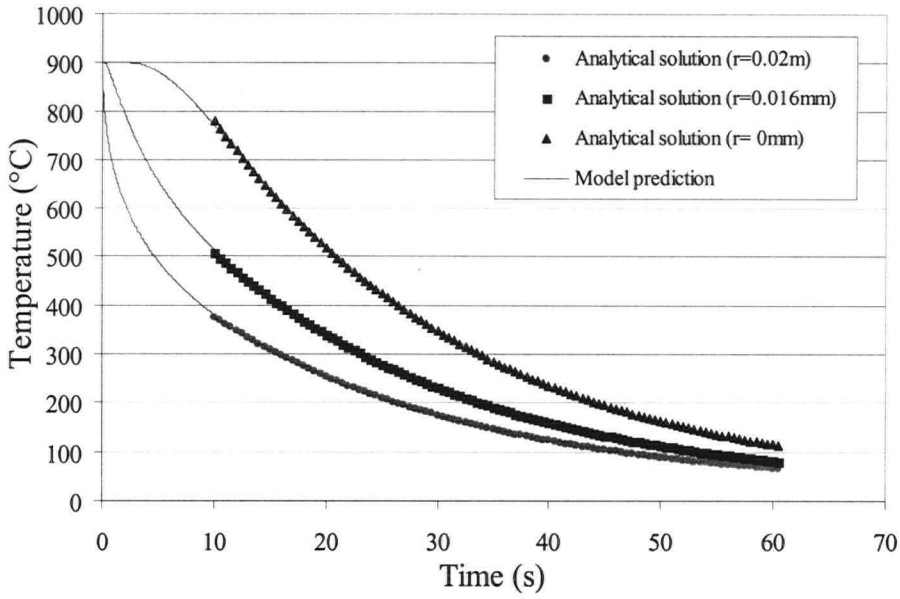

Figure 5.5 - Comparison of the model predicted temperature history against the results from an analytic solution for various positions from the centre of the tube.

Verification against ABAQUS™

Because the solutions from Heisler charts and model predictions can only be compared at times greater than ten seconds (i.e., $t > 10$ s), the 2-D thermal conduction model was also verified against the commercial FE code, ABAQUS™. This was done by using ABAQUS™ to simulate the thermal response in the steel cylinder as described previously and subject to a fixed heat flux (1000000 W/m^2) on the cylinder surface and also on the left end of the cylinder. The ABAQUS™ predicted thermal histories at particular positions (distance from left end of cylinder, $z = 0.01$, and radius $r = 0.0$, 0.016, 0.02 m) are compared to those calculated by the 2-D thermal conduction model. A typical comparison is shown in Figure 5.6, which indicates that the developed 2-D thermal

model is capable of predicting the temperature history in the 2-D axisymmetric sample very accurately.

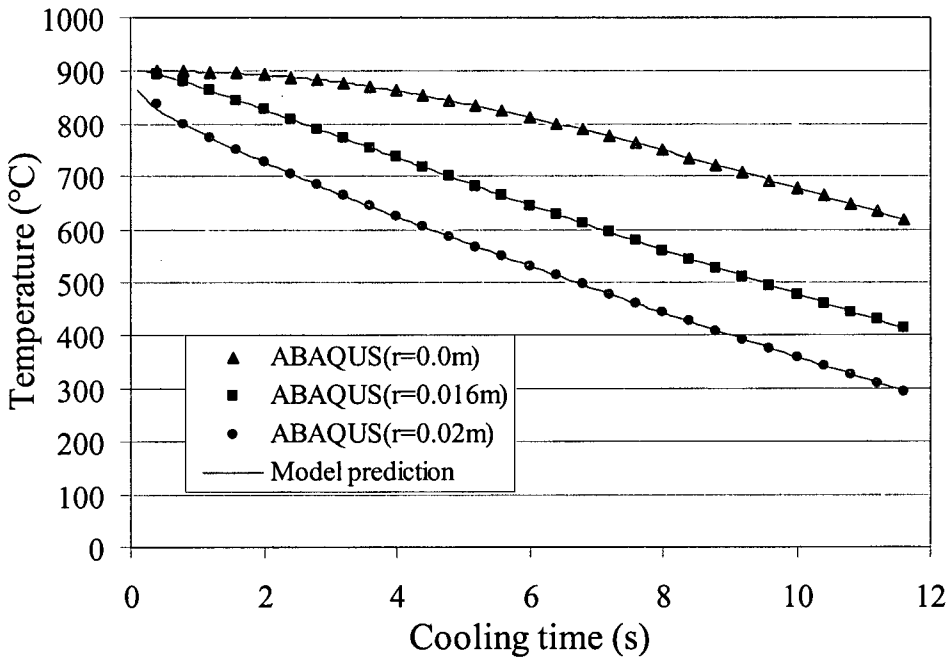

Figure 5.6 - Comparison of the 2-D thermal conduction model predictions against ABAQUS™ predictions for cooling of a cylinder with a heat flux of 1000000W/m^2/K applied to cylinder surface and one end.

5.3. Development of 2-D Inverse Heat Conduction (IHC) model

The algorithm used for the IHC model is presented in Figure 5.1. One important technique used in the IHC model is the multiple future time step method [62]. This method was chosen as it guarantees both convergence and accurate results from the IHC model. The following section will explain the multiple time step method used in the IHC model in detail.

5.3.1 Multiple future time step method

With a correctly chosen element size and time step, the FE thermal conduction model can reproduce the temperature history experienced at various locations within the sample accurately. As a result, the IHC model, which relies heavily on accurate predictions of the thermal conduction model, should predict the boundary heat flux quite accurately as well. However, one of the inherent drawbacks of the IHC problem is that it will diverge when the time step is too small due to the lag of the measured temperature inside the sample as shown in Appendix D. Hence, the time step used in the IHC method should be large enough to ensure convergence. This requirement is contrary to that needed in the FE conduction algorithm, which requires a small time step for accurate results. To overcome this problem, the multiple future time step technique [62] was adopted in developing the IHC model. In this technique, a small time step, $\Delta t(FEM)$, is used to calculate the temperature distribution in the sample whereas a large time step, $\Delta t(IHC)$, is used to estimate the heat flux for the inverse calculation as shown in Figure 5.7. Thus, convergence in the IHC algorithm and accuracy of the FEM conduction model are maintained.

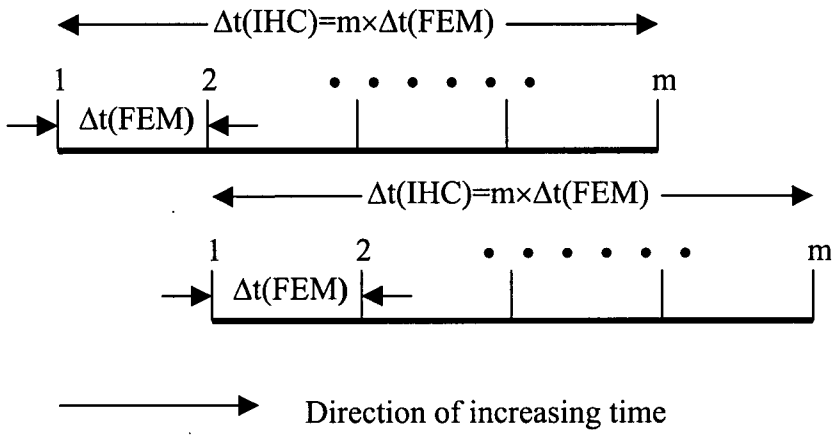

Figure 5.7. Multiple future time step method.

5.3.2 Verification of IHC model

The 2-D transient IHC model was verified against the commercial FE code, ABAQUS™. This was done by using ABAQUS™ to simulate the thermal response in a range of steel geometries (tubes and cylinders) subject to a known surface heat flux. The ABAQUS™ predicted thermal history at a particular position - i.e., at the location of a hypothetical thermocouple - was then input into the 2-D IHC model so that the applied heat flux could be back-calculated and compared to the original applied heat flux.

5.3.2.1 Solid cylinder geometry

The geometry and thermo-physical properties of the sample used to verify the IHC model is the same as that used to verify the 2-D FE thermal conduction model code (i.e., a steel cylinder with length 0.1 m and a radius of 0.02 m). The hypothetical thermocouple location is assumed to be 2 mm from the quenched surface and at an axial position of 0.05 m along the cylinder (i.e., z = 50mm). It is the thermal history experienced at this location that was input to the IHC model. Two cases with quite different heat fluxes were used to conduct the verification, namely: 1) a heat flux that varies linearly as a function of cooling time as shown in Equation 5-8:

$$q=(1-t/100)\times 10^6 \qquad (5\text{-}8)$$

where q is the heat flux in W/m^2 and t is the time in seconds, and 2) a heat flux which varies in a non-linear fashion as a function of surface temperature (i.e., a typical boiling curve). In both cases, heat transfer at the ends of the cylinder was assumed to be zero. As

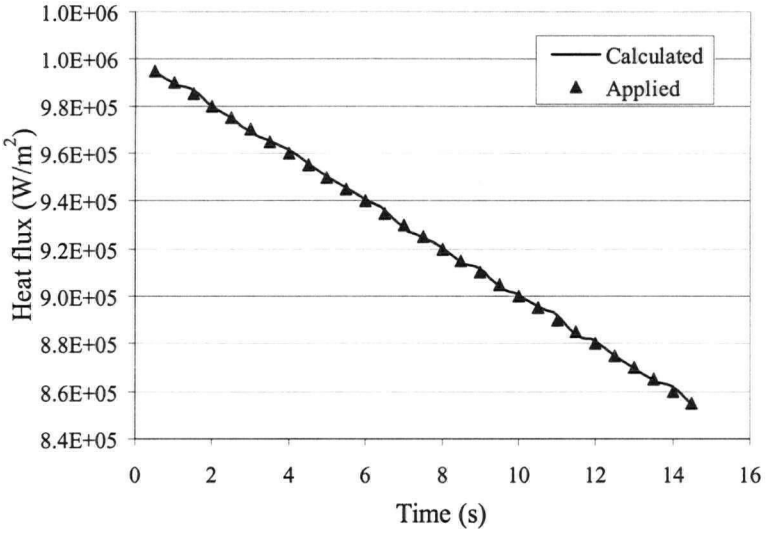

a) Heat flux as a function of time

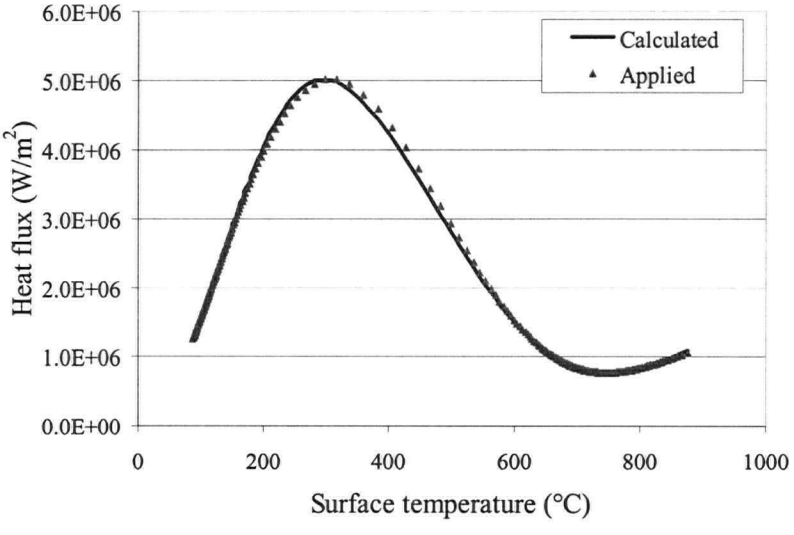

b) Heat flux as a function of surface temperature

Figure 5.8 – Comparison of the heat fluxes predicted using the IHC model to those applied in ABAQUS for: a) a heat flux which varies as a function of time and b) a boiling curve where the heart flux varies as a function of surface temperature.

can be seen in Figures 5.8 excellent agreement is achieved between the IHC model-predicted and applied heat fluxes.

5.3.2.2 Tube geometry

Further validation work was done on the IHC model to assess its capability to accurately predict the applied heat flux in a tube where both inner and outer diameter quenching occurred at the same time. To verify the model predictions for this situation, two different boiling curves were applied to the inner and outer diameter of a tube at the same time. Heat transfer at the ends of the tube was assumed to be zero. The geometry used for this verification is shown in Figure 5.9 and was assumed to have an inner radius of 0.029 m, an outer radius of 0.04 m and a length of 0.1 m. The thermo-physical properties used for the material are the same as the cylinder case and are given in Table 5.1. Two temperature profiles were generated in ABAQUS at hypothetical thermocouple locations of r_1 = 0.0305 m and r_2 = 0.0385 m from the centre of the tube at an axial location of z = 0.05 m and then input to the IHC model. As shown in Figure 5.10, again the comparison between the heat fluxes applied in ABAQUS and the predictions made using the IHC model are excellent.

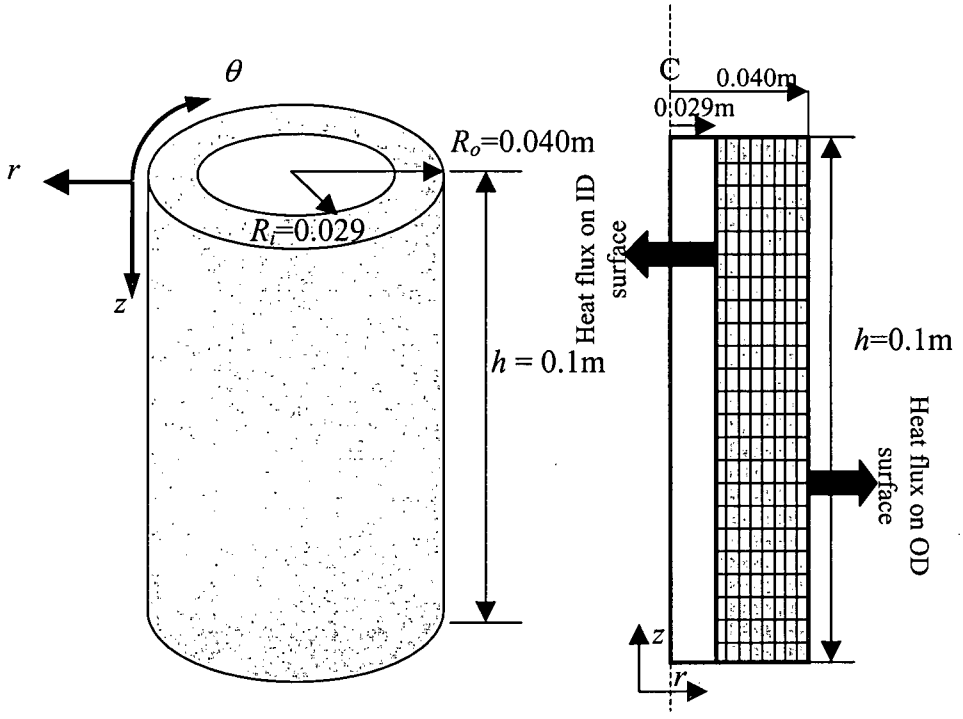

Figure 5.9 – Tube geometry used to verify IHC model predictions against ABAQUS. In this case a boiling curve at both the inner and outer diameter locations of the tube were applied at the same time.

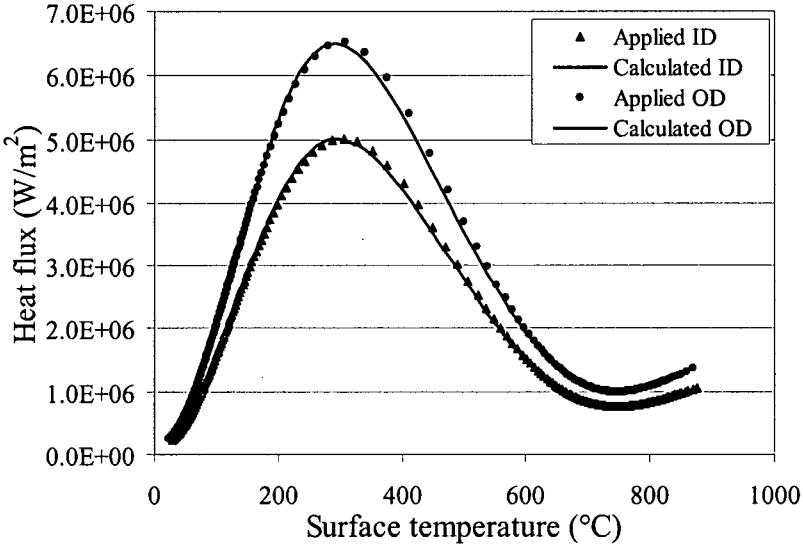

Figure 5.10 - Comparison of model predicted and applied boiling curves using ABAQUS™.

5.4 Inclusion of phase transformation kinetics into the IHC model

5.4.1 Effect of latent heat on sample thermal field

During the cooling of steel products, phase transformations can occur as the steel is quenched from a high temperature where the structure is austenite to a lower temperature where it transforms into equilibrium (ferrite/pearlite) or non-equilibrium (bainite/ martensite) products. During these transformations, latent heat is evolved and can influence the temperature profile in the material significantly. Hence, it becomes necessary to include the phase transformation kinetics and associated latent heats into the IHC model. Typical enthalpy values for the possible equilibrium and non-equilibrium transformation products in steels are given in Table 5.2. A quick calculation ($\Delta T = \frac{\Delta H}{C_p}$) indicates that these heats of transformation are equivalent to about 120-200 °C increase in the sample temperature and hence could have a significant influence on the thermal history experienced by the steel during cooling.

Table 5.2 – Enthalpy data associated with typical phase transformations in steel [11].

Transformation	Enthalpy (kJ/kg)
Austenite – ferrite	75.2
Austenite – pearlite	92.0
Austenite – bainite	92.0
Austenite – martensite	83.6

5.4.2 Incorporation of phase transformation kinetics into the IHC model for AISI 52100 steel

One of the most common equations, which has been used to successfully model isothermal phase transformation kinetics in steels, is the classic equation proposed by Avrami [109] and shown in Equation 5-9:

$$X = 1 - \exp(-bt^n) \tag{5-9}$$

where X is the fraction transformed, t is the transformation time, and b and n are empirically determined constants. In general, b is a kinetic parameter that represents both the nucleation and growth rates, whereas n is related to the geometry of the growing phase and the conditions of nucleation.

In order to make the Avrami equation applicable to non-isothermal or continuous cooling situations, the principle of additivity is used. This principle states that a transformation occurring under continuous cooling conditions can be considered as a series of isothermal events, in which the phase transformation is treated as a function only of the fraction transformed and the temperature. Using this principle, a continuous cooling curve can be broken up into a series of small isothermal events which are then summed together as shown in Figure 5.11.

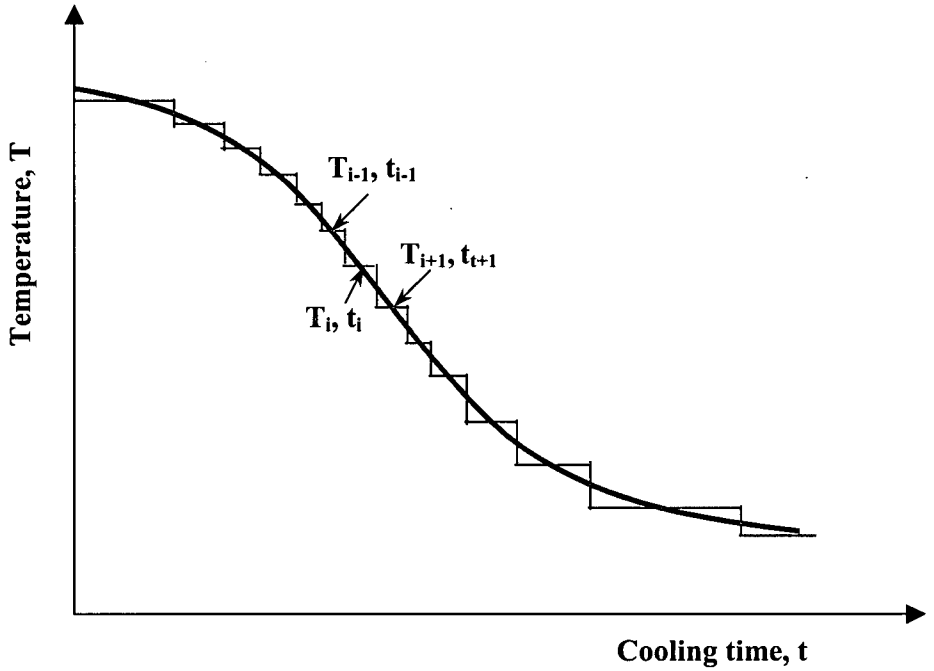

Figure 5.11 - Principle of additivity showing how a continuous cooling curve can be approximated as a series of isothermal events.

Using the principle of additivity, the amount of austenite, at temperature, T_i, which transforms in time, t_i, can be calculated using the Avrami equation as shown in Equations 5-10 – 5-12.

$$t_{i,initial} = \left[\frac{-\ln(1-X_{i-1})}{b}\right]^{1/n} \tag{5-10}$$

$$t_{i,total} = t_{i,initial} + \Delta t \tag{5-11}$$

$$X_i = 1 - \exp(-bt_{i,total}^n) \tag{5-12}$$

In these equations, X_{i-1} is the fraction of austenite already transformed; $t_{i,initial}$ is the time required to complete the transformation of fraction X_{i-1} at the temperature condition, T_i,

$t_{i,total}$ is the total phase transformation time that occurs under temperature T_i and experiences an initial time $t_{i,initial}$ which is representative of X_{i-1} and a time increment Δt.

Equation 5-10 is used to calculate the time required to finish the transformation of fraction X_{i-1} under the temperature T_i condition. Equation 5-11 assumes that the total phase transformation occurs under temperature T_i and experiences an initial time which is representative of X_{i-1} and a time increment Δt. Under such conditions, the Avrami equation can be used to calculate the total transformed fraction X_i.

The actual amount of transformed austenite ΔX_i at temperature T_i in time t_i is the difference between X_i and X_{i-1} as shown in Equation 5-13.

$$\Delta X_i = X_i - X_{i-1} = 1 - \exp\left(-bt_{i,total}^n\right) - X_{i-1} \tag{5-13}$$

The latent heat generation rate $\dot{Q}$ that is released at temperature T_i can then be calculated according to Equation 5-14:

$$\dot{Q}_i = \Delta X_i \times \rho \times \Delta H / \Delta t \tag{5-14}$$

where ΔH is the enthalpy (J/kg) associated with the phase transformation.

Unlike the transformation of austensite to pearlite or bainite, the transformation of austensite to martensite is athermal, i.e., the amount of martensite formed is only related to the temperature and is independent of time. For the transformation of austensite to martensite, in an AISI 52100 steel the martensite transformation start temperature (M_s) is estimated to be is 245°C [123], and the martensite transformation finish temperature (M_f)

is 30°C [123]. The amount of martensite transformed can then be estimated using Equation 5-15 [124].

$$x = 1 - \left[\frac{T - M_f}{M_s - M_f} \right]^{2.5} \tag{5-15}$$

where x is the fraction transformed of martensite, T is the temperature, M_f is the martensite finish temperature and Ms is the martensite start temperature.

5.4.3 Validation of the IHC model including phase transformation kinetics

A commercially significant high carbon steel (AISI 52100) was used in this investigation and the associated phase transformation kinetics for this steel were incorporated into the IHC model. Since this is a hypereutectoid steel, only the austenite to pearlite, austenite to bainite and austenite to martensite phase transformations were incorporated into the IHC model. The chemical composition of this steel is given in Table 4.1 of Chapter 4.

In order to model the austenite to pearlite and austenite to bainite phase transformation kinetics, the "***b***" and "***n***" used in the in Avrami equation were determined as a function of temperature from an Isothermal-Transformation (IT) diagram for AISI 52100 [122]. At a fixed temperature, the transformed phase fraction X_m and the time t_m (m can be 1%, 50% and 99% etc.) can be obtained from an IT diagram, and then with the help of this information, the Avrami equation can be used for determining the coefficients b and n. The variation in these coefficients as a function of temperature can be seen in Figure 5.12. In the model "n" was taken as a constant of 1.32 and a linear interpolation

was done to determine "*b*" based on the temperature. In the IHC model, the martensite transformation was modeled using Equation 5-15.

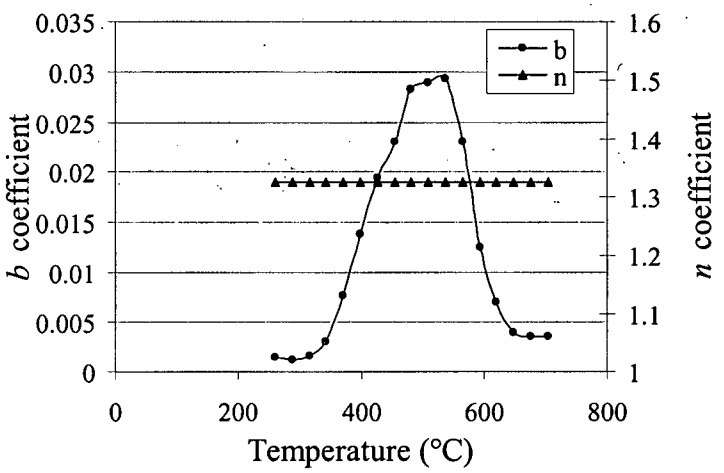

Figure 5.12 – Coefficient's of ***b*** and ***n*** used in the Avrami equation to model the kinetics of the austenite to pearlite and austenite to bainite transformations in an AISI 52100 steel.

To validate the IHC model including the phase transformation kinetics, an instrumented AISI 52100 steel tube, with an outer diameter of 80 mm, an inner diameter of 58 mm and a length of 406 mm was heated in an electric furnace to 870°C. Once at temperature, the tube was taken out of furnace and allowed to air-cool in the test chamber. During cooling, the temperature history in the sample was recorded and was then input into the IHC model to calculate the heat flux at the surface of the tube during the air cool. The results from the IHC model calculation were then compared to an analytical calculation based on known principles of radiation and natural convection. During the calculation of thermal conduction model and IHC model, it is assumed that the tube surface is exposed to radiation and air natural convection, the two ends of tube

have an adiabatic boundary condition and the inner surface of the tube also has an adiabatic boundary condition.

Under air cooling conditions, heat can transfer from the tube to the surrounding air in two ways, namely: radiation and natural convection. The total heat flux experienced by the tube during air cooling is the sum of both the natural convection and radiation components as shown in Equation 5-16. Details of the formulation for this equation are given in Appendix B.

$$q = 2.44\times10^{-8}T_w^4 + 0.328(0.6+1.94(T_w - 298)^{0.1667})^2 \times (T_w - 298) \qquad (5\text{-}16)$$

In equation 5-16, T_w is tube surface temperature (K), and q is the total heat flux transferred from tube to the surroundings by radiation and natural convection (W/m^2). In the above equation, the ambient temperature is assumed to be 298 K.

The calculated heat flux under air-cooling conditions is shown in Figure 5.13.

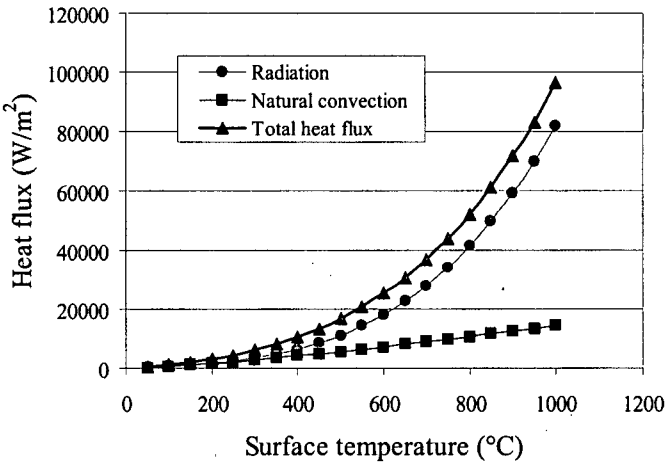

Figure 5.13 - Calculated heat flux associated with natural convection and radiation during air cooling of the AISI 52100 tube.

Figure 5.14 shows the measured temperature history in the tube during the air cool process. As can be seen in the figure an obvious recalesence occurs in the temperature-time profile around 700°C. This is consistent with the formation of pearlite at this temperature and the evolution of latent heat during the phase transformations.

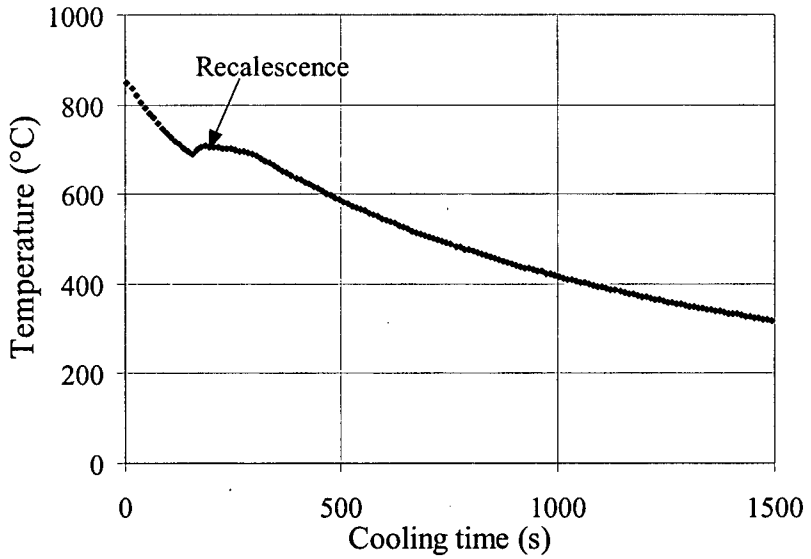

Figure 5.14 - Measured temperature profile during air cooling of AISI 52100 tube showing the recalescence due to latent heat.

The measured temperature-time data from the air-cooling test was put into the IHC model to predict to heat flux boundary condition. This was then compared to the heat flux calculated using the theoretical considerations and as can be seen in Figure 5.15 excellent agreement between the theoretical analysis and the calculated heat flux for the IHC model including phase transformations. In comparison, if the IHC model was used without accounting for the phase transformations and associated latent heat, the model

would predict a negative heat flux at 700°C where the phase transformation (PT) occurred.

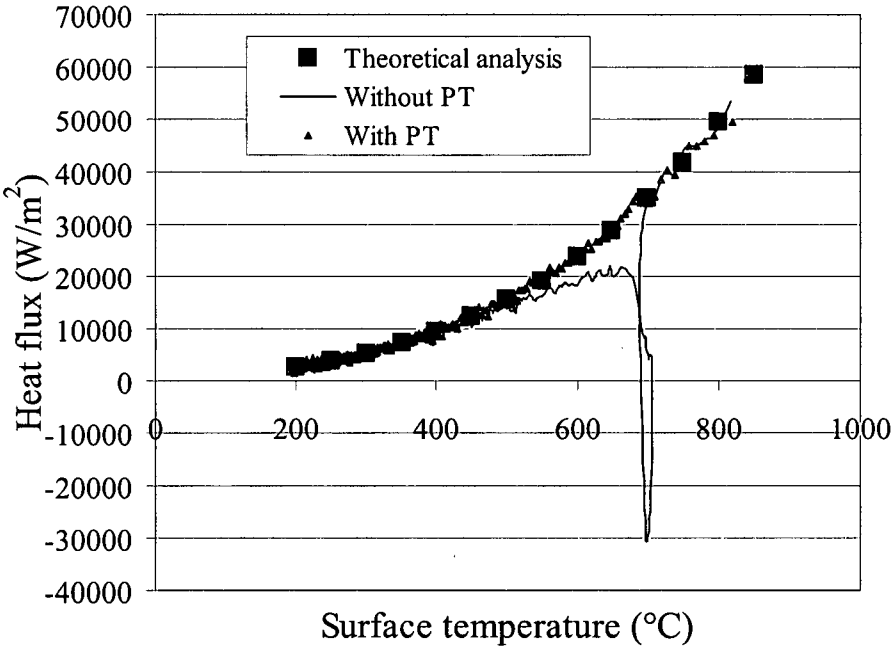

Figure 5.15 - Comparison of IHC model predictions both with and without phase transformations to the theoretical prediction of the heat flux as a function of temperature.

6.0 SENSITIVITY ANALYSIS OF THE IHC MODEL

6.1 Sensitivity analysis

When using an IHC model to predict the heat flux at the surface of the sample based on the thermal response in the sample at a known interior location, there are many parameters that can affect the accuracy of the calculated results. These parameters can be categorized into three groups, namely: (1) material thermal properties such as thermal conductivity, specific heat, density and latent heat evolution due to phase transformations, (2) calculation parameters within the model such as time step and (3) thermocouple location. In this section the effect of these factors will be discussed in detail. The geometry used for the sensitivity analysis is the same as shown in Figure 5.9 of chapter 5. The material properties used for the base case are shown in Table 6.1.

Table 6.1 – Material thermal physical properties used for the sensitivity analysis (T is the temperature in °C).

Thermal conductivity, k (W/m/K)	Specific Heat, C_p (J/kg/K)	Density, ρ (kg/m^3)
-0.027021×T+47.293	0.13459×T+498.03	-0.34516*T+7843.5

6.1.1 Effect of thermal conductivity

Thermal conductivity is a material property that quantifies the ability of a material to transfer heat from high temperature to low temperature. Generally, the higher the

thermal conductivity of a material, the easier it is for heat to flow through the material. If the thermal conductivity input into the IHC model is higher than the actual one, then the predicted heat flux will be higher than the real one. This can be deduced from the heat conduction equation shown below:

$$q = k\frac{dT}{dx} \cong k\frac{T_{t/c} - T_s}{d} \tag{6-1}$$

where q is the surface heat flux (W/m^2), k is thermal conductivity (W/m/K), $T_{t/c}$ is the measured thermocouple location temperature (K), T_s is surface temperature (K) and d is the distance from the thermocouple location to the surface of the sample (m).

Although the influence of thermal conductivity appears quite obvious, the associated influence of an incorrect value for the thermal conductivity on the predicted boiling curves is not as obvious and the influence of this will vary as the severity of the quench varies. To quantify this effect, the thermal conductivity was varied by +/-15% at each temperature location as shown in Figure 6.1.

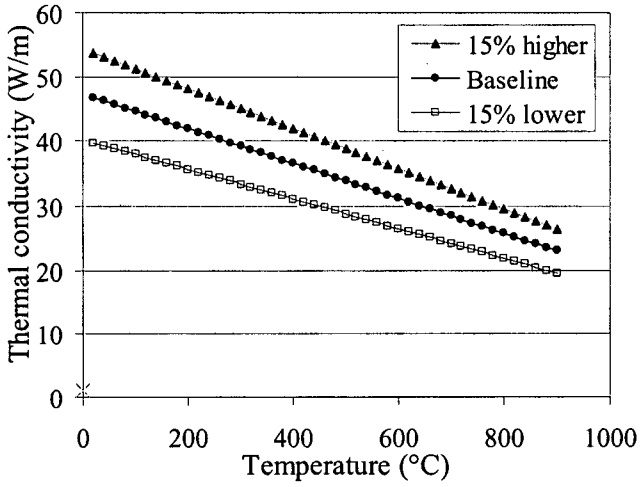

Figure 6.1 – Thermal conductivity values used in the sensitivity analysis.

Figure 6.2 shows the effect of thermal conductivity on the calculated boiling curves under different quench conditions ranging from an extremely severe quench where the peak heat flux $= 1.5\text{x}10^7$ W/m^2, to a more moderate water quench where the peak heat flux $= 2.5\text{x}10^6$ W/m^2. As can be seen, the effect of a correct value of thermal conductivity is not only displayed in the magnitude but also on the shape of boiling curve. A higher thermal conductivity will produce a higher heat flux and shift the boiling curve to the right, whereas, a lower thermal conductivity value will predict a lower heat flux, and shift the boiling curve to the left. This can be deduced from the heat conduction equation shown in Equation 6-1. After being rearranged, Equation 6-1 becomes:

$$T_s \cong T_{T/C} - \frac{qd}{k} \tag{6-2}$$

For a fixed surface heat flux and the measured temperature, a higher thermal conductivity will predict a higher surface temperature, and thus the boiling curve will be

shifted to the right. On the other hand, a lower thermal conductivity will predict a lower surface temperature, and thus the boiling curve will be shifted to the left.

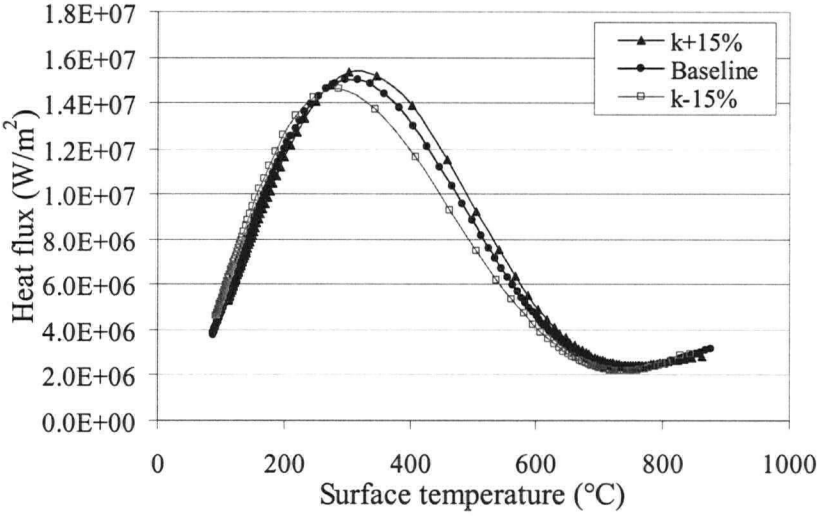

a) High

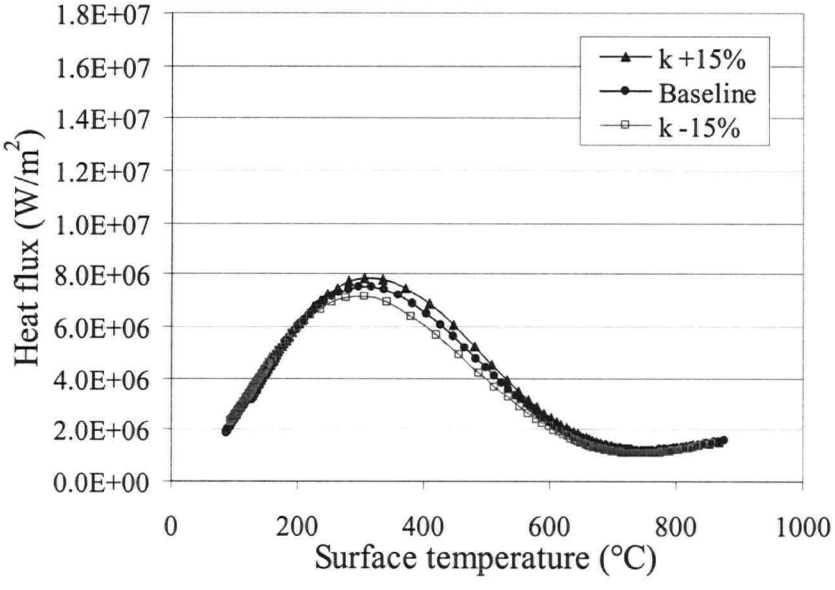

b) Medium

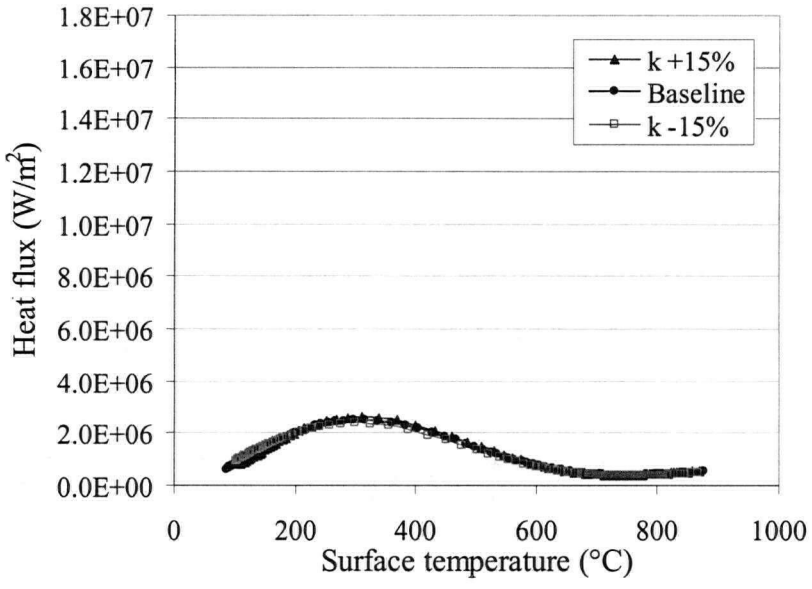

c) Low

Figure 6.2 – Effect of a +/-15% error in the thermal conductivity values of the material on the calculated boiling curves for three different heat flux conditions, namely a) high, b) medium and c) low.

6.1.2 Effect of volumetric specific heat

The volumetric specific heat ($C_p \times \rho$) represents the ability of a unit volume of material to give out heat energy as the material temperature drops. Therefore, the higher the volumetric specific heat for a material, the more heat the material will give out as the temperature goes down. If the value of the volumetric specific heat is higher than the actual one, more heat will be given out by the sample and hence, the calculated heat flux will be higher than the real one. Conversely, if a small volumetric specific heat is used in the IHC model calculations, it means the less heat can be given out by sample, and the

calculated heat flux will be lower than it should be. To quantify this effect, the volumetric specific heat was varied by +/-15% as shown in Figure 6.3 (because the variation in volumetric specific heat can be achieved by the change on either density or specific heat, i.e. $115\% \times (C_P \times \rho) = (115\% \times C_P) \times \rho = C_P \times (115\% \times \rho)$, only the variation of specific heat is shown in Figure 6.3).

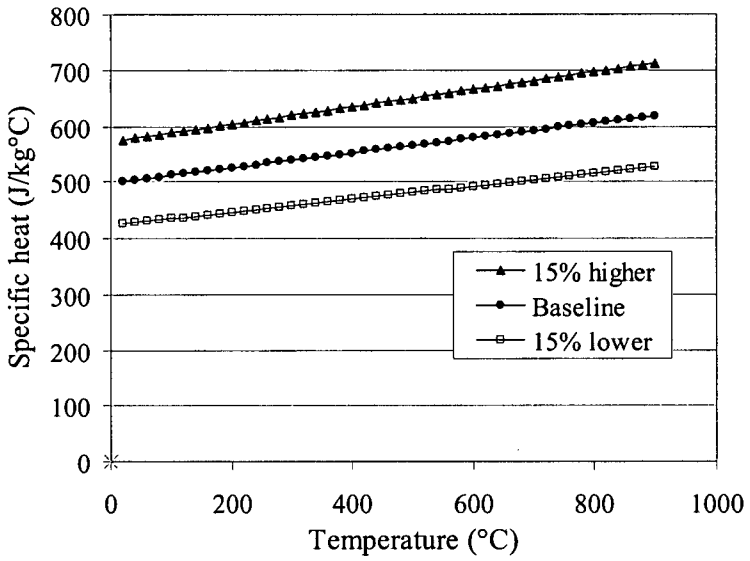

Figure 6.3 – Volumetric specific heat values used in the sensitivity analysis.

Figure 6.4 shows the effect of volumetric specific heat on the calculated boiling curves using the IHC model under different quench conditions ranging from an extremely severe quench where the peak heat flux $= 1.5 \times 10^7$ W/m^2 to a more moderate water quench where the peak heat flux $= 2.5 \times 10^6$ W/m^2.

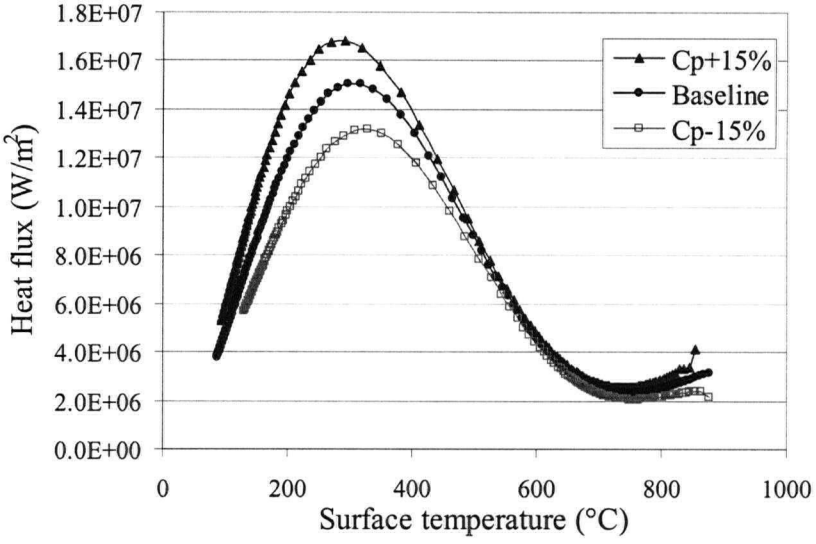

a) High

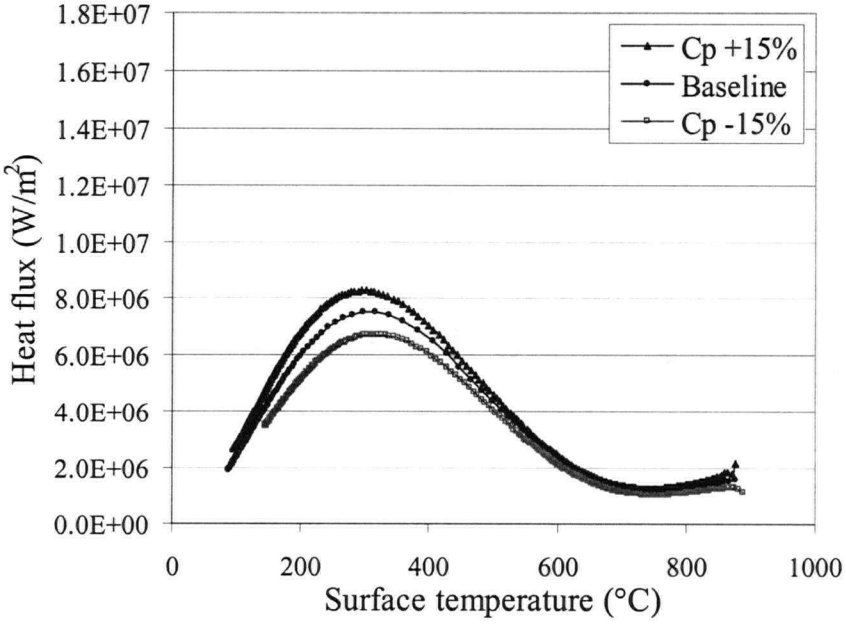

b) Medium

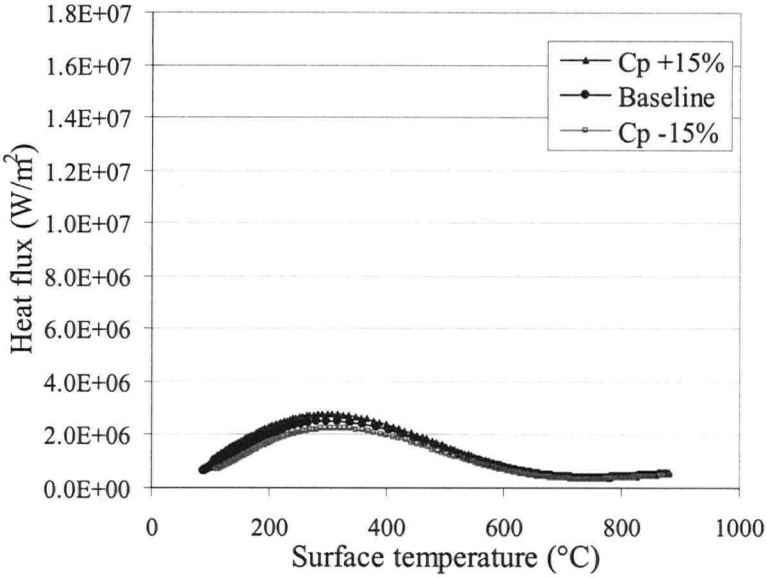

c) Low

Figure 6.4 – Effect of a +/-15% change in the volumetric specific heat values of the material on the calculated boiling curves for three different heat flux conditions, namely a) high, b) medium and c) low.

As shown in Figure 6.4, the volumetric specific heat has a significant effect on the calculated heat flux. When a higher volumetric specific heat is used in the IHC calculation, the calculated heat flux will be higher than the real one, whereas when a lower volumetric specific heat is used, the calculated heat flux will be lower than the real one.

6.1.3 Effect of time step

As pointed out previously, the time step used in the IHC calculation is a very important factor that affects the convergence of the model calculation. In the IHC model

a larger time step makes convergence of the calculated result easier. But a large time step can reduce the accuracy of the calculated heat flux. The following section will demonstrate the influence of time step on the model predictions.

During a water quench process, the heat flux exerted on the sample surface by the water can be represented by a continuous curve as shown in Figure 6.5 (applied). During the IHC model calculation, the heat flux curve is divided into many small sections that have a length equal to the time step used in the analysis. For each of these sections, only one heat flux value (the average heat flux over the time interval) can be estimated by the IHC model. Hence, the calculated heat flux curve is represented by a series of non-continuous dots that are the average calculated values for each small section. The accuracy of the calculated heat flux depends strongly on the length of the sections, i.e. the time step, as shown in Figure 6.5. When the time step used in the IHC calculation is large, the heat flux estimated by the model will deviate from the applied value at times where the heat flux changes dramatically. However, when the time step used in the IHC calculation is small enough, the model calculated heat flux will be very close to the applied one.

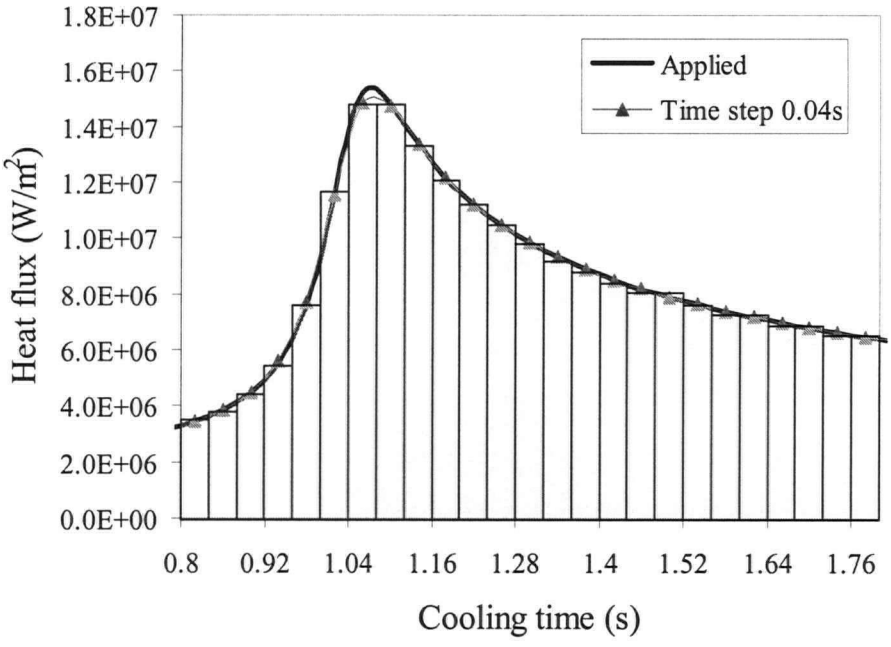

a) time step = 0.04s

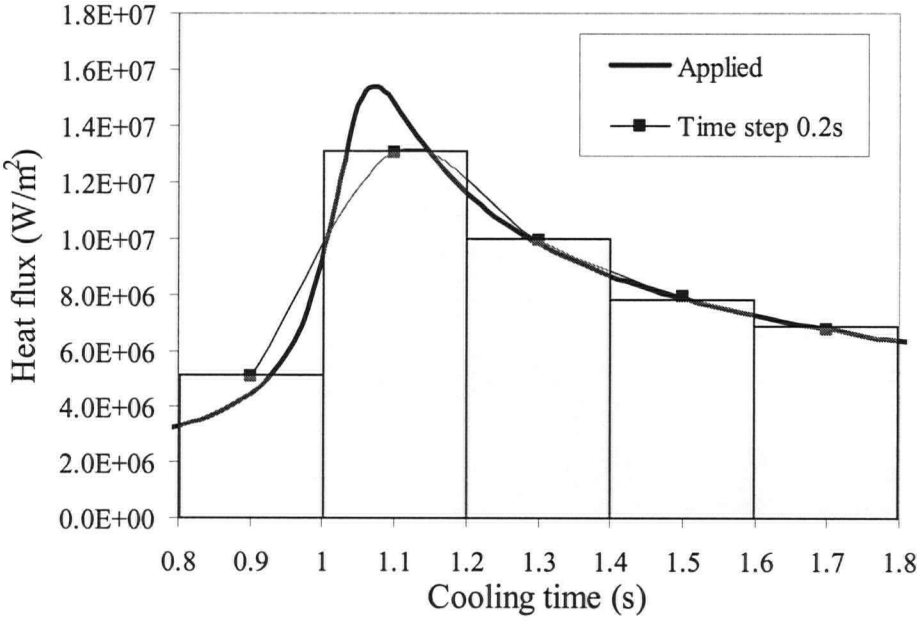

b) time step = 0.2s

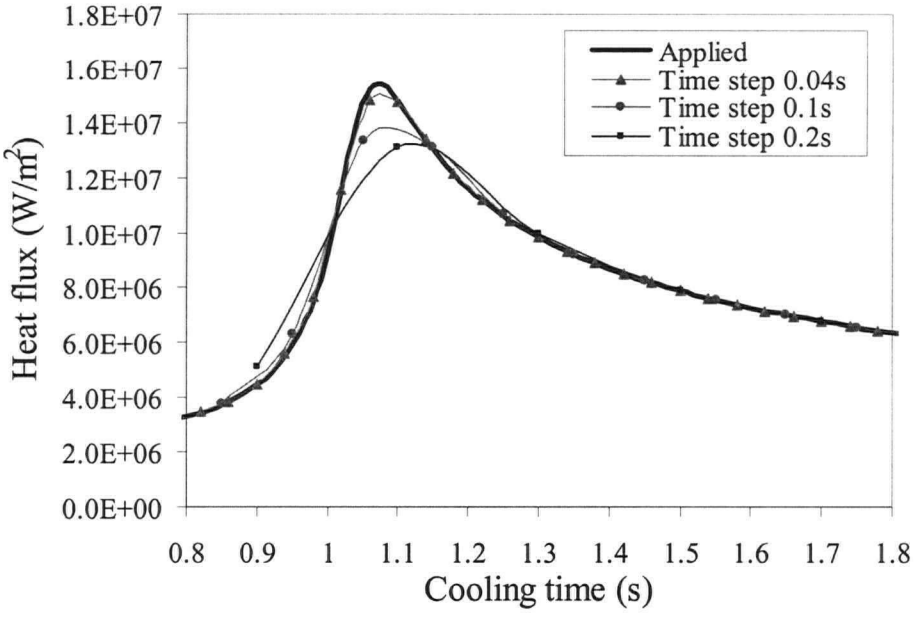

c) comparison to applied

Figure 6.5 - Effect of time step used in IHC calculation on the calculated heat flux showing: a) time step = 0.04s, b) time step = 0.2s and c) comparison to applied.

The inverse time step, $\Delta t(IHC)$, used in the IHC model has a very strong effect on the calculated boiling curve as shown in Figure 6.6. As the time step decreases, the calculated result is closer to the actual heat flux being applied to the boundary. However, as the time step is increased, the calculated boiling curve stretches out as compared to the applied one so that the peak is significantly lower than what was applied.

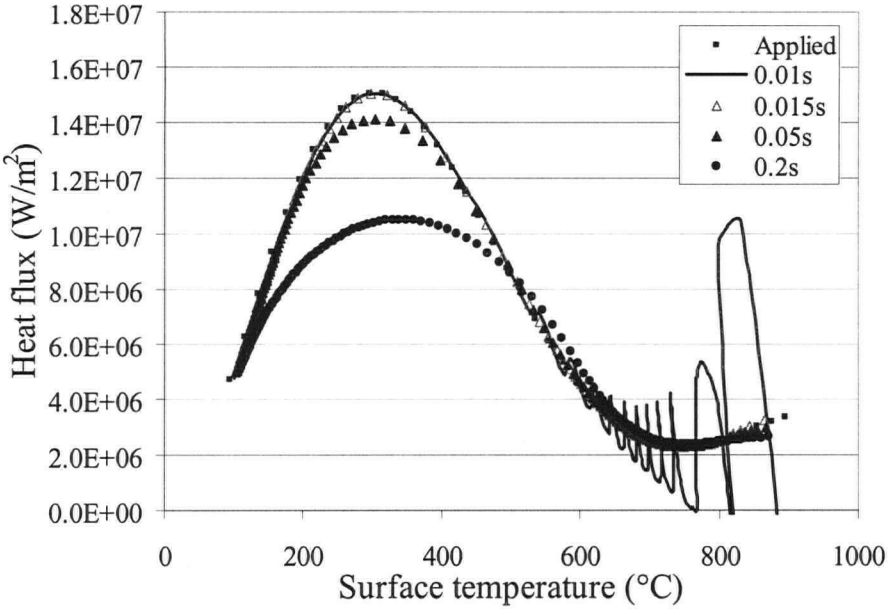

a) High

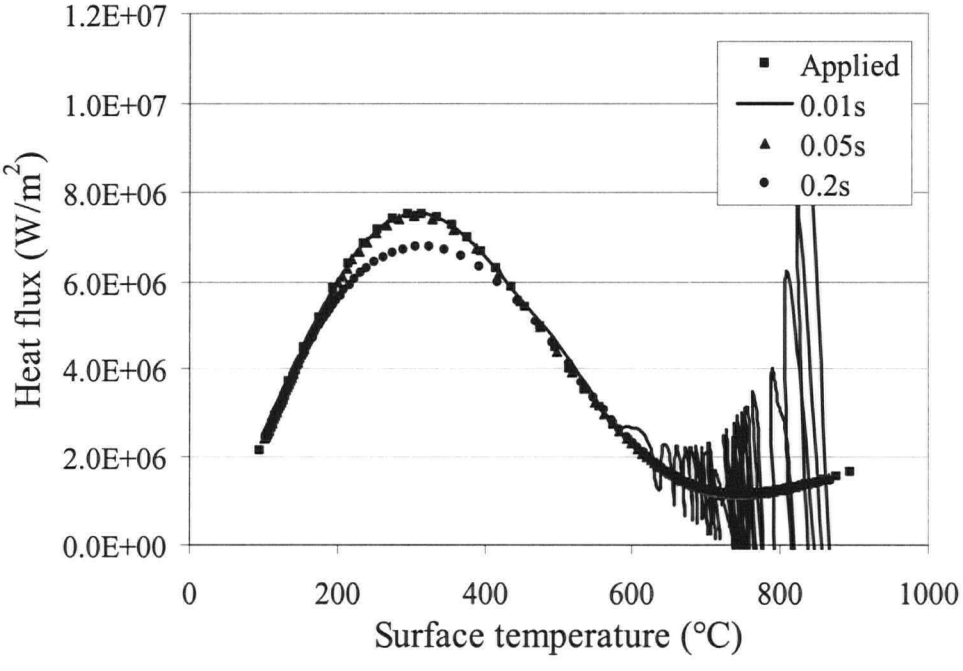

b) Medium

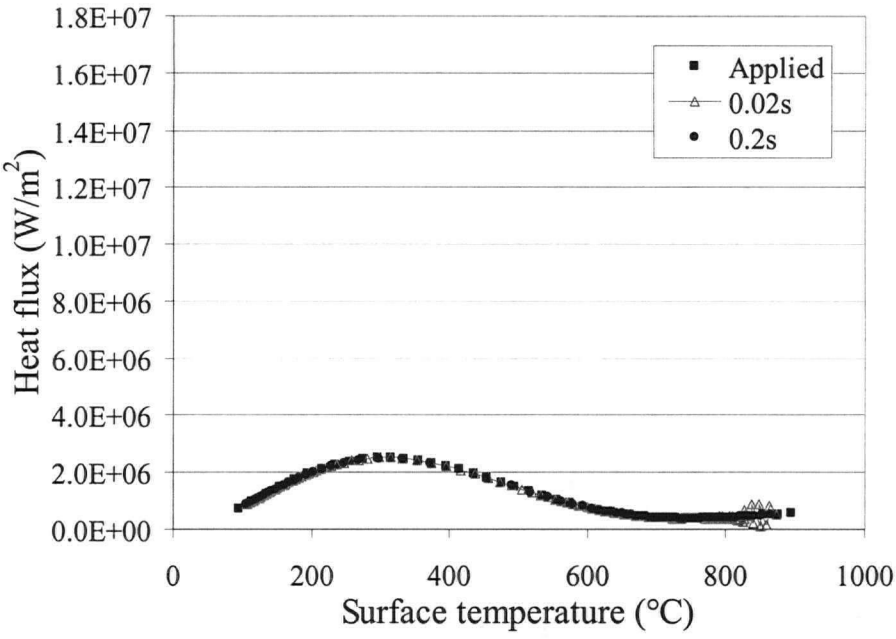

c) Low

Figure 6.6 - Effect of time step on the calculated boiling curve for three different heat flux conditions, namely, a) high, b) medium and c) low.

As stated previously, during the IHC model calculation, the estimated heat flux is an average heat flux during a time step, this is equivalent to the applied boiling curve being represented by bars that have the height of the average heat flux and the same width as the time step. As a result, when the time step is small, the assemblage of these small increments of heat flux will represent the applied boiling curve very well. However, at larger time steps, the calculated heat flux will be closer to the average of the applied heat flux and it will cause the calculated boiling curve to stretch out. As can be seen in Figure 6.6, this sensitivity to time step increases dramatically as the severity of the quench increases. In order to accurately predict a boiling curve, a sensitivity analysis to the time step should be done and the time step used in the IHC model should be small

enough to ensure that accurate results are obtained. On the other hand, if too small a time step is used in the IHC model, it will cause the calculations to diverge. The selection of the time step used in the IHC model calculations must take these two criteria into consideration; a small time step to ensure accurate results but not too small so that the calculation results diverge. The selection of time step depends not only on the magnitude of the heat flux but also on thermocouple location and material thermal properties. Determination of the "best" time step to use for each condition was done by trial and error in this study.

As shown in Figure 6.6, under high heat flux conditions, a time step of ~0.015s produces accurate results. However, when the time step used in the IHC model is smaller than 0.01s, the calculations from the IHC model start to diverge. As the heat flux is lowered the time step required to produce accurate results as compared to the applied curve increases.

The temperature-time data used to develop this sensitivity analysis was based on model predictions hence there was no noise in the data. In reality, the measured data will contain some noise and this means that the time step required to achieve a convergent solution will be larger.

6.1.4 Effect of the accuracy of thermocouple position

During a quench test, the thermocouple is embedded in the sample to measure the temperature history. Due to the damping and lagging of the measured sample inner temperature, the thermocouple should be located as close to the quenched surface as possible (for our tests, the distance of the thermocouple from the quenched surface is

around 1.0 mm). Accurate measurement of the thermocouple distance from the surface is very important, as a very small measurement error can produce a large error in the calculated heat flux, especially under severe quench conditions. When the measured thermocouple distance from the quenched surface is smaller than the actual one, the calculated heat flux will be lower than the real heat flux. However, if the measured distance is larger than the real distance, the calculated heat flux will be higher than the real heat flux.

Determination of the thermocouple position relative to the quench surface can be difficult, especially if the test sample has a very rough surface or a very complicated shape. In some cases [18], the surface roughness can be around 1.0 mm, and it is very difficult to determine the thermocouple position accurately. Under such conditions, it is better to place the thermocouple a little further away from the quenched surface, and then the effect of surface morphology on the measured temperature will be reduced.

The effect of thermocouple position on the calculated boiling curves is shown in Figure 6.7. As can be seen under high quench intensities, the accuracy of thermocouple position during the quench is very important; small errors in the thermocouple position can produce large errors in the calculated boiling curve. Under low quench intensities, there is nearly no effect on the calculated boiling curve even when there is 0.2 mm error in the measured thermocouple position.

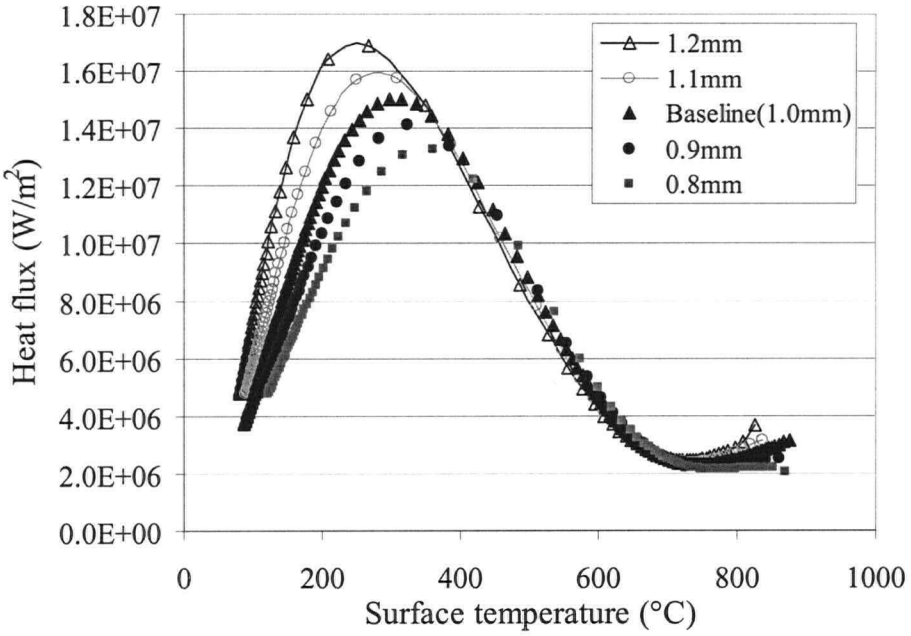

a) High

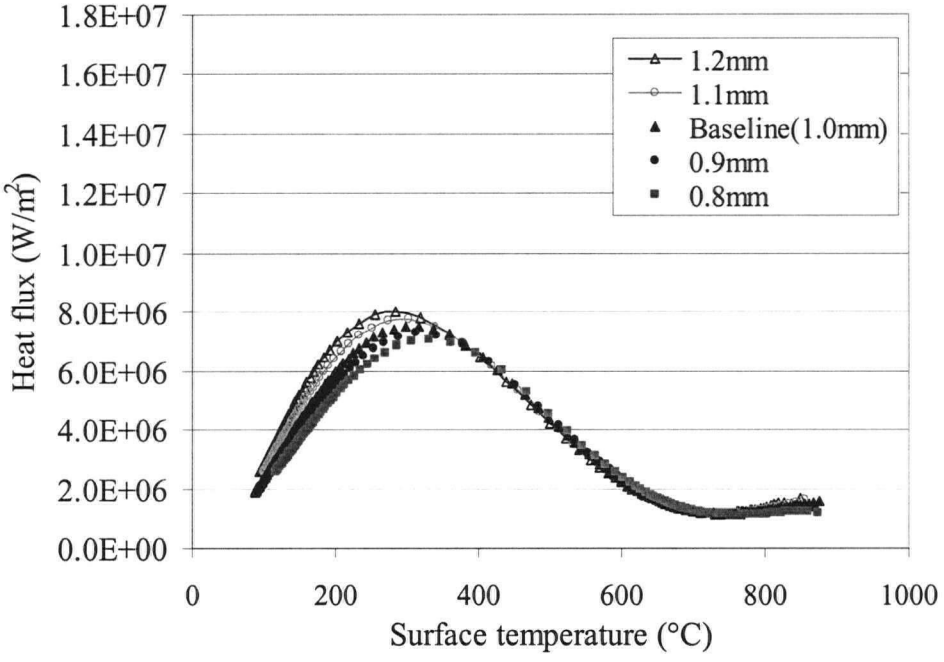

b) Medium

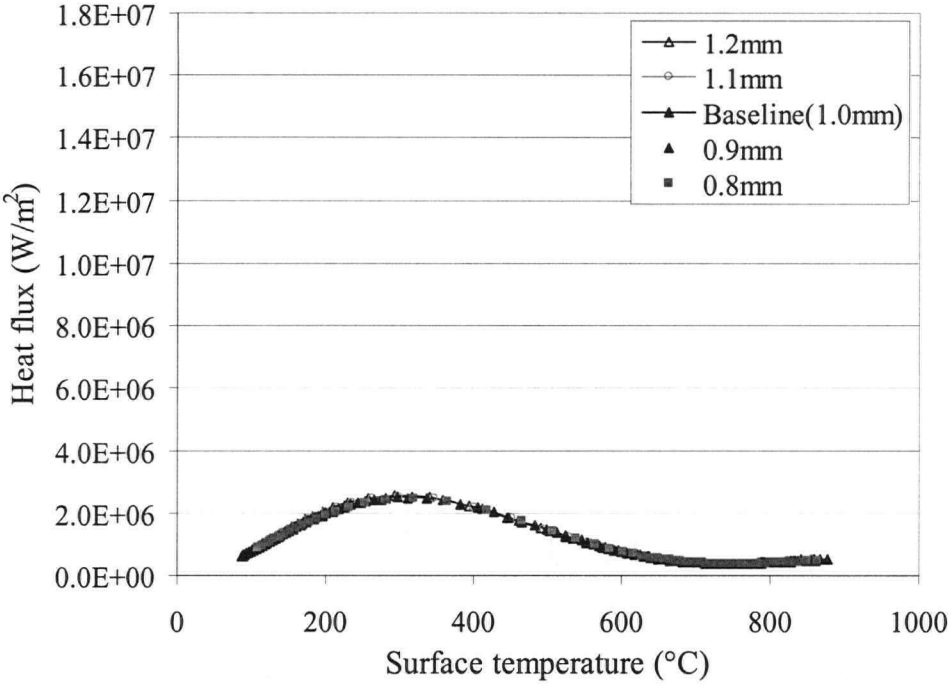

c) Low

Figure 6.7 - Effect of T/C position on the calculated boiling curve for three different heat flux conditions, namely a) high, b) medium and c) low.

6.1.5 Effect of latent heat on the calculated boiling curve during the quench process

Figure 6.8 shows the effect of latent heat on the calculated boiling curve under two different quench processes. This analysis was done using a hypothesized heat flux on a sample surface to calculate the temperature distribution in the sample using the thermal conduction model that includes the latent heat associated with phase transformation. This calculated temperature profile in the sample was then put into the IHC model to calculate the surface heat flux. For the analysis, the calculation domain is the same as stated in section 5.4.3 of chapter 5, with the two ends as well as the inner surface of the tube

assumed to have an adiabatic boundary condition. As can be seen in Figure 6.8, under a high heat flux condition, the calculated heat fluxes (both without latent heat and with latent heat) will be the same as the applied heat flux when the temperature is higher than 250°C. This is due to the fact that the transformation of austensite to pearlite and bainite is suppressed. From a heat evolution point of view, the only noticeable phase transformation that occurs is austensite to martensite. This causes the calculated heat flux to deviate from the applied one when the temperature is below 250°C, in the model which does not take phase transformations into account.

As can also be seen in Figure 6.8, when the applied heat flux is lower, the phase transformations can start to occur at a higher temperature. This can then have a more noticeable impact on the predicted boiling curve if the IHC model does not take the phase transformation kinetics and associated latent heat into consideration.

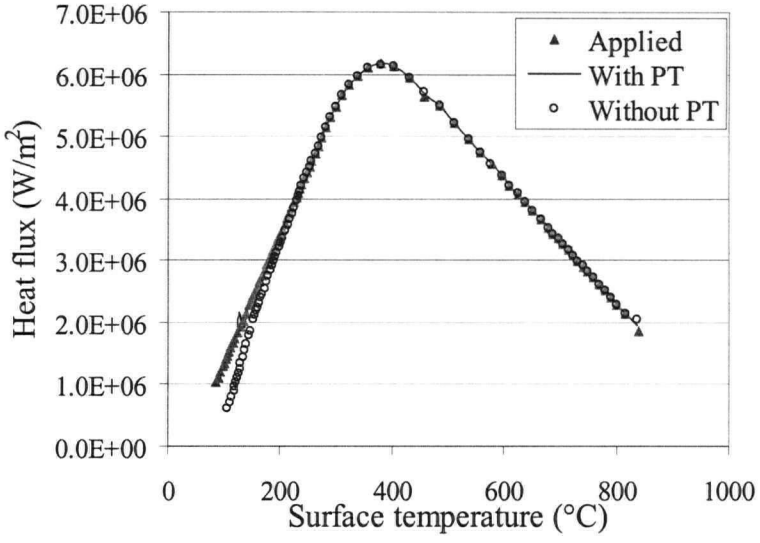

a) high heat flux

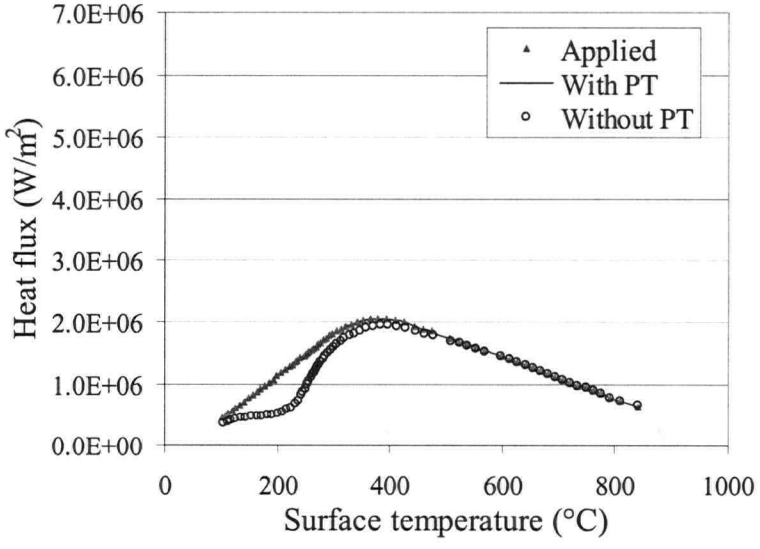

b) medium heat flux

Figure 6.8 – Comparison of calculated boiling curve to the applied one when phase transformations are not taken into account for: a) a high heat flux and b) a medium heat flux.

7.0 TEMPERATURE MEASUREMENT DURING QUENCHING

A key component to accurate quantification of the boiling water heat transfer during a water quench operation is measurement of the thermal history experienced at a known location in a sample. Although not anticipated directly at the start of the research, an important component of this research has been to analyze and investigate experimental methods to accurately measure the thermal history in the sample during a water quench operation including using both surface as well as sub-surface thermocouples.

The calculation of the IHC model is based on the temperature obtained from a quench test, in which the measured temperature is assumed to be accurate. Invariably, the measured temperature has some error associated with it due to the method used to install the thermocouple as well as the inherent thermocouple characteristics. As a result, the calculated boiling curves can contain some inaccuracies if the measured temperature history that is used as input to the model is incorrect. This problem becomes exaggerated under very high heat flux conditions, typical of a water quench, where a slight error in the temperature history measurement can lead to a large error in the calculated boiling curve. A confounding problem is that under these very large heat flux conditions, the ability to measure the temperature history accurately is quite difficult. In this section, the error associated with various temperature measurement techniques that can be used during quench tests are evaluated and methods to correct for these errors in the IHC model are determined.

The methods used to measure the temperature during a quench test can be divided into two groups according to the location where the measurement is being made: these include: surface temperatures, which are obtained at the quenched sample surface, as well as sub-surface temperatures, which are acquired at an inner location in the tested sample.

Generally, when using the IHC method, thermal histories measured using sub-surface thermocouples can produce some inaccuracies in the heat flux predictions as well as diverging solutions, as the measurement made by the thermocouple can be slightly delayed due to heat conduction in the sample from the quenched surface to the tip of the interior thermocouple junction. One important factor, which affects the accuracy of the measured temperature when using a thermocouple, is the thermal contact resistance between the thermocouple and sample. The effect of this factor can be quantified by calculating the time constant for the thermocouple, τ^+, as discussed in the literature review in the section on thermocouple dynamics. As the time constant of the thermocouple increases, the measured temperature lags progressively behind the true temperature and results in increasing error in the estimated surface temperature. So, a method must be found to determine the time constant of the thermocouple and either minimize or eliminate it, if possible. In the quench tests, all the sub-surface thermocouples were welded to the sample at the bottom of the T/C hole, so the thermal contact resistance between the thermocouple and the sample is completely eliminated. Another drawback of using a sub-surface thermocouple is that it produces a lagged and damped temperature response as shown in Appendix D due to the thermal conduction between the thermocouple tip and boundary surface. Hence, if possible, it is preferable to be able to measure the thermal response at the surface of the sample and use it as input to

the IHC model. The disadvantage of a surface temperature is that it is a very localized measurement that can be influenced by many local surface characteristics such as surface morphology as well as the formation and detachment of water bubbles during the water quench. More importantly, the installation of a surface thermocouple can change the surface fluid flow pattern and alter the local nature of the heat transfer. In the following sections, both sub-surface and surface temperature measurement techniques will be discussed as well as analyzed to determine the estimated errors in temperature measurement caused by these two methods.

7.1 Sub-surface temperature measurement

7.1.1 Thermocouple installation

When installing thermocouples into an interior location in the sample, the thermocouple itself can have an effect on the surrounding thermal field, as the thermocouple material properties are usually quite different from those of the sample being tested. As shown in Figure 7.1, a typical thermocouple will include the thermocouple wires as well as some insulation (typically MgO) to ensure that the two wires remain separated as well as insulating them from the thermocouple sheathing.

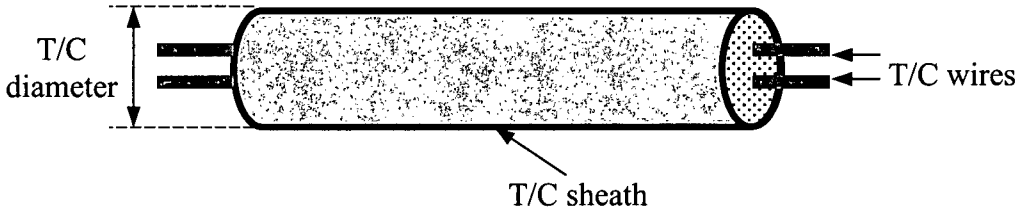

a) outward appearance of thermocouple.

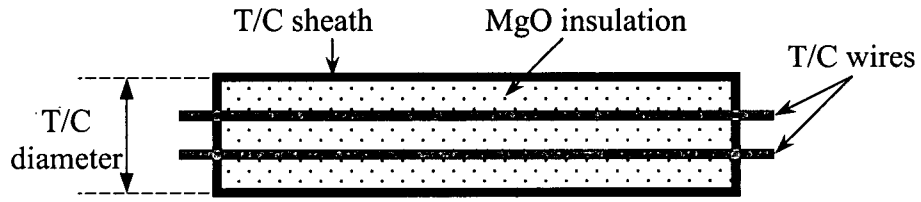

b) detailed x-sectional view inside a thermocouple.

Figure 7.1 - Sketch of thermocouple showing: a) outward appearance of thermocouple as well as b) detailed x-sectional view inside a thermocouple.

During a quench test, the sub-surface thermocouple is usually installed into the sample from the back as close as possible to the quenched surface, so that a fast response to changes in the surface heat flux can be obtained. Figure 7.2 shows a schematic of a typical thermocouple installed from the back surface of a quenched sample. During the quench test, the temperature in the sample will drop due to the heat transfer from the sample to the water. However, due to the thermocouple hole and MgO insulation, heat cannot transfer from the back of the sample to the tip of the thermocouple as quickly as it does in other parts of the sample. Hence, the measured temperature will be lower than the "true" temperature experienced by the rest of the sample during the quench test.

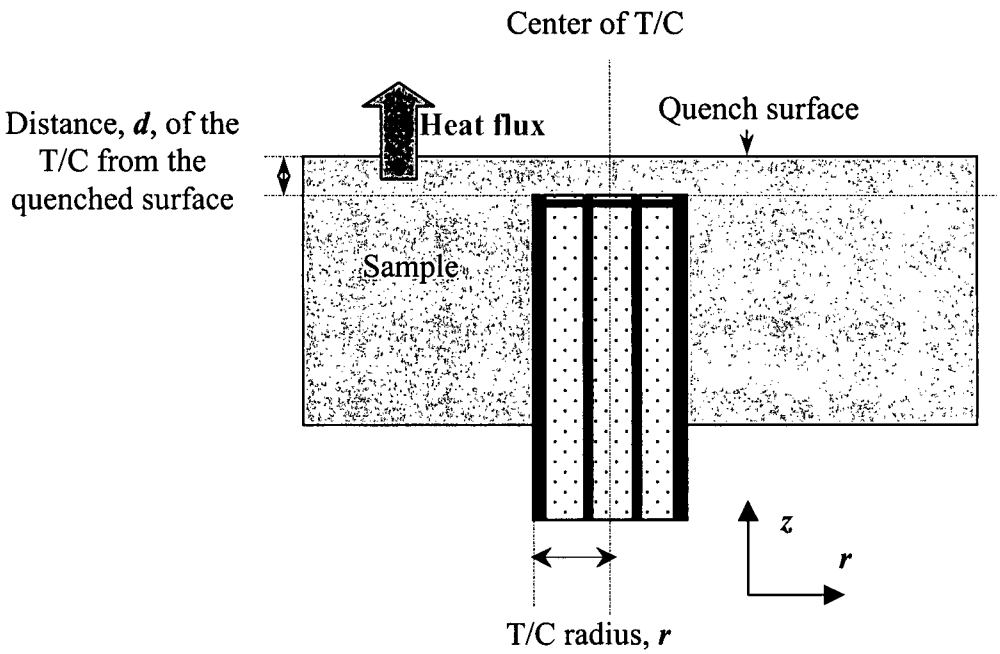

Figure 7.2 - Schematic of sub-surface thermocouple installation.

7.1.2 Effect of thermocouple hole on the sample thermal field

In order to analyze the potential effect of the thermocouple installation on the sample thermal field during a quench test, an assumed heat flux was applied to the quenched surface and the 2-D FEM heat conduction model was used to calculate the thermal field in the quenched sample. To quantify the influence of the thermocouple installation on the thermal field, the material properties of the MgO insulation were taken into account. This ensured that the calculated temperature would be similar to that measured during a quench test with a sub-surface thermocouple. To examine the subsequent influence on the boiling curves, the temperature-time history predicted by the FEM conduction model was then used in the IHC model to estimate the applied heat flux on the quenched surface. These values could then be compared to what had originally

been used in the FEM conduction model and an estimate of the error quantified. For the simulation, the thermocouple was assumed to be 1.5 mm from the quenched surface, and its diameter was 1.0 mm. The thermal properties used for the test sample and MgO insulation are shown in Table 7.1 and 7.2 respectively.

Table 7.1 -Material properties used for the AISI 316 stainless steel in the simulation.

Density ρ, kg/m^3	Specific heat *Cp*, J/kg K	Conductivity *k*, W/m K	
		T≤780°C	T>780°C
7865	460	10.717+0.014955×T	12.076+0.013273×T

Table 7.2 - Material properties used for the MgO in the simulation.

Density ρ, kg/m^3	Specific heat *Cp*, J/kg K	Conductivity *k*, W/m K
2800	950	3.5

The domain used for the FE simulation is shown in Figure 7.3. As can be seen, a section of the sample around the thermocouple was included in the analysis with dimensions of r = 5 mm and a thickness, z, of 11 mm. For the simulation, a 2-D axisymmetric analysis was performed around the centerline of the thermocouple with boundary and initial conditions as follows:

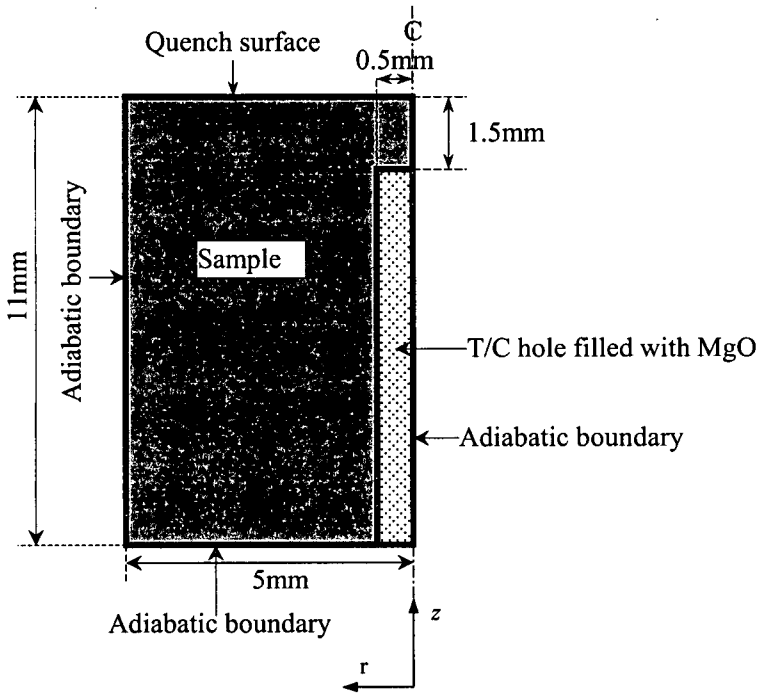

Figure 7.3 – Schematic of the domain used for the sub-surface thermocouple analysis.

At the left side of the domain, r = 5 mm, at all z positions (i.e., z = 0 to 11 mm) an adiabatic condition exists

$$-k\frac{\partial T}{\partial r}\bigg|_{r=5mm} = 0 \tag{7-1}$$

1) At the bottom of the domain, z = 0 mm, at all r positions (i.e., r = 0 to 5 mm) an adiabatic condition exists

$$-k\frac{\partial T}{\partial z}\bigg|_{z=0} = 0 \tag{7-2}$$

2) At the centerline of the sample, r = 0 mm an adiabatic condition exists

$$-k\left.\frac{\partial T}{\partial r}\right|_{r=0} = 0 \tag{7-3}$$

3) At the quenched surface, $z = 11$ mm at all r positions (i.e., $r = 0$ to 5 mm)

$$-k\left.\frac{\partial T}{\partial z}\right|_{z=11} = h(T - T_c) = q \tag{7-4}$$

where q varies as a function of sample surface temperature as shown in Figure 7.4.

5) The initial condition is given by:

$$T(r,z)\big|_{t=0} = T_i(r,z) = 1050\ ^\circ\text{C} \tag{7-5}$$

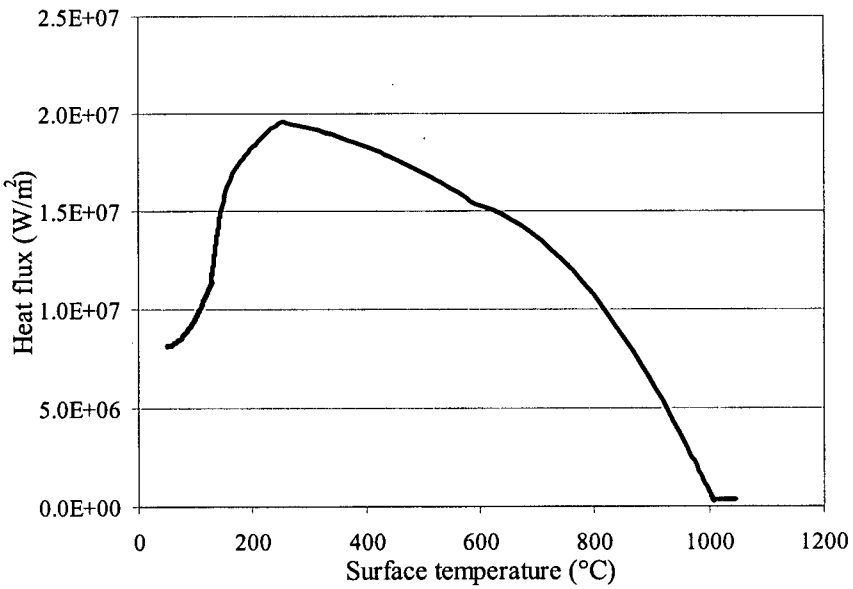

Figure 7.4 – Applied heat flux used in the simulation to calculate the influence of the T/C hole on the thermal field in the sample.

The calculated thermal history in the sample at a position at the center of the T/C (i.e., r = 0 mm, z = 9.5 mm) and 0.5 mm, 1 mm and 5 mm away from it (i.e., r = 0.5, 1, and 5 mm, z = 9.5 mm) is shown in Figure 7.5. As can be seen, at the center of the T/C the thermal history is considerably different than a position away from the T/C. When the thermocouple is inserted from the back surface of the sample, the temperature at the center of the thermocouple drops more quickly than the temperature in other parts of the sample due to the lower value of the thermal conductivity of the MgO as compared to the steel. As can be seen, the difference between the temperatures measured at the T/C tip and other parts of the sample can be over 100°C. Figure 7.6 shows how the thermal history in the sample would be perturbed spatially due to the presence of the T/C in the sample. As can be seen the effect of the thermocouple on the thermal field in the sample will diminish as the distance, r, away from the thermocouple increases. In this case, when the distance away from the T/C is greater than ~4 mm, the thermocouple installation appears to have no influence on the sample thermal field.

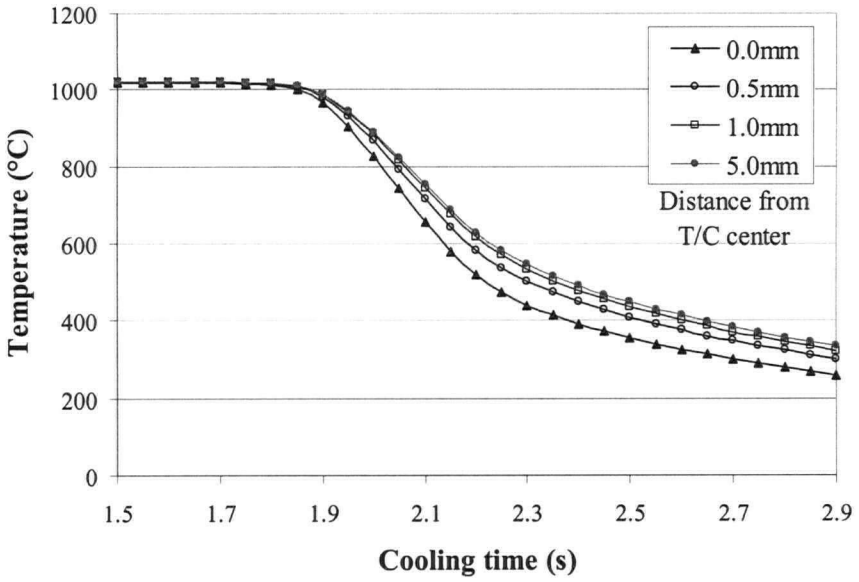

Figure 7.5 - Calculated thermal history in the quenched sample at positions, r, away from the centerline of the thermocouple (z = 9.5 mm).

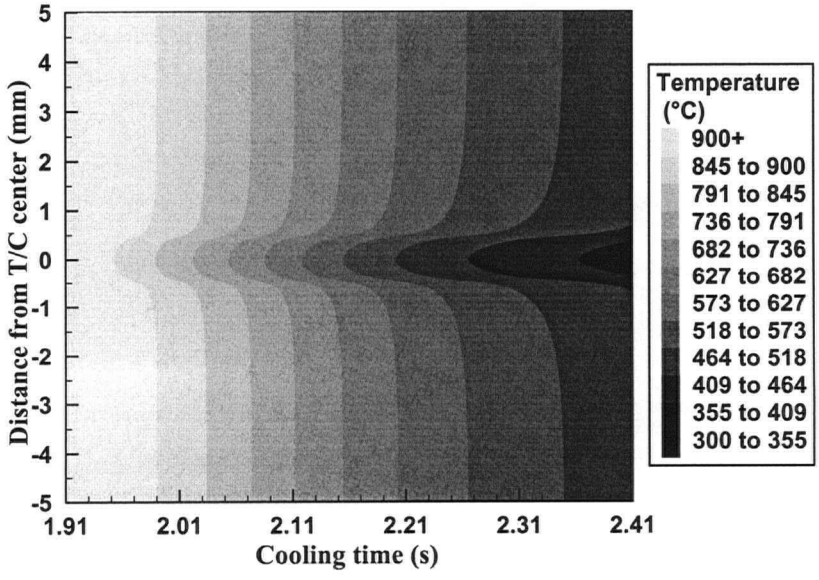

Figure 7.6 - Calculated perturbation in sample thermal history due to the presence of the thermocouple.

However, the effect of the sub-surface thermocouple on the sample thermal field in the *z*-direction is only localized around the T/C tip and the hole. Hence, it has nearly no effect on the surface temperature of the sample directly above it (z = 11 mm). This result can be seen in Figure 7.7, which shows the calculated surface temperature histories on the quenched surface at different r locations from the tip of the T/C, namely r = 0.0 mm (at the center of the T/C), 3.0 mm and 5.0 mm from T/C location. As can be seen, the installation of the sub-surface T/C has no effect on the sample surface temperature distribution.

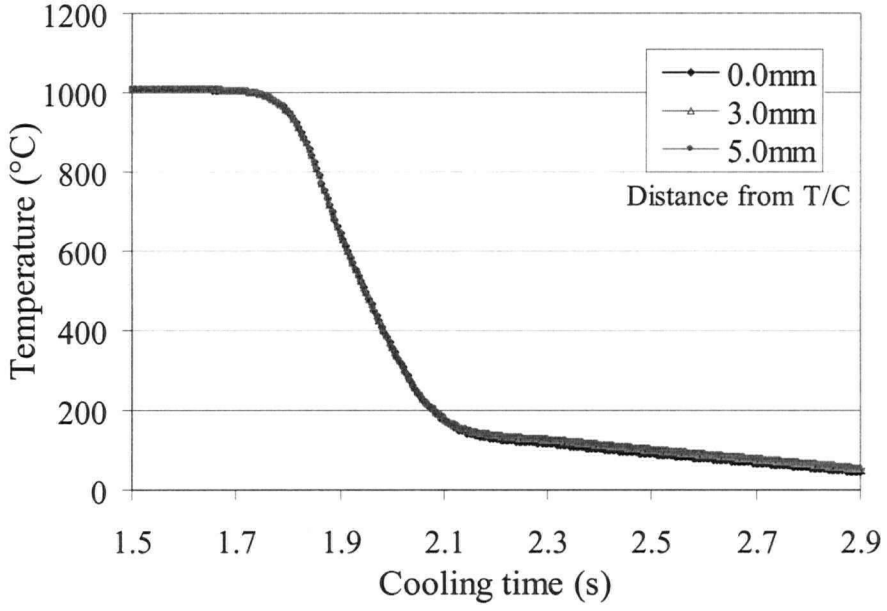

Figure 7.7 - Calculated thermal history at the surface of the quenched sample at positions, r, away from the centerline of the thermocouple (z = 11.0 mm).

If the thermal histories calculated at the T/C location were inputed into the IHC model without taking into account or correcting for the thermocouple installation, then the calculated boiling curve would be significantly higher than the actual one. Figure 7.8

shows the calculated boiling curves as compared to the applied ones for the analysis outlined above, if the thermocouple hole was not taken into account. For the calculation, the domain used is the same as shown in Figure 7.3 except the T/C hole is not included in the analysis and the entire domain is considered to be steel. The boundary conditions and initial condition are the same as used in the previous analysis and are shown in Equation 7.1 to Equation 7.5. As can be seen in Figure 7.8, the calculated boiling curve is significantly higher than the applied one.

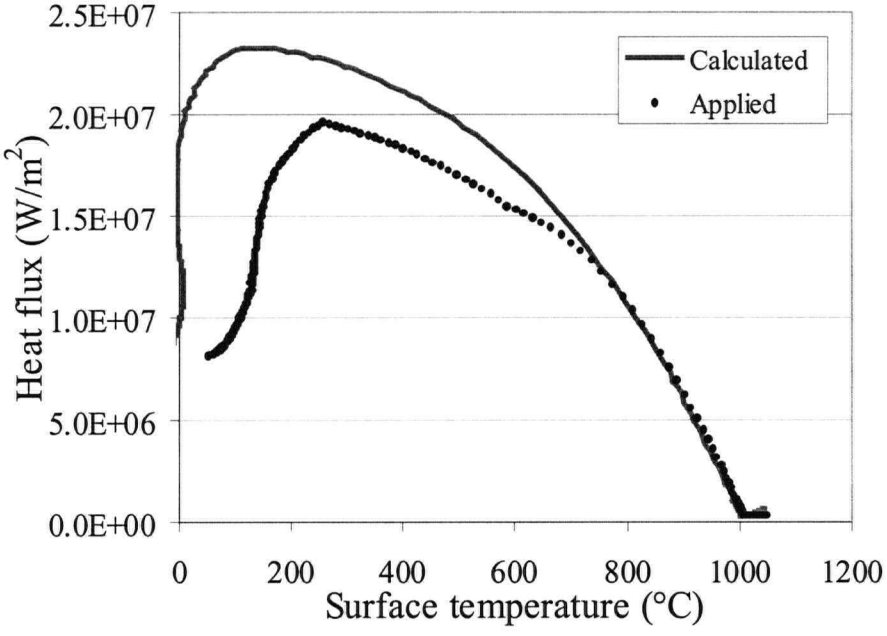

Figure 7.8 – Comparison between applied and calculated heat flux when the T/C hole is not included in the analysis.

As can be seen in Figure 7.5, under the heat flux conditions applied, when the thermocouple is inserted from the back of the sample, the thermocouple measures a lower temperature than the "true" one, so the calculated heat flux from this temperature will be

higher than the applied one, and the shape of the calculated heat flux curve will shift upwards to higher heat fluxes as well as to the left. The error in the predicted peak heat flux is ~20%, hence the effect of the thermocouple hole on the temperature field in the sample must be taken into consideration.

7.1.3 Experimental verification of analysis

In order to verify the approach used to account for the T/C installation on the measured temperature history in the sample at the T/C location, an experiment was run using the AISI 52100 tube material with T/C's instrumented at both 90° and 45° from the back of the sample as shown in Figure 7.9. The T/C's were spatially located close to the center of the nozzle such that the water flow conditions experienced at the surface of the tube would the same in both thermocouple locations. It is expected that the thermocouple installed at an angle of 45° to the quenched surface should produce temperature-time data that more closely reflects what is experienced by the sample.

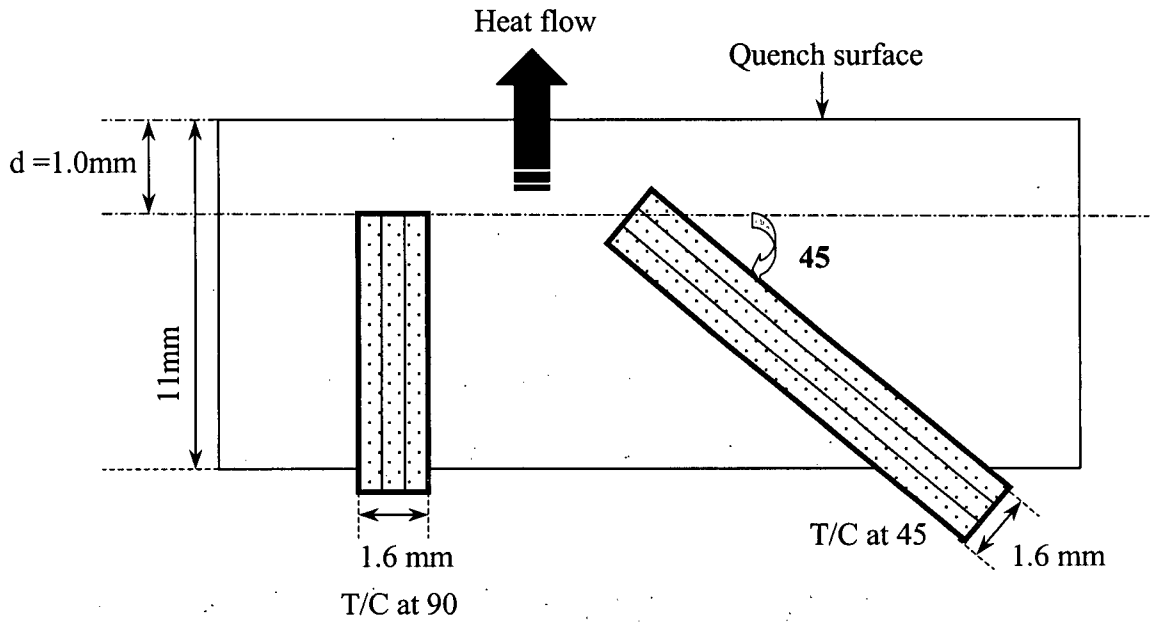

Figure 7.9 – Cross-sectional schematic of an AISI 52100 tube from the ID to the OD showing thermocouple installation at both 45 and 90° to the quenched surface from the back of the sample (d = 1.0 mm).

A water quench experiment was run under the conditions outlined in Table 7.3 and the measured temperature data from the two T/C's were put into the IHC model to estimate the surface heat flux during the quenching test.

Table 7.3 – Quench test conditions used for AISI 52100 tube to assess differences between T/C's at 45° and 90°.

Water flow rate (l/s)	Tube start temperature (°C)	Tube geometry (mm)	T/C hole diameter (mm)
1.27	850	ID = 58, OD = 80	1.6

The measured temperature-time data from the two T/Cs are shown in Figure 7.10. As can be seen the thermal history measured by the T/C at 45° is quite different than that measured by the T/C at 90°.

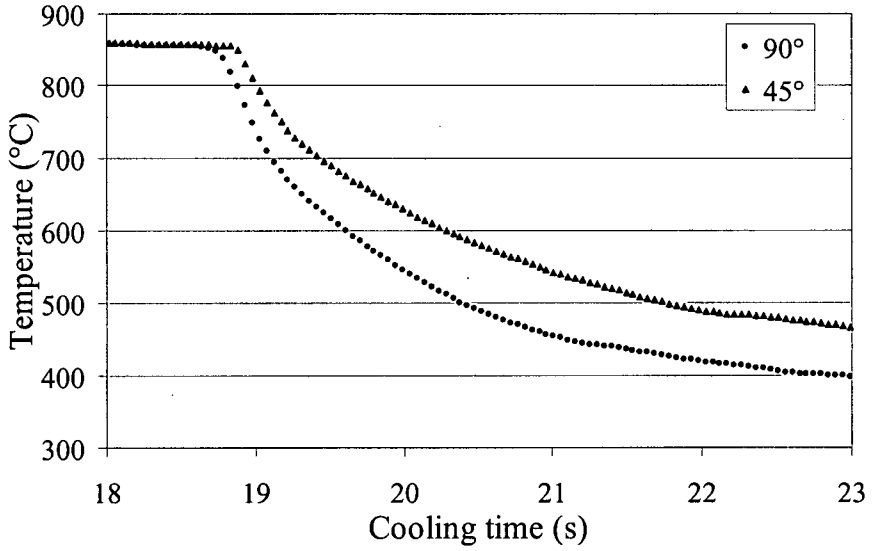

Figure 7.10 – Measured thermal history in the tube during a water quench test for the T/C at 90° and 45°.

From the above measurements, it is very clear that the installation of thermocouple from the back of the sample at 90° impedes the heat supply to the thermocouple tip, and hence accelerates the temperature drop measured by the thermocouple during the quench process.

Figure 7.11 shows the calculated boiling curves if this data is then inputted into the IHC model. As can be seen, if the T/C insulation is not taken into account for the T/C installed at 90° to the quenched surface, then the predicted boiling curves are

significantly higher than they should be. When the T/C insulation is taken into account the results between the T/C at 45° and 90° are more similar.

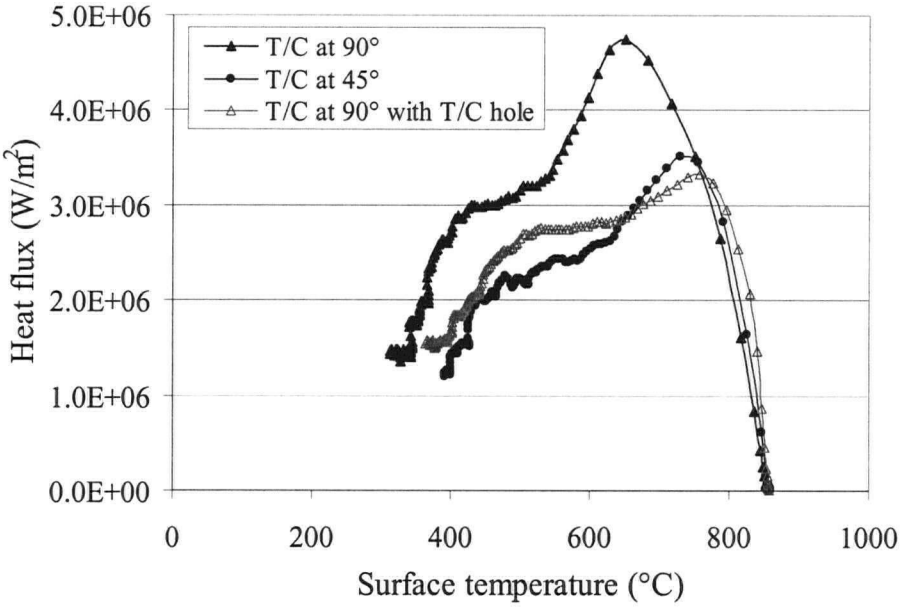

Figure 7.11 – Comparison of the calculated boiling curves using measured data from T/C's oriented at 90° and 45°, as well as the influence on the predicted curves when the T/C hole is accounted for with the measured data from the 90° T/C.

This provides some experimental verification that the method used to account for the T/C hole in the IHC model is correct. There will be some error in these calculations as the tube used during the test had a curved surface however to simplify the analysis it was considered to be flat on top.

7.1.4 Effect of other factors on need to include T/C hole in IHC analysis

The amount of perturbation on thermal field experienced by the sample during a quench operation due to the presence of the T/C will be influenced by a number of factors

including: the properties of the thermocouple being installed (e.g., diameter and distance from the quenched surface), the severity of the quench at the surface of the sample as well as the thermal conductivity of the material being quenched. This section will explore some of these factors and quantify the influence each of them can have on the perturbation of the sample thermal field around the T/C. For all of the analysis done, the domain and boundary conditions described in section 7.1.2 were used unless otherwise indicated.

Thermocouple installation – The influence of the T/C diameter and distance from the quenched surface were investigated to quantify how much of an influence they would have on the calculated heat flux or boiling curve on the sample surface during a quench operation.

To determine the influence of the thermocouple diameter on the calculated heat flux, two diameters were compared namely: 1 mm versus 0.6 mm. As can be seen in Figure 7.12, as the T/C diameter decreases, the effect of the thermocouple on the sample thermal field will be reduced; the calculated heat flux will be closer to the applied one. So, the smaller the thermocouple the less will be the disturbance on the sample thermal field.

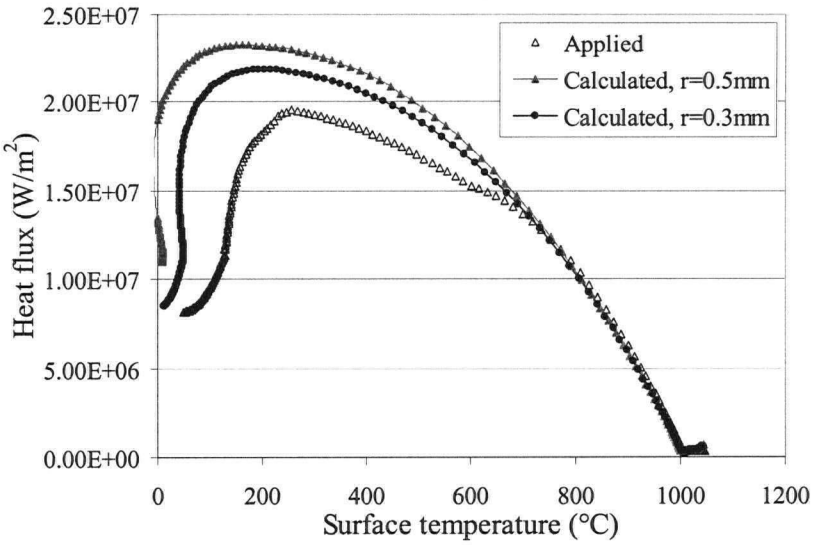

Figure 7.12 - Effect of thermocouple diameter on the calculated heat flux when the T/C hole is not taken into account in the analysis.

The distance of the thermocouple from the quenched surface was also studied to determine its influence on the sample thermal field and the calculated heat flux. Surprisingly, the distance of the thermocouple from the quenched surface had no obvious effect on the calculated heat flux, as shown in Figure 7.13. This implies that the thermocouple can be put any distance from the quenched surface without aggravating the disturbance of the sample thermal field. However during a quench test, the thermocouple should be put as close as possible to the quenched surface so that the detailed changes of the surface heat flux can be captured. If the T/C is too far away from the quenched surface, it will only be able to measure the damped and lagged temperature.

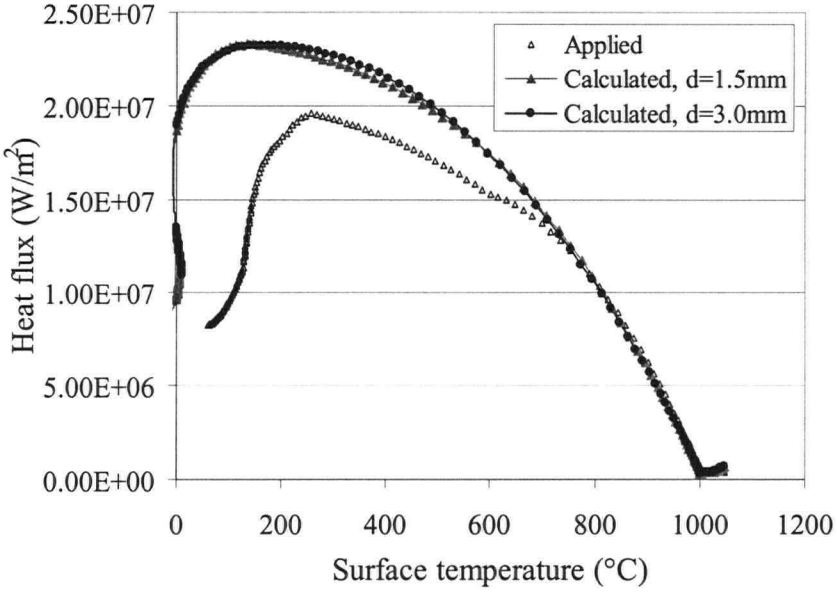

Figure 7.13 - Comparison between the calculated and applied heat flux when the T/C hole is not taken into account for conditions where the distance of the tip of the thermocouple from the quenched surface varies from 1.5 mm to 3.0 mm.

Magnitude of applied heat flux - The magnitude of the applied heat flux on the quenched surface also has a significant effect on the level of perturbation caused by the presence of the T/C and hence the calculated heat flux curve. Figure 7.14 shows the influence of the magnitude of the heat flux on the calculated results. As can be seen, as the magnitude of the heat flux is lowered, the difference between the applied and predicted values is lowered. This means that, at low heat fluxes, the effect of the thermocouple hole on the measured thermal history and the calculated boiling curve using the IHC model will decrease.

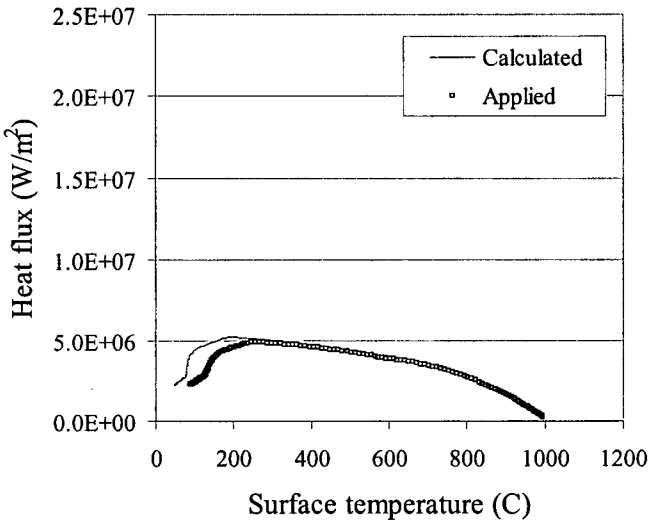

a) Peak heat flux = ~5 MW/m^2

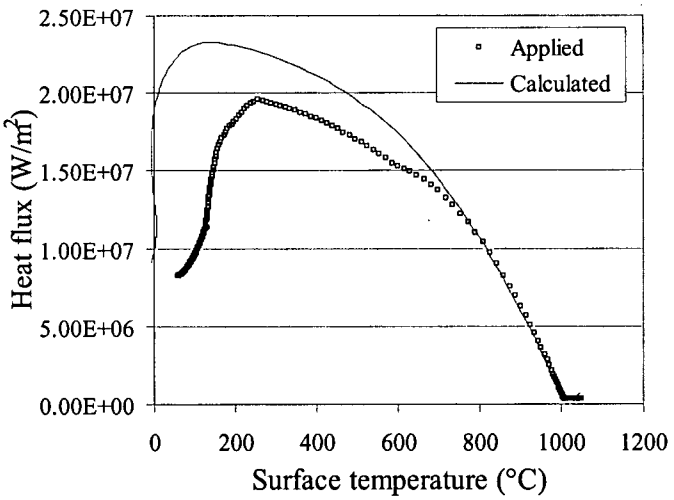

b) Peak heat flux = ~20 MW/m^2

Figure 7.14 - Comparison between the calculated and applied heat flux when the T/C hole is not taken into account for: a) a peak heat flux = ~5 MW/m^2 and b) a peak heat flux = ~20 MW/m^2.

Material properties - The effect of the thermocouple installation on the sample thermal field also depends on the material properties of the sample. For example, because aluminum has a very high thermal conductivity relative to steel, the heat in the sample is able to transfer much more quickly to the thermocouple tip and hence compensates for the temperature drop experienced at the tip of the T/C due to the thermocouple hole; the effect of the thermocouple hole on the sample thermal field is lessened. Figure 7.15 shows the effect of thermocouple hole on the calculated heat flux when an aluminum alloy was chosen as material being quenched. The thermal properties used for this analysis are given in Table 7.4. As can be seen, when using aluminum alloy as the test material, the thermocouple installation has nearly no effect on sample thermal field.

Table 7.4 - Material properties used for the aluminum in the simulation.

Density ρ, kg/m^3	Specific heat Cp, J/kg K	Conductivity k, W/m K
2700	870	165.0

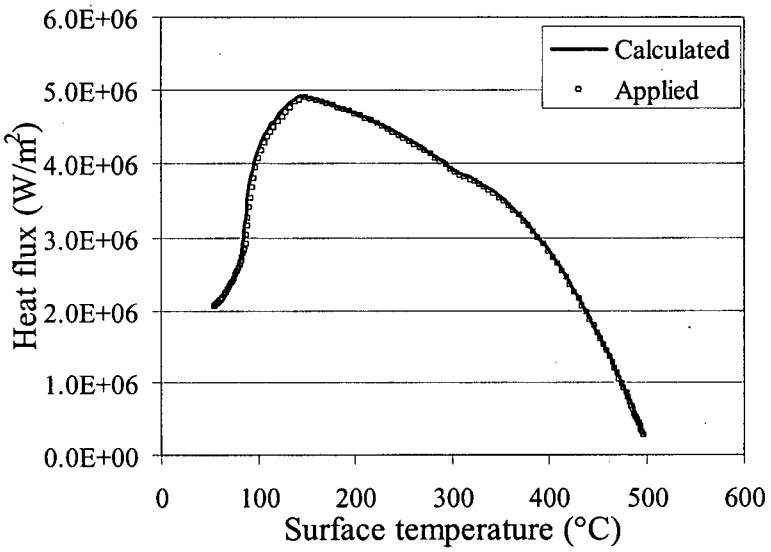

a) Aluminum

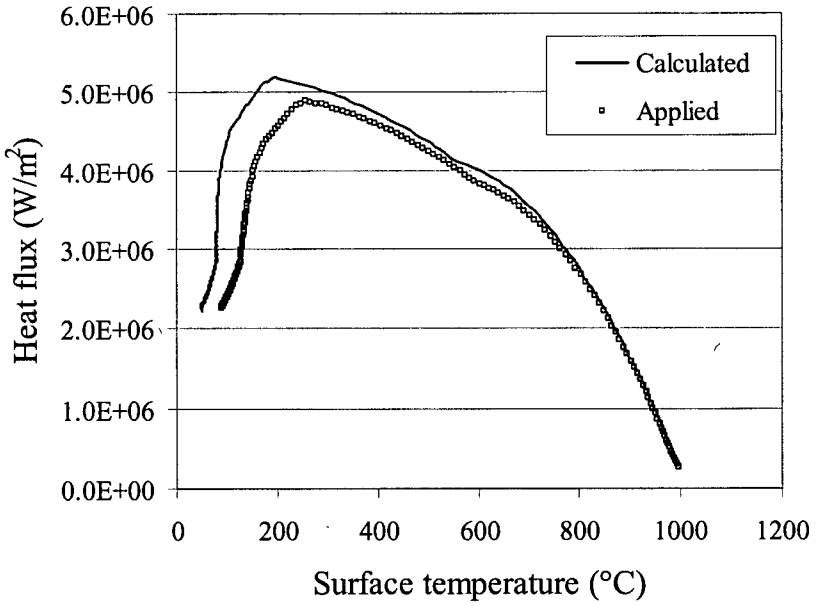

b) Steel

Figure 7.15 - Comparison between the calculated and applied heat flux during a quench operation when the T/C hole is not taken into account for: a) aluminum and b) steel.

A general method to determine the necessity of taking the T/C hole or installation into consideration during a quench test is to calculate the Biot number (Bi) for the test conditions and material being studied. The Biot number is a comparison of the internal thermal resistance to the external thermal resistance (at the quenched surface) as shown in Equation 7-6:

$$Bi = \frac{hL}{k} \tag{7-6}$$

where Bi is the Biot number, h is the heat transfer coefficient at the surface of the quenched sample in $W/m^2°C$, L is the characteristic dimension of the material being cooled (in this case the diameter of the thermocouple) in meter, and k is the thermal conductivity of the material being quenched in W/m°C.

A large Biot number means that the internal thermal resistance is much higher than the external thermal resistance. During a quench process, a large Biot number implies that the thermal resistance at the surface is much lower, and that the thermal energy in the sample mainly flows to the quenched surface. As a result, very little heat flows in the transverse direction in the sample to compensate for the temperature drop at the thermocouple tip due to presence of the T/C hole. So the effect of the thermocouple hole on the sample thermal field must be taken into consideration. Whereas, a small Biot number means the external thermal resistance is much higher than the internal thermal resistance and the transverse heat flow to the T/C tip will be much higher. In this case the effect of thermocouple hole on the sample thermal field can be ignored without impairing the calculated heat flux.

As shown in Figure 7.16, the Biot number for the quench test being performed can be calculated based on the material being tested, the heat flux at the surface of the sample and the diameter of the T/C hole. Hence, in situations where the Biot number is less than 0.1 then the T/C hole can be ignored, as the internal thermal resistance is much smaller than the external thermal resistance.

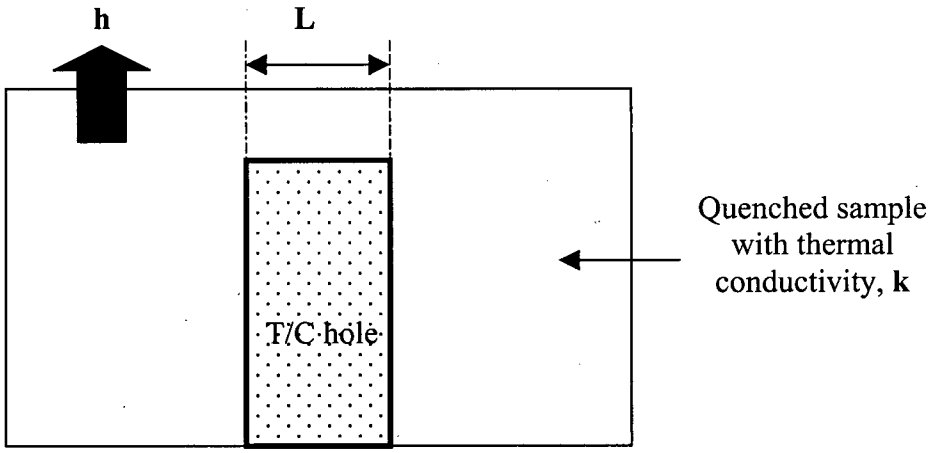

Figure 7.16 – Schematic of quenched sample and T/C hole indicating parameters that can be used to calculate the Bi number.

Figure 7.17, shows the quench conditions for different materials where the T/C hole must be included in the IHC analysis to obtain accurate results. For the steel material, which is assumed having a thermal conductivity of 20 W/m°C, the thermocouple insulation must be taken into consideration when heat transfer coefficient at the surface is higher than 1000 $W/m^2°C$ (T/C hole diameter is 2 mm) or 2000 $W/m^2°C$ (T/C hole diameter is 1 mm). But for the aluminum alloy, which is considered to have a thermal conductivity of 160 W/m°C, the thermocouple insulation can be ignored even

when the heat transfer coefficient at the surface is as high as 16000 W/m^2°C (T/C hole diameter is 1 mm) or 8000 W/m^2°C (T/C hole diameter is 2 mm).

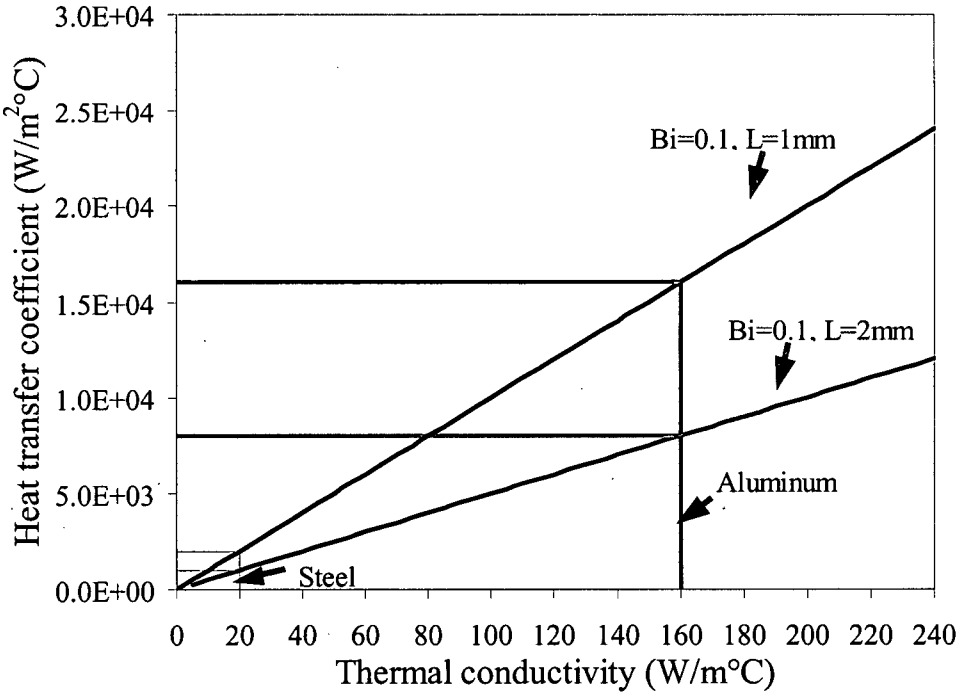

Figure 7.17 – Effect of thermal conductivity *k*, heat transfer coefficient *h* and thermocouple radius, *r* on the Biot number. Under quench conditions where the Biot number is greater than or equal to 0.1 the T/C hole will need to be included in the IHC.

7. 2 Surface temperature measurement and its error

As indicated earlier, two main techniques can be used to measure the temperature of the sample during a quench test namely: sub-surface techniques where the thermocouple is located at some known inner location in the sample and surface temperatures where the temperature is obtained at the surface of the sample where the

quench operation is occurring. The advantage of measuring the temperature right at the quench surface is that there is no lag in the measured surface temperature, and thus there is no restriction on the time step used in the IHC calculation. As a result, some water quench experiments were conducted on the AISI 316 stainless steel flat plate instrumented with both surface as well as sub-surface thermocouples at the same spatial location on the sample so that the calculated boiling curves and the two techniques to measure the temperature could be compared.

7.2.1 Experimental results

Figure 7.18 shows schematically how the thermocouples were installed in the stainless steel plate for the experiments. As can be seen in this diagram, the distance (d) between the surface thermocouple and sub-surface thermocouple is ~1 mm and to ensure that both thermocouples experienced the same quench conditions, care was taken to ensure that the thermocouples were located on top of each other or at the same spatial location in terms of r and θ. This ensured that both thermocouples experienced the same test conditions during the quench. Chapter 4 outlines the test conditions used for these tests and a total of 2 tests were run.

The measured temperature profile from one of the tests is shown in Figure 7.19a and the calculated boiling curves using the temperature-history measured by the surface and sub-surface thermocouples are shown in Figure 7.19b. For the case of the sub-surface thermocouple the T/C hole was included in the analysis.

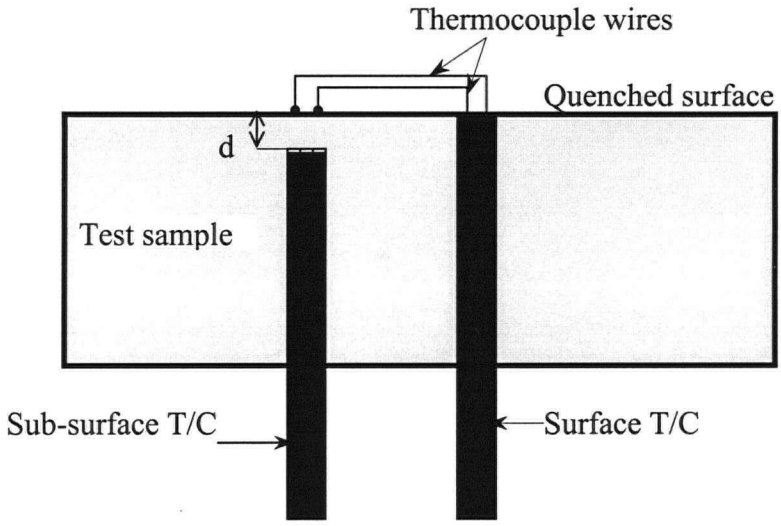

Figure 7.18 - X-sectional schematic of the flat plate showing how the surface and sub-surface thermocouples were instrumented in the sample during the quench tests.

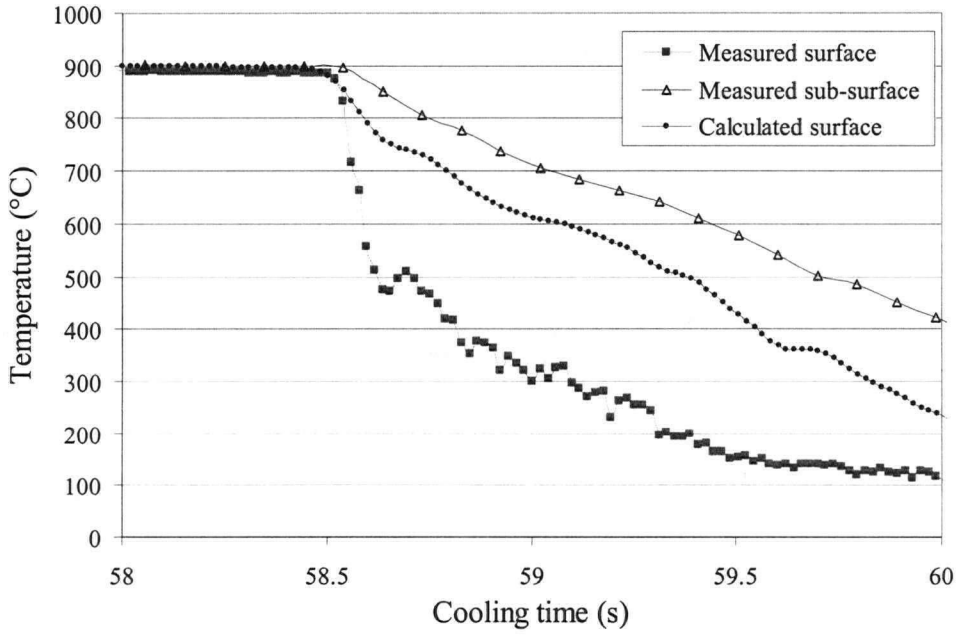

a) Temperature-history using both surface and sub-surface T/C's.

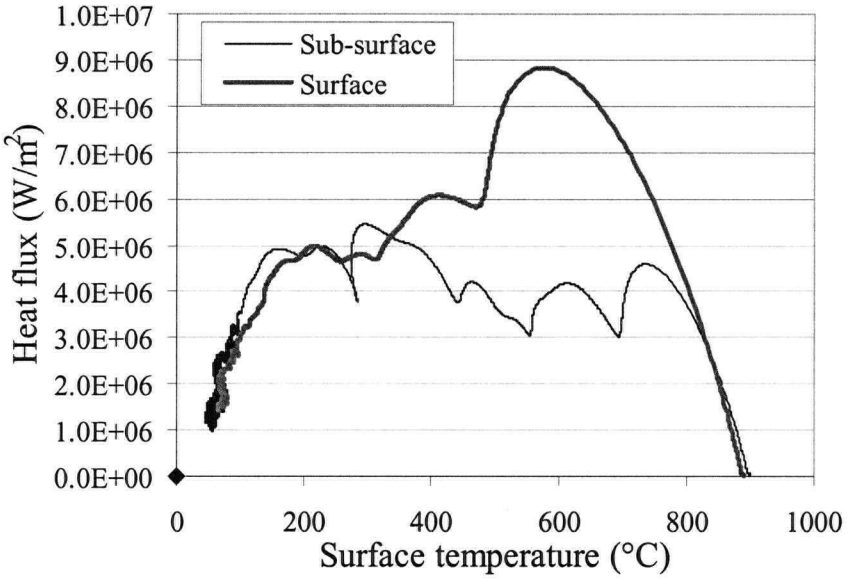

b) Calculated boiling curves using measured temperature-time data from both the sub-surface (T/C hole included in analysis) and surface T/C's

Figure 7.19 – Results from quench tests to assess differences in measurement techniques showing: a) Temperature-history using both surface and sub-surface T/C's and b) Calculated boiling curves using measured temperature-time data from both the sub-surface (T/C hole included in analysis) and surface T/C's.

As can be seen in Figure 7.19a, as expected the temperature–time history measured at the surface drops more quickly than the measured temperature-time at an interior location in the sample. However, if the boiling curve calculated using the sub-surface temperature data is used to calculate the temperature-time history at the surface, one can see that the predicted or calculated temperature-time history at the surface is quite different than what was measured. Figure 7.19b shows the calculated boiling curves using the measured data from the two different techniques and, as can be seen, the

boiling curves are quite different both in shape and magnitude. In this case the boiling curve calculated using the measured surface data goes to significantly higher heat fluxes than that predicted using the measured sub-surface data and compensating for the T/C hole. Ideally, the calculated boiling curves using the measured data from these two thermocouples should be same as they are predicting the heat flux at the same surface location on the sample.

Since the calculated boiling curve using data from the sub-surface thermocouple has taken the thermocouple hole into account, we are confident that this boiling curve represents the actual heat flux experienced by the material at this surface location on the sample. Hence, we need to determine why the surface thermocouple produces incorrect results. In order to understand why the surface T/C measured much lower temperatures than were actually experienced by the material during the quench test, a theoretical analysis combined with mathematical modeling using the IHC model was done and is outlined in the following section.

7.2.2 Theoretical analysis of surface T/C

Figure 7.20 shows a detailed sketch of the surface thermocouple wire welded to sample surface. As can be seen the heat transfer that occurs in this situation is very similar to the heat transfer that occurs from an extended fin surface. The analysis of heat transfer during fin cooling is well known and can be found in detail in many basic heat transfer textbooks [125].

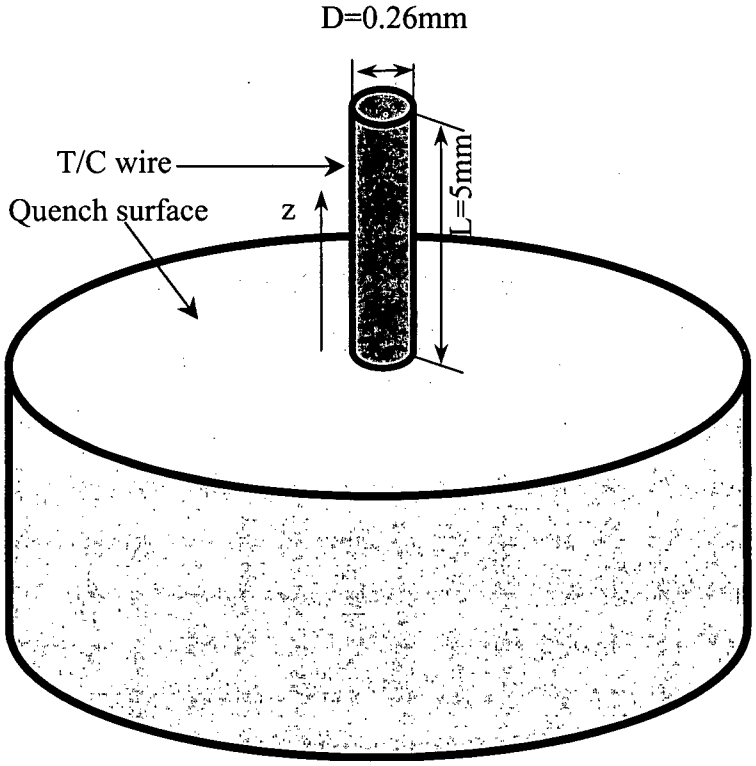

Figure 7.20 – Enlargement of the quenched surface showing a detailed sketch of a thermocouple wire welded to the sample surface

In Figure 7.20, the thermocouple wire is welded to the sample surface and hence there is no contact thermal resistance between the wire and the surface. The dimensional data for the T/C wire used in the analysis is given in Table 7.5.

Table 7.5 – Dimensional data for the T/C wire used in the analysis.

Length L, m	Diameter D, m	Cross-sectional area A, m^2	Perimeter P, m
0.005	0.00026	5.309×10^{-8}	8.168×10^{-4}

In the analysis, the water temperature on the quenched surface, T_w, was assumed to remain constant at 15°C and the material properties for the Chromel wire were used (Table 7.6).

Table 7.6 - Material properties of the thermocouple wires [126].

T/C wire	Density ρ, kg/m^3	Specific heat C_p, J/kg K	Conductivity k, W/m K
Chromel	8730	447	19.2
Alumel	8600	522	29.7

To do this analysis the T/C wire was assumed to be a pin or spine fin as shown in Figure 7.20. The governing equation shown in Equation 7-7 was used along with the boundary conditions shown in Equations 7-8 and 7-9:

$$\frac{d^2T}{dz^2}+\frac{hP}{kA}(T-T_w)=0 \tag{7-7}$$

where h is the heat transfer coefficient acting on the T/C wire surface, P is the perimeter of the T/C wire, k is the thermal conductivity of the T/C wire, A is the cross section area of the T/C wire, and T_w is the water temperature.

At the point of contact between the thermocouple wire and the quenched surface, a fixed temperature is assumed, so at $z = 0$, the boundary condition is given by Equation 7-8.

$$T = T_s = 800°C \tag{7-8}$$

where T_s is wall temperature.

At $z = L$ (at the tip of the T/C wire) it is assumed that little or no heat is transferred from the end of the wire because the cross-sectional area at the tip is considered to be small (1.3%) compared to the remaining surface area of the wire. So, at $z = L$, the boundary condition is

$$\left.\frac{dT}{dz}\right|_{z=L} = 0 \tag{7-9}$$

The temperature of the thermocouple wire can then be calculated using Equation 7-10 [125]:

$$\frac{T - T_w}{T_s - T_w} = \frac{\cosh[mL(1 - z/L)]}{\cosh(mL)} \tag{7-10}$$

where, T is temperature of the T/C wire and m is given by Equation 7-11.

$$m = \sqrt{\frac{hP}{kA}} \tag{7-11}$$

The heat transfer rate at $z = 0$ (the thermocouple wire junction), q_z, can then be obtained using Equation 7-12.

$$\frac{q_z}{kAm(T_s - T_w)} = \tanh(mL) \tag{7-12}$$

Using the above equations, the axial temperature distribution in the T/C wire and the heat flux at the thermocouple junction (z=0) can be calculated respectively as shown in Figures 7.21 and 7.22.

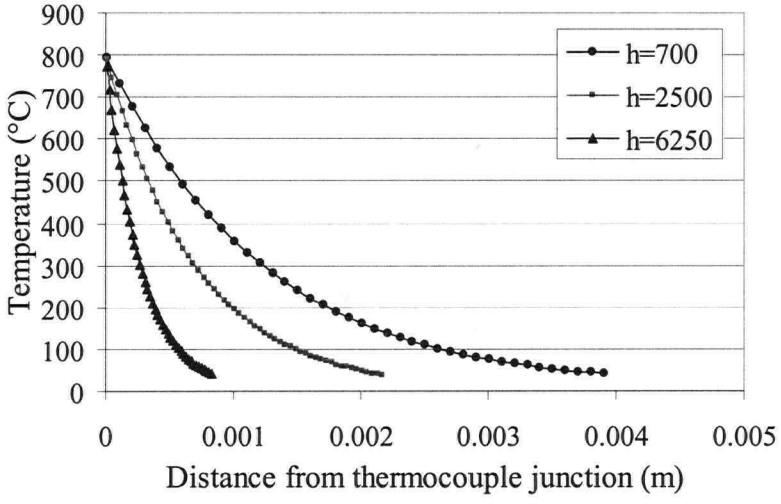

Figure 7.21 – Calculated axial temperature distribution in the thermocouple wire at steady state under three different heat transfer coefficient conditions, calculated using Equation 7-10.

As can be seen in Figure 7.21, as the surface heat transfer coefficient, h, increases, the axial distance along the T/C wire that heat will conduct decreases. When the heat transfer coefficient is h = 6250 W/m^2°C, the heat conduction distance is only ~1 mm. This means that, although the wire is 5 mm in length, the majority of heat that transfers from the wire to the surroundings occurs in the wire only 1 mm away from the junction point.

The relationship between the applied heat flux around the thermocouple wire and the heat flux at the wire junction, where the thermocouple wire extracts heat from the sample, is shown in Figure 7.22.

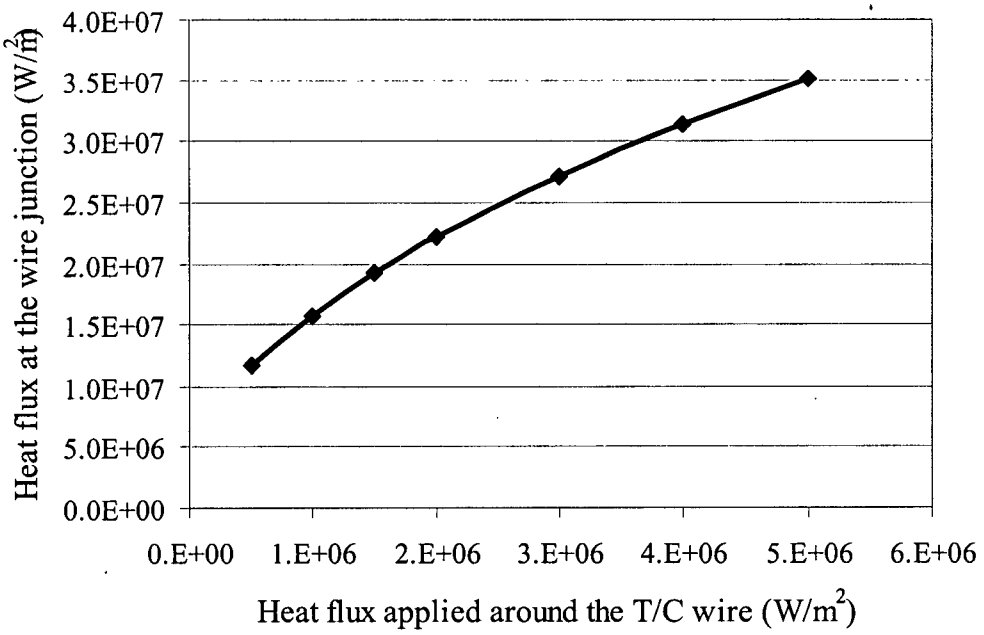

Figure 7.22 - Calculated heat flux at wire junction under different heat flux conditions, calculated using Equation 7-12.

It can be see that depending on the magnitude of the applied heat flux, the heat flux experienced by the thermocouple wire at the thermocouple wire junction is increased by about 10 times. Under water quench conditions, the heat flux is usually is in the range of $2.0\text{-}6.0\times10^{6}$ W/m^2. Using data from Figure 7.22, it can be seen that under these conditions the heat flux at the T/C wire junction would be $\sim23\text{-}37\times10^{6}$ W/m^2. As a result, the measured temperature at the T/C junction point will drop much more quickly than the temperature in other parts of the sample away from the T/C wire. Therefore, it

can be expected that the use of a surface T/C technique to measure the temperature during a quench test will have a large effect on the sample thermal field around the wire junction and produce erroneous measured results. The following section will calculate the expected influence of the surface T/C wire on the temperature distribution in the sample during a quench test using the FE conduction and IHC model developed during the course of this research.

7.2.3 Mathematical simulation of the surface temperature during a quench test when a surface T/C is used

From the above analysis, it is obvious that the heat transfer at the surface of the sample where the T/C wire is located will be much larger than the heat transfer experienced by the material at other parts of the sample away from the wire. This is shown schematically in Figure 7.23.

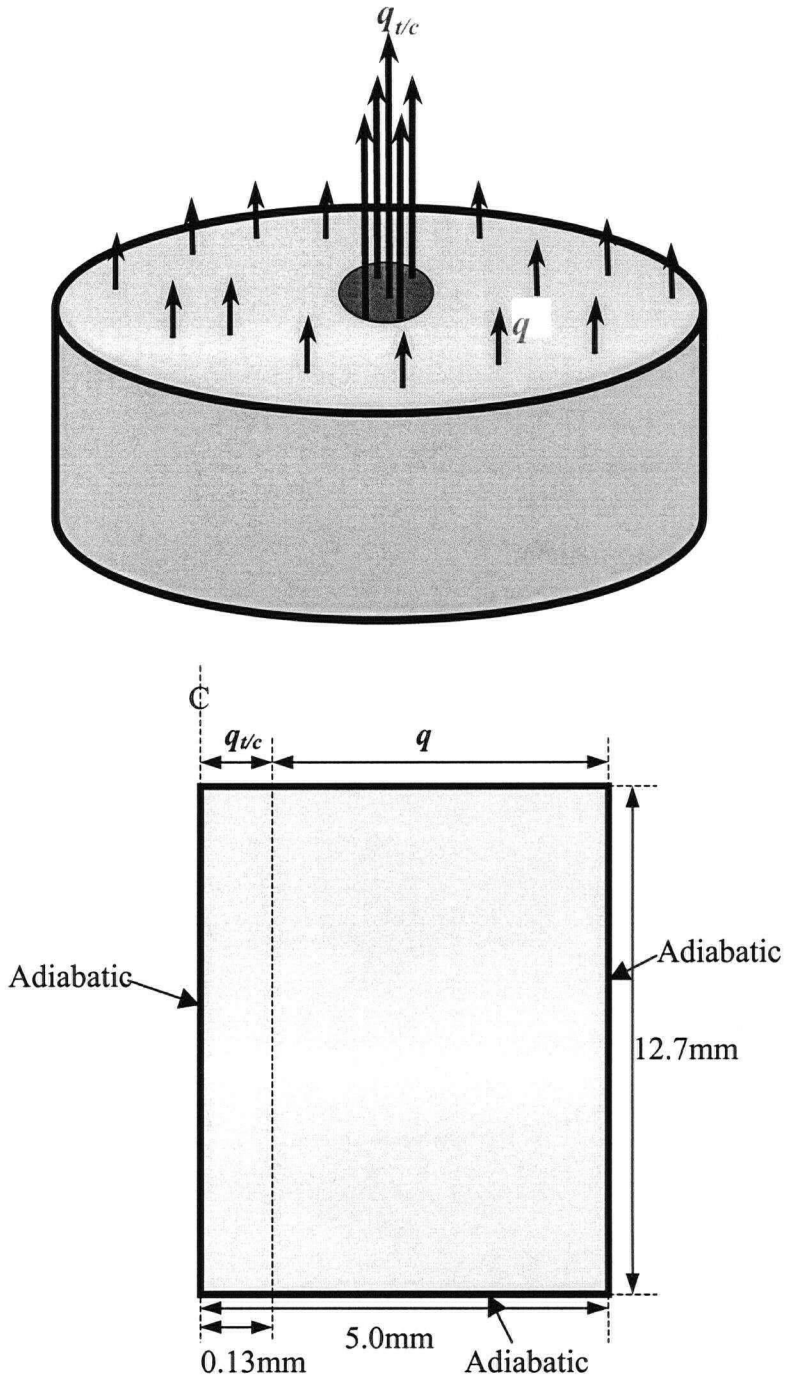

Figure 7.23 – Schematic diagram illustrating the two different heat fluxes being applied to the surface of the sample during the water quench in the case where a surface T/C is used to measure the temperature-time data ($q_{t/c}$ is about 10x larger than q).

In order to account for this, different heat fluxes should be applied on the sample surface consistent with the influence of the T/C wire on the applied heat flux. For the analysis, the heat flux as a function of surface temperature calculated using the measured sub-surface temperature was used as q and is shown in Figure 7.19b.

For the analysis, it was assumed that $q_{t/c}$ was 10x larger than q. This approximate assumption is based on the theoretical analysis and calculated results shown in Figure 7.22.

After applying the heat flux q and the assumed heat flux $q_{t/c}$ on the sample, the temperature at the thermocouple junction and the area around the thermocouple junction can be calculated. The calculated results are shown in Figures 7.24a and b

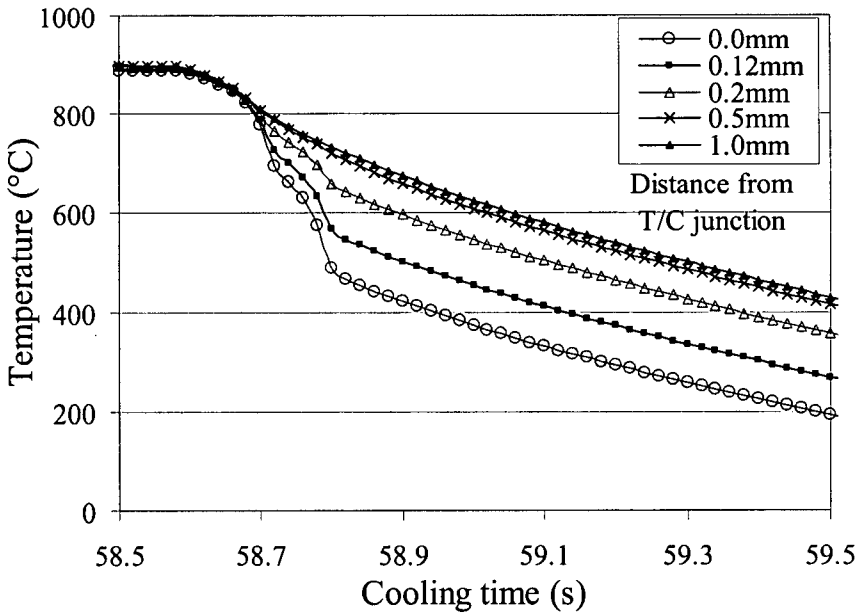

a) Predicted thermal history on the quenched surface at positions, r, away from the centerline of T/C junction.

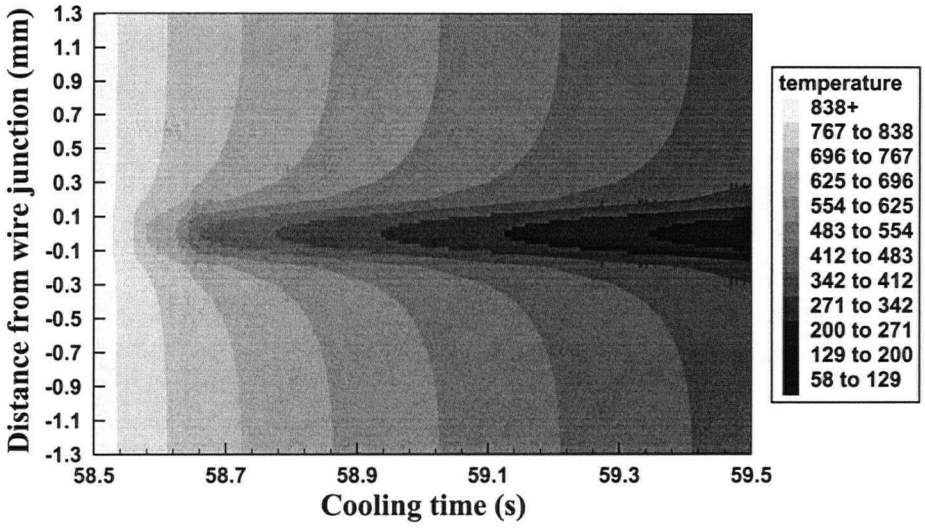

b) Illustration of this effect as a function of time and distance away from the T/C wire.

Figure 7.24 – Predicted perturbation in the sample thermal field around the T/C wire showing: a) predicted thermal history on the quenched surface at positions, *r*, away from the centerline of T/C junction and b) illustration of this effect as a function of time and distance away from the T/C wire.

It can be seen that at the beginning of cooling, due to the lower heat flux, the temperature at the wire junction would not be much different from the surface temperature at other locations. However, as the quenching process proceeds, the surface heat flux increases and the difference between the wire junction temperature and surface temperature of the sample becomes larger and reaches a peak of about 300°C at a cooling time of 59 second. It can also be noticed from Figure 7.24, that the spatial effect of the thermocouple wire on the sample surface is localized and is confined to the very small area around the T/C wire junction point. As the distance away from the wire junction increases, the effect of the thermocouple junction will gradually disappear. When the

distance is larger than ~1.0 mm, the effect of the thermocouple on the sample thermal field will vanish completely.

Using the model results, we can see that the calculated temperature at the thermocouple junction agrees quite well with the measured surface temperature as shown in Figure 7.25.

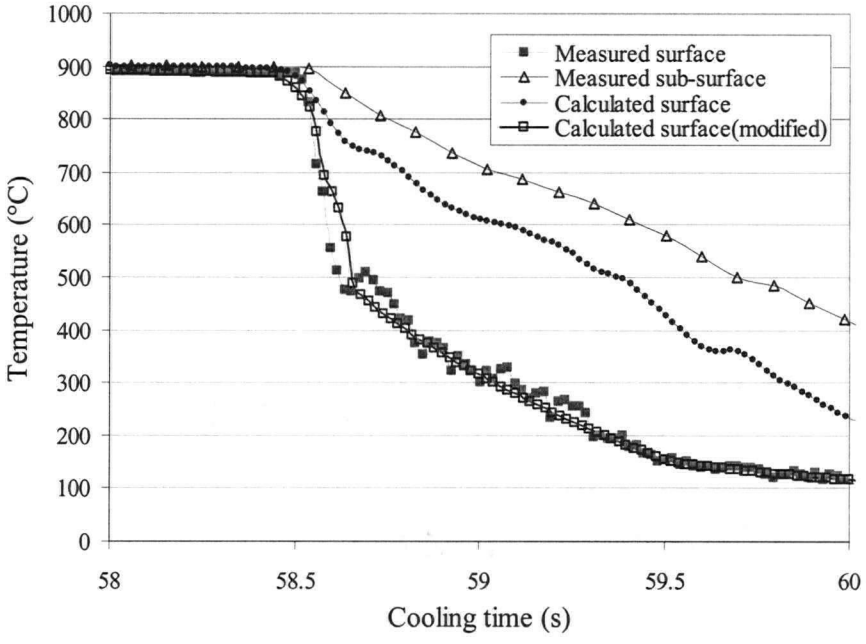

Figure 7.25 - Comparison between the calculated and measured surface temperatures using the surface T/C.

From this analysis, it can be concluded that during the quench process, instead of measuring the "real" surface temperature, the surface thermocouple generates a much lower surface temperature as the local heat flux conditions experienced at the point where the T/C is located are quite different from the rest of the sample. As a result, it was decided to use the sub-surface technique of measuring the sample temperature and

compensation for the T/C hole in our study to quantify the influence of sample start temperature and thickness of the boiling curves.

8.0 RESULTS AND DISCUSSION

The objective of this research was to develop a quantitative understanding of the boiling water heat transfer that occurs during water spray cooling of some ferrous alloys including a high carbon steel (AISI 52100) which would undergo a phase transformation during the water quench as well as a stainless steel (AISI 316) which would not undergo a phase transformation during a water quench. Towards this goal, the work has focused on the development of a 2-D inverse heat conduction (IHC) model capable of calculating the heat transfer boundary condition at the surface of the steel product based on the thermal history at a known location in the quenched sample. Part of this model development has included performing a detailed sensitivity analysis to identify model, material and measurement parameters that influence the accuracy of the model predictions and quantify the influence on the accuracy of the model predictions if inaccuracies in any of these parameters exist. These results have been presented in Chapter 6 of this thesis.

A key component to accurate quantification of the boiling water heat transfer during a water quench operation is measurement of the thermal history experienced at a known location in a sample. Although not anticipated directly at the start of the research, an important component of this research has been to analyze and investigate experimental methods to accurately measure the thermal history in the sample during a water quench operation including using both surface as well as sub-surface thermocouples. This data and analysis has been presented in Chapter 7 of this thesis.

Finally, the influence of sample start temperature, spatial location on the sample and sample thickness on the resulting boiling curves was quantitatively assessed for AISI 316 steel plates. As outlined in the experimental section, these tests were conducted on flat circular plates made from AISI 316 stainless steel. As mentioned previously, a stainless steel flat plate was chosen to do these measurements as geometrically it simplified the interaction of the water on the surface of the sample. In addition, using stainless steel avoided other complicating factors such as scale formation while reheating to the test temperature and the interaction of the scale with the water spray during the quench test as well as phase transformations during the quench process.

The quench operation involved a single circular cone nozzle which was positioned above the plate and the sample was instrumented with a number of T/C's inserted from the back of the sample to within 1 mm of the quenched surface and positioned across the entire diameter of the plate. In total, 7 T/C's were used for each test and in this way, the quench conditions experienced by the plate both within the water spray zone and outside of it could be assessed. For all calculations in this section, the geometry and boundary conditions used in the IHC model are similar and involve accounting for the T/C hole in the analysis. The geometry used in the IHC model is shown in Figure 7.3 and the boundary conditions are given in Equations 7-1 to 7-4 of Chapter 7. The initial condition is similar to Equation 7-5 with the measured test temperature just prior to the water quench being the start temperature.

8. 1 Water flow distribution on the quenched surface

During the quench tests, a circular cone nozzle was used to spray the cooling water onto the surface of the sample. As shown schematically in Figure 8.1, after initially hitting the surface of the sample, the water flowed horizontally to the edges of the plate. In this case the diameter of the test plate was larger than the spray diameter of the nozzle, so two distinct zones could be defined on the sample surface during the quench operation, namely: 1) a direct spray zone (T/C's 2-6) and 2) a water flow zone (T/C 1 and 7). The interaction of the water with the surface of the sample in each of these zones is quite different. In the direct spray zone, the water is sprayed onto the surface of the sample directly from the nozzle and hence the impingement velocity is quite high, whereas in the water flow zone, the water flows horizontally across the surface and the impingement velocity is much lower.

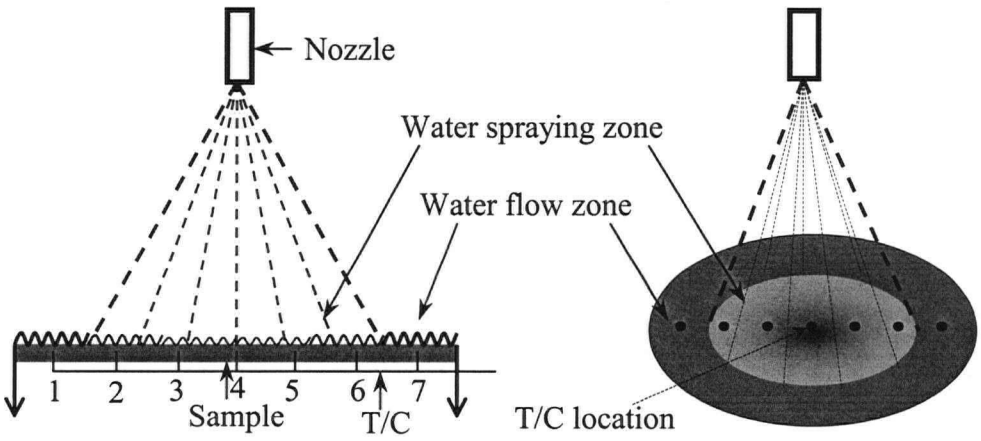

Figure 8.1 - Cooling water spray pattern on surface of plate.

To determine if there was any spatial variation in each of the zones the temperature history measured by the T/C's in each of these zones was compared. As can

be seen in Figure 8.2, thermocouples 2-6 which were all positioned within the water spray zone exhibit very similar behaviour. Similarly T/C's 1 and 7, in the water flow zone also exhibited very similar behaviour. Figure 8.3 shows the calculated boiling curves in these two regions using the measured data as input to the IHC model. As shown in Figure 8.3, boiling curves generated using either a heat flux or heat transfer coefficient exhibit similar trends and distinct regions of film, transient and nucleate boiling as well as convection cooling can be identified, especially in the water spray zone.

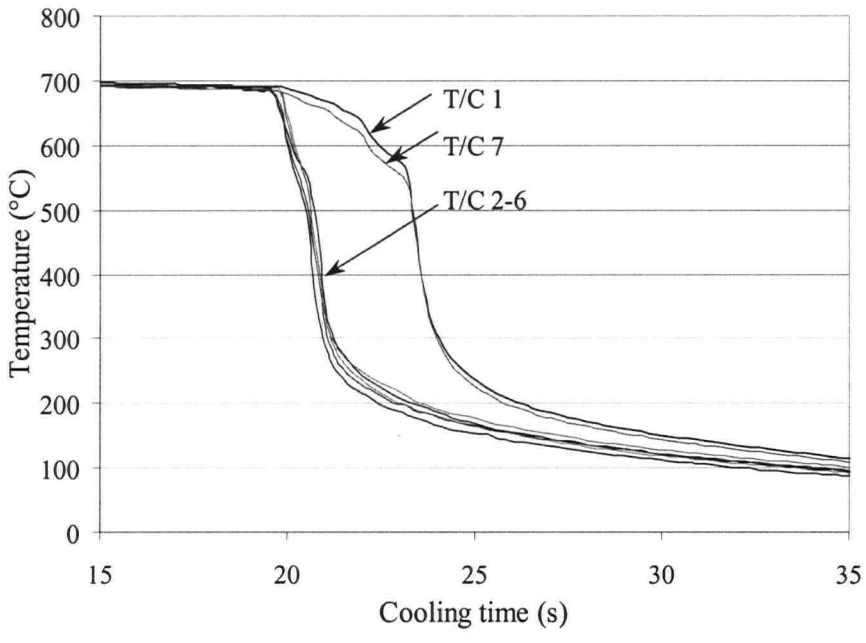

Figure 8.2 – Typical temperature history measured by each of the thermocouples during a water quench test, indicating the two zones on the plate namely: the water spray zone (T/C's 2-6) and the water flow zone (T/C 1,7).

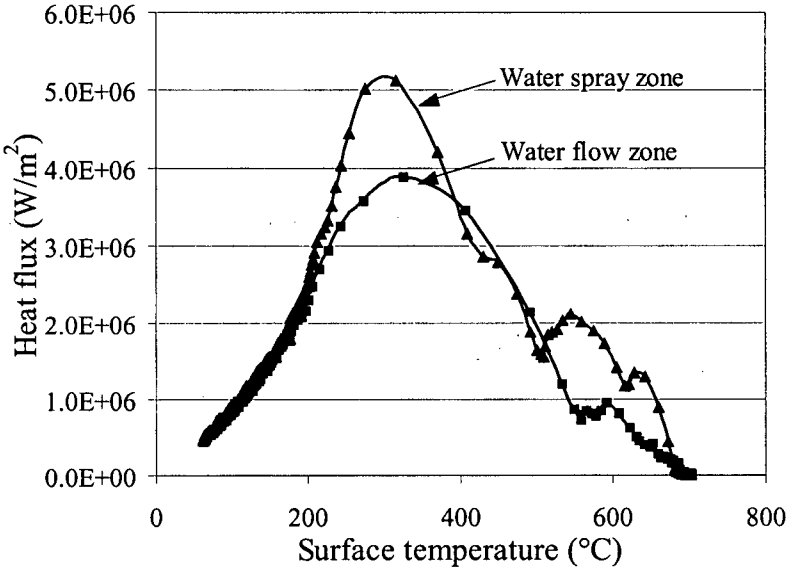

a) boiling curves expressed using heat flux.

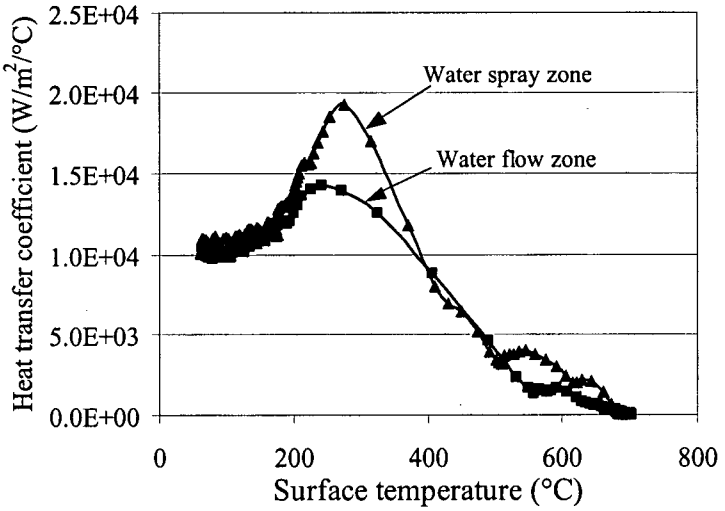

b) boiling curves expressed using heat transfer coefficient.

Figure 8.3 - Calculated boiling curves in the different zones across the plate sample during a quench test: a) boiling curves expressed using heat flux, and b) boiling curve expressed using heat transfer coefficient.

Since very little variation in the heat transfer occurs in the radial direction in the water spray zone or water flow zone, the heat transfer can be assumed to occur in only one dimension (z) – through the thickness of the plate in each zone respectively. At the boundary between the water spray and water flow zones there will be some heat flow as these two zones have different quenching intensity and hence the assumption of heat flow in only the z-direction would be inaccurate.

8. 2 Measured cooling curves and calculated boiling curves

The cooling curve is the temperature history measured in the test sample during the quench process. When the location at which the temperature is being measured is very close to the quenched surface, the measured cooling curves can reflect the detailed changes in the surface heat transfer. Historically, much analysis has been done based on measured cooling curves when accurate calculation of the surface heat transfer could not be done. The advantage of examining the cooling curve is that it is the most direct reflection of the heat transfer process, and when measured accurately, close to the quenched surface, it can capture very tiny changes in surface heat flux. The disadvantage of using a cooling curve is that it cannot quantify the heat flux on the quenched surface – a critical parameter for mathematical modeling of any quench process. Today, cooling curves are becoming less important as more sophisticated and accurate IHC models are being used to calculate the boiling water curves under a given quench condition.

Figure 8.4 shows a typical cooling curve and its calculated boiling curve during a quench test where the starting temperature of the sample was above the Leidenfrost point.

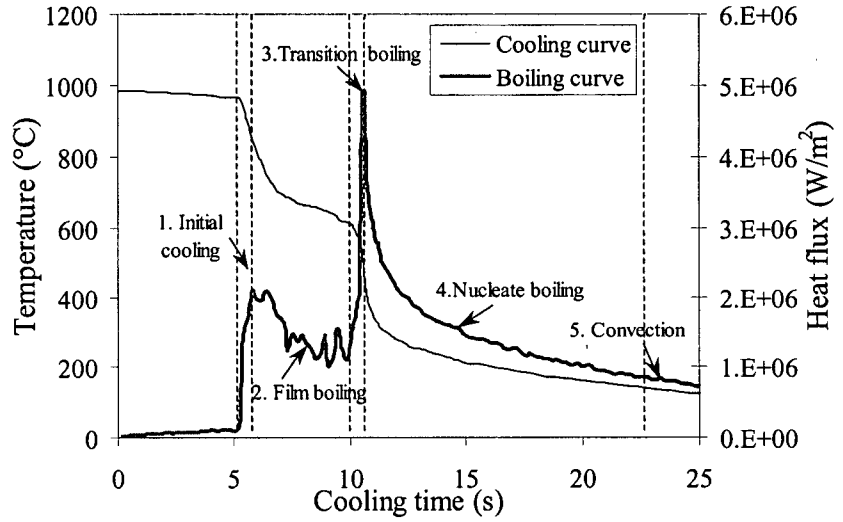

a) Measured cooling rates and calculated boiling curves

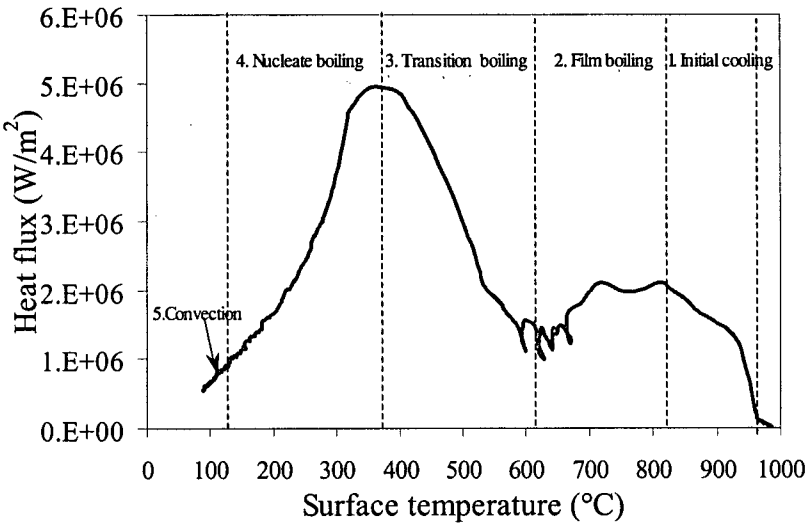

b) Calculated boiling curves

Figure 8.4 – Quench test in the water spray zone where the sample start temperature was above the Leidenfrost point showing: a) the measured cooling curve and b) the calculated boiling curve (T_{start} =1000°C, water flow rate = 1.27 l/s, water temperature 15 °C)

As can be seen in Figure 8.4, after being taken out of furnace the sample cooled slightly due to natural convection and radiation, hence the calculated heat flux in this region is small (around $2\sim5\times10^5$ W/m^2). At around 5 second, water began to spray on the sample surface and the sample temperature dropped about 100°C. In this region, the heat flux increased to 2.0×10^6 W/m^2, this is considered to be an initial cooling region, where the water first starts to interact with the hot surface. This feature is characteristic for a transient quench process and during steady-state boiling this region would never be seen. After the initial cooling period (~1 second), a water vapor film covered the sample surface, and the heat flux decreased gradually. This film boiling region lasted for 5 seconds and the heat flux dropped to $\sim1.0\times10^6$ W/m^2. At ~600°C, the quenching process moved into a transition boiling region and the measured temperature in the sample drops very quickly. In this region the heat flux increases dramatically to $\sim5.0\times10^6$ W/m^2. The transition boiling region usually only lasts a very short time (less than 1 second) as the sample temperature drops very quickly due to high heat flux. After reaching a peak heat flux (5.0×10^6 W/m^2), the heat flux begins to go down, and thus the quenching process enters the nucleate boiling region. The nucleate boiling region usually lasts for a longer time compared to the other boiling regions, and it typically is over when sample temperature reaches ~130°C. Below this temperature, the quenching process is characterized by convection cooling as the there is no vapor nucleating on the surface of the sample.

The relationship between the calculated heat flux and surface temperature is shown in Figure 8.4b. In this figure, the different regions of the boiling curve can be seen

more clearly. As shown, although some regions such as the initial cooling and transition occur in a very short period of time, they can span a large temperature range.

Compared to the steady state boiling curve that has four distinct regions (convection, nucleate boiling, transition boiling and film boiling), the transient boiling curve for a quench process when the sample temperature is above the Leidenfrost point, has one additional region, which corresponds to the initial interaction of the water on the hot surface of the sample or the initial cooling. During the initial cooling region, the boiling heat transfer mechanism is very similar to the nucleate boiling region, i.e., the heat flux increases with the increase in the number of bubbles on the surface of the sample.

One important aspect of the initial cooling region is that it can be confused with transition boiling. This point is illustrated in Figure 8.5, which shows the measured cooling curves and calculated boiling curves for a sample whose start temperature was below the Leidenfrost point. Due to the low initial sample temperature, after a very short time in the initial cooling zone (~0.2 seconds), the quenching process goes directly to the nucleate boiling zone without experiencing the transition zone. If one is looking at the calculated boiling curve (Figure 8.5b), it is very easy to think the quenching process experienced transition boiling and nucleate boiling regions. The big difference between transition boiling and initial cooling is that, in the initial cooling zone, the heat flux will increase as the amount of water vapor increases, but in the transition boiling zone, the reverse is true.

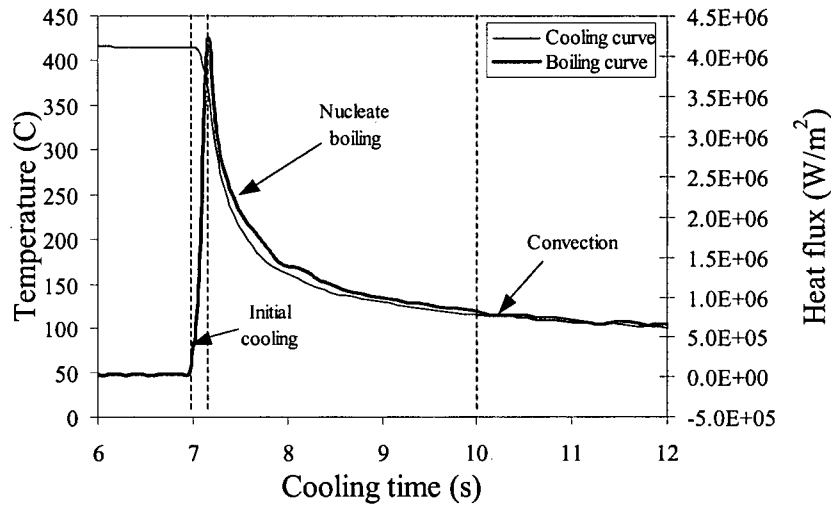

a) Measured cooling curves and calculated boiling curves

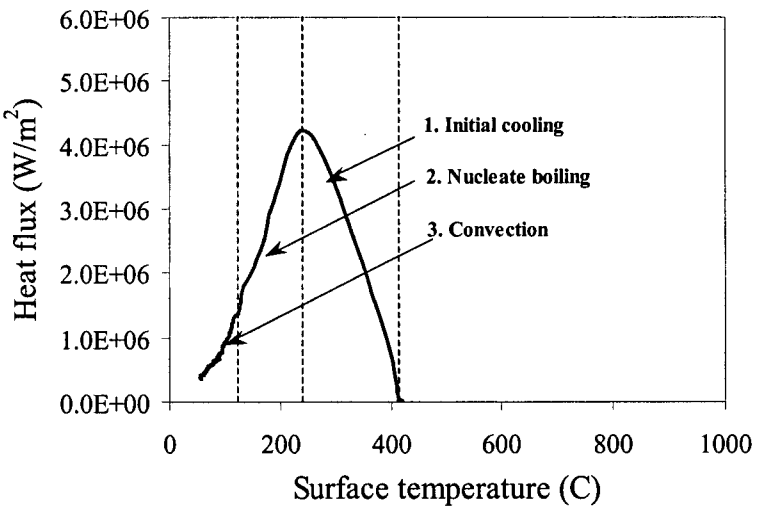

b) Calculated boiling curves

Figure 8.5 – Results from a quench test in the water spray zone where the start temperature of the sample is below the Leidenfrost point showing: a) the measured cooling curves and b) calculated boiling curves. (T_{start} = 425°C, water flow rate = 1.27l/s, water temperature 15°C)

8. 3 Effect of initial sample temperature on boiling heat transfer

Under steady-state conditions, assuming everything else is the same, the boiling curve will not depend on the start temperature of the sample and the same boiling curve can be used to predict how the heat flux changes as the sample temperature changes. The reason for this is that under steady-state conditions, the sample surface temperature is maintained at a fixed level until the nucleation, growth and detachment of the vapor or bubbles reaches a steady state. As a result, regardless of the surface temperature history the sample has experienced, the sample produces the same heat flux for a given temperature.

Much of the research to date on boiling water heat transfer in industrial metals and materials operations such as casting, hot rolling and heat treating has assumed that the boiling water curves do not change as a function of the start temperature of the sample and although relationships between boiling water curves and water flow rate, water impingement angle, water temperature, sample morphology, etc. have been studied, no work has been done on how the sample starting temperature can influence the boiling curves; the assumption being that, similar to steady-state boiling curves, no effect will occur and that the same boiling curve can be used regardless of sample start temperature. In fact, little regard has been given to the fact that for most industrial practices the quenching process is not steady state but transient.

Under transient boiling conditions, the water vapor on the sample surface at a given temperature does not have enough time to reach a steady-state condition as the sample temperature decreases too quickly due to the water quench. So, the heat flux

under transient boiling conditions depends not only on the surface temperature, but also how long the surface temperature can stay at a given temperature, (i.e., *dT/dt)*; the longer the surface temperature can stay at a given temperature the more the boiling curve will approach the boiling curve under steady-state conditions. As a result, for industrial practice, boiling curves obtained under steady-state conditions have very limited application and the effect of initial sample temperature on boiling heat transfer must be taken into consideration.

Figure 8.6 illustrates the influence of the sample start temperature (400-1000°C) on the calculated boiling curves under transient quench conditions in both the water spray zone as well as the water flow zone. As can be seen the initial sample temperature has a significant effect on boiling heat transfer during the quenching process and as the start temperature decreases below the Leidenfrost point, the boiling curve changes dramatically.

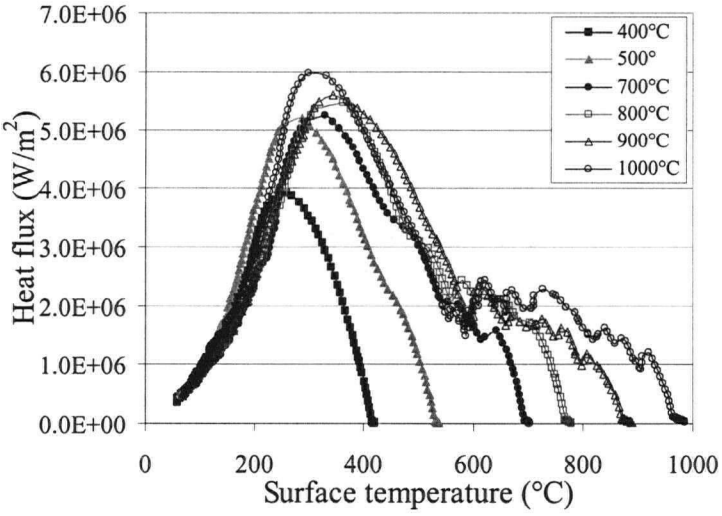

a) Water spray zone

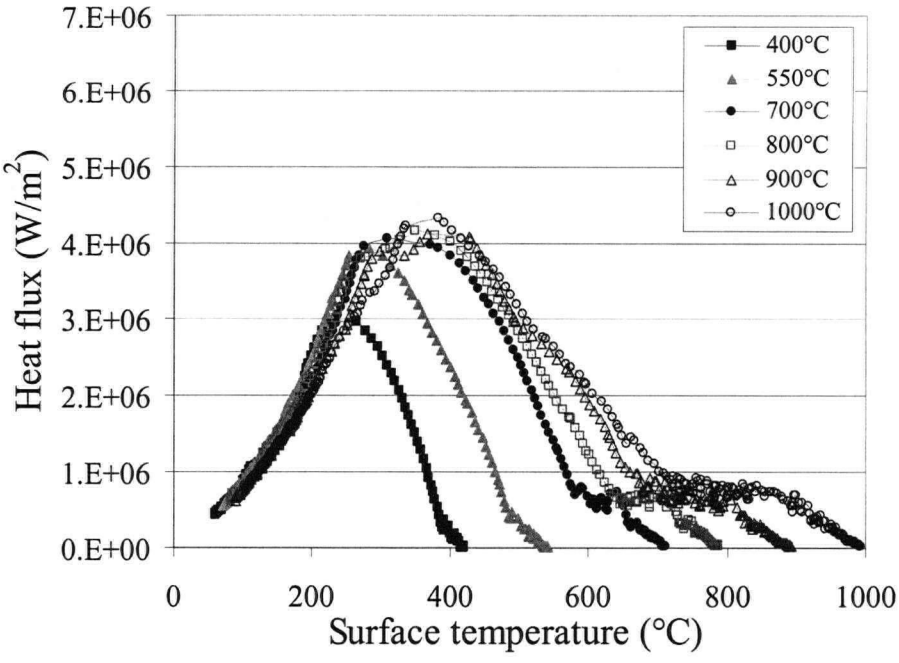

b) Water flow zone

Figure 8.6 Calculated boiling curves from measured data at different initial start temperatures for: a) the water spray zone and b) the water flow zone (Water flow rate = 1.262 l/s, water temperature 15°C).

From Figure 8.6a, it can be seen that the Leidenfrost temperature in the water spray zone is ~600°C. When the sample initial temperature is higher than the Leidenfrost temperature, the quenched sample will experience the four distinct stages of boiling heat transfer (film boiling, transition boiling, nucleate boiling and convective cooling) after a short initial cooling region. As can be seen, the boiling curves will coincide after the initial cooling stage is completed, in the film boiling region, and then follow the full boiling curve throughout the rest of the quench process. This indicates that under these

conditions, the initial sample temperature has very little effect on the boiling heat transfer if the sample start temperature is significantly higher than the Leidenfrost temperature.

When the sample start temperature is lower than the Leidenfrost temperature, the sample will experience the initial cooling stage for a short period of time, and then will go directly to the nucleate boiling zone; the sample will not experience either the transition or film boiling regions even though the start temperature of the sample corresponds to the temperature under which transition boiling should occur. Once the boiling heat transfer reaches the nucleate boiling region, the heat flux will follow the full boiling curve down through the nucleate and convective cooling regimes regardless of the sample start temperature. For this case, a critical aspect of the boiling curve is the initial cooling stage as this will dictate how quickly the heat flux will change as the surface temperature of the sample changes.

When the sample start temperature is close to the Leidenfrost temperature, the situation is slightly more complicated. After the initial cooling region, the sample surface temperature will be very close to the Leidenfrost temperature (maybe higher or lower), and the sample will enter the transition boiling zone. But in the transition boiling zone, compared to a boiling curve developed from a sample which has a much higher initial start temperature, the heat flux will be lower as the surface temperature drops more quickly. The change in the surface temperature of the sample with time depends on the temperature gradient in the sample, which determines the capacity of the sample to supply heat to the surface.

From a computer modeling perspective, the influence of the start temperature of the sample on the resulting boiling curve can easily be calculated based on the fully developed boiling curve (i.e., the boiling curve generated with a sample at a initial temperature significantly higher than the Leidenfrost point) as well as knowing the rate of change in the heat flux as a function of surface temperature during the initial cooling region. Essentially, a line is drawn from the sample start temperature with a slope or rate of change of the heat flux with sample temperature similar to that seen in the initial cooling region. This line represents the initial cooling experienced by the sample and continues until it intersects the fully developed boiling curve. Using this method, very little data are required to capture the influence of sample start temperature on a transient boiling curve.

Figure 8.7 illustrates that this method that can be used to estimate the influence of the sample start temperature on the boiling curve during a transient cooling process in the water spray zone. In Figure 8.7, the fully developed boiling curve, which is very close to the boiling curve under steady state, can be obtained by doing quenching tests at a very high sample initial temperature. As can be seen, the method is relatively simple and produces very accurate results.

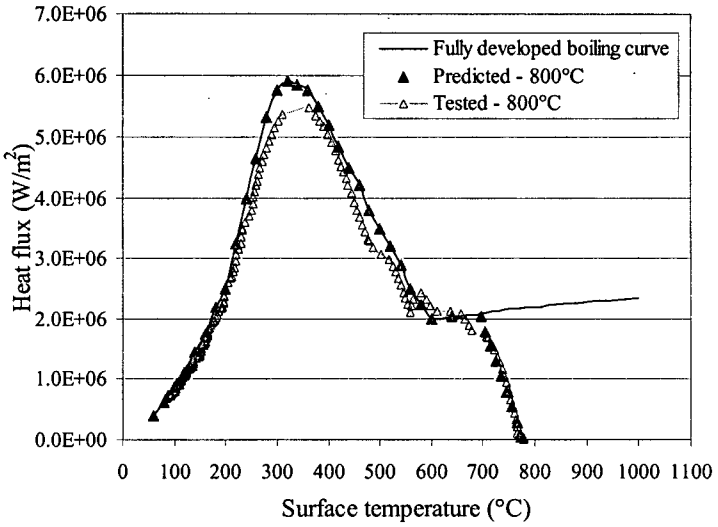

a) Sample start temperature is greater than the Leidenfrost temperature

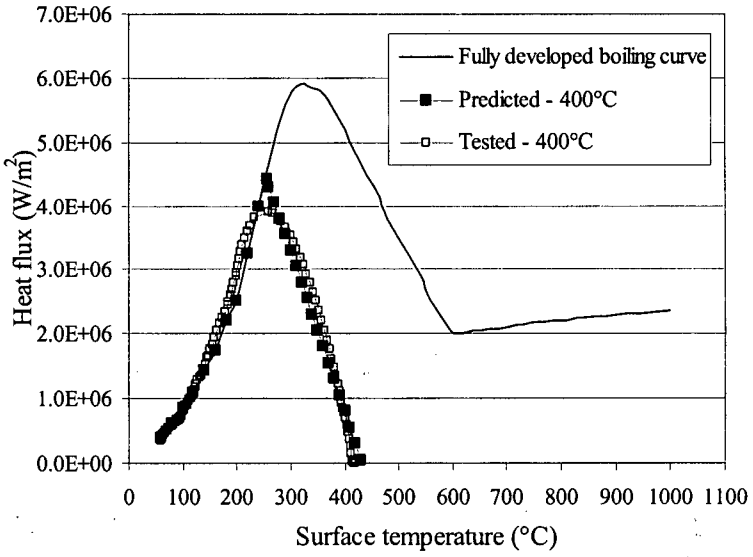

b) Sample start temperature is below the Leidenfrost point

Figure 8.7 – Method to estimate the influence of sample start temperature on the boiling curve in the water spray zone for: a) a case where the sample temperature starts above the Leidenfrost point and b) a case where the sample start temperature starts below the Leidenfrost point.

8.4 Effect of sample thickness on boiling heat transfer

It is obvious that the boiling heat transfer during a transient quench process depends strongly on the surface temperature history experienced by the sample. Hence, the sample thickness should have some impact on the boiling curves as it will determine the ability of the sample to supply heat to the surface of the sample and hence the temperature history at the surface. In order to answer this question, quench tests were done on plates of different thickness to determine what effect sample thickness would have on boiling water heat transfer during a quench process. The test procedure and sample geometries used for this study are outlined in Chapter 4 of this thesis.

Figure 8.8 shows the results obtained from these tests and as can be seen, under the studied conditions, the plate thickness appears to have no effect on boiling heat transfer.

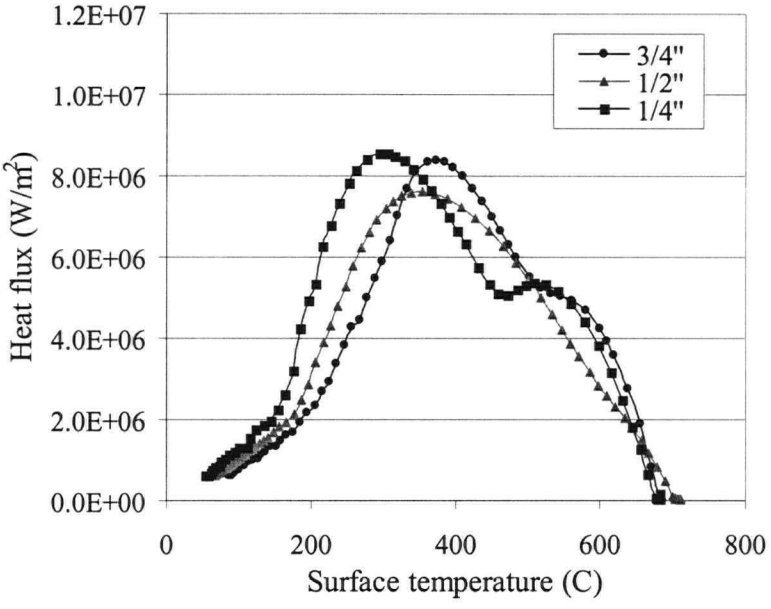

a) Water spray zone

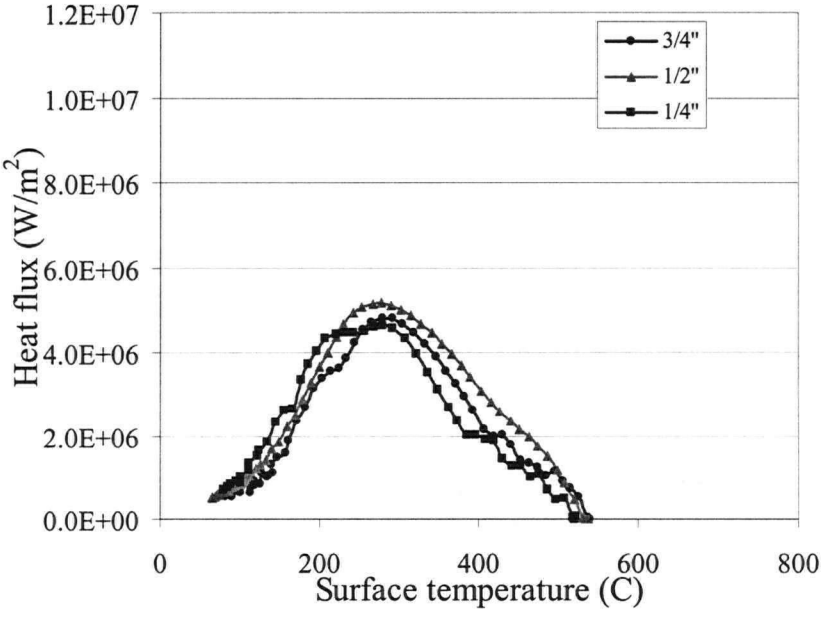

b) Water flow zone

Figure 8.8 - Effect of sample thickness on the calculated boiling curve (water flow rate = 1.27 l/s, initial temperature 520°C) for: a) water spray zone and b) water flow zone.

Theoretically, the sample thickness should have an impact on the boiling curve during a transient quench process since a thinner sample has a lower thermal capacity to supply heat to surface as compared to a thicker sample. In order to determine why this effect was not seen for these test results, computer modeling of the quench process under different quench intensities was done. The results from these calculations will be shown in the following section.

8.5 Analysis of the quench process with samples of different thickness

A model of the quench process during the test condition was simulated by applying an assumed boiling curve in the 2-D FE thermal conduction model to calculate the thermal field in the three samples with different thickness. As shown in Figure 8.9, the applied boiling curve was from one of the calculated boiling curves in Figure 8.8a, which represents the typical heat flux experienced during a water quench. The 2-D FE thermal conduction model was then used to predict the thermal history at any location inside the samples as well as at the surface of the sample during the quench operation. The modeling results from this analysis are shown in Figures 8.10 – 8.11.

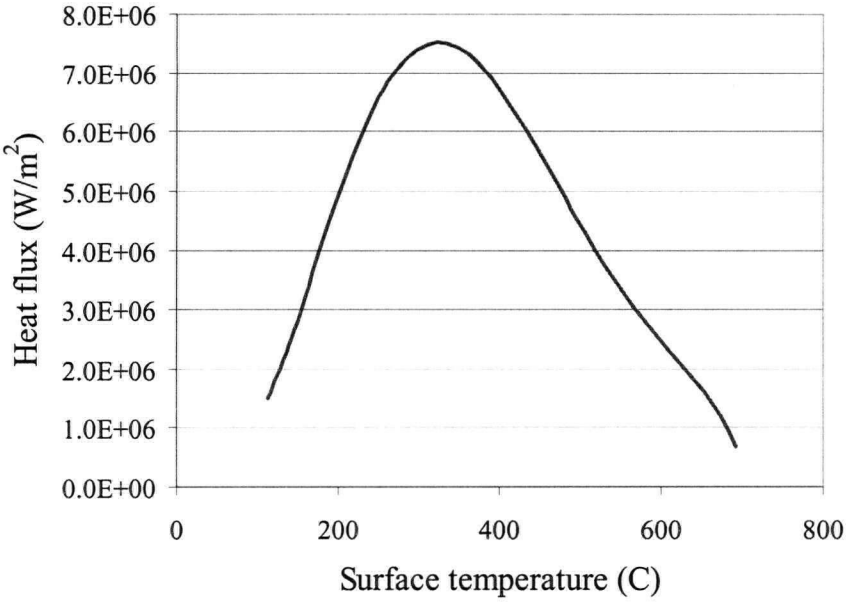

Figure 8.9 – Boiling curve used in the 2D FE conduction model to simulate quench conditions.

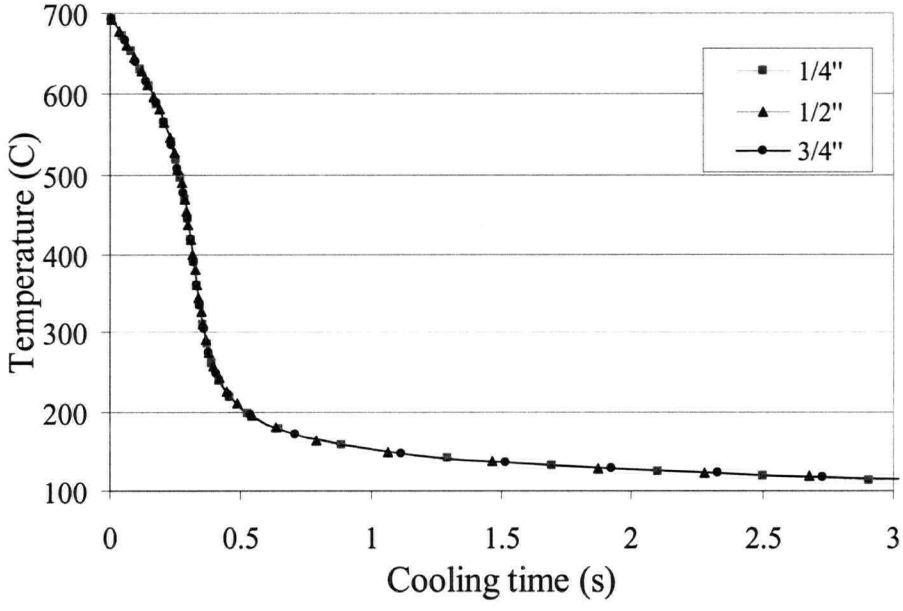

Figure 8.10 – Model-predicted thermal history experienced at the surface of the sample for different thickness samples.

As can be seen in Figure 8.10, under the studied quench conditions, the thermal histories at the surface for each of the samples is almost same. Because the difference in sample thickness does not have any effect on sample surface thermal history under the studied quench conditions, it will have no effect on boiling heat transfer, and thus will have no effect on the calculated boiling curves.

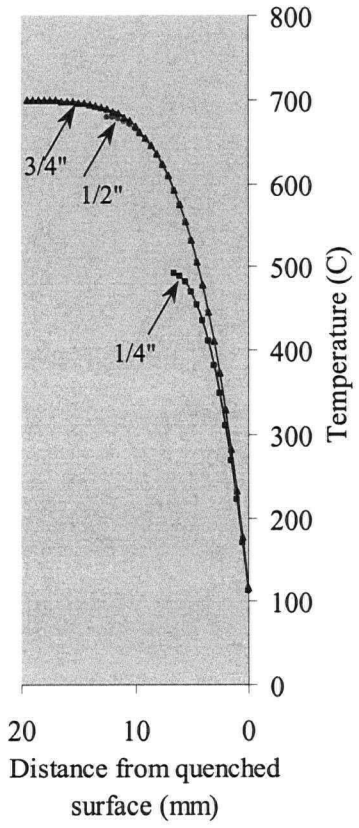

Figure 8.11 – Thermal profile through the sample from the quenched surface to the interior for each sample of different thickness after 3 seconds of cooling.

As can be seen in Figure 8.11, for the sample with a ¼'' thickness, the temperature at the back surface will be much lower than the temperatures at the same

location for the other two samples, because heat can be supplied to that position for the two thicker sample. For the sample of ½'' thickness, the back surface temperature is only slightly lower than the temperature of ¾'' sample at that location. The most important thing about Figure 8.11 is that, no matter what the temperature at the back of the sample is, the temperature gradient across the sample thickness is concentrated close to the quenched surface, and the temperature gradients for all three samples are very similar at the locations around sample surface. As a result, in this case, the sample thickness will have no effect on the calculated boiling curves and this explains why this effect was not observed during our experiments.

CHAPTER 9. SUMMARY AND CONCLUSIONS

9.1 Summary

The design, analysis and control of many metallurgical and materials operations hinges, in part, on being able to quantify the heat transfer occurring at the boundary of the components being processed. In many cases, the components are not processed at steady state; rather they are subject to transients that can encompass large variations in temperature and rates of change in temperature. In light of the need for quantification of heat transfer boundary conditions, and the challenges associated with accurately quantifying heat fluxes during industrial operations, engineers are increasingly turning to Inverse Heat Conduction (IHC) models to quantify surface heat fluxes. In these methods, the surface heat transfer is calculated based on knowledge of the temperature at some known interior location in the product.

Critical to the accurate determination of the surface heat flux is a precise inverse heat conduction model as well as accurate temperature measurement during the quench test. This research has explored the factors that can affect the accuracy of an inverse heat conduction model including material properties, time step used in the model and the assumed thermocouple location.

The research has also done extensive analysis as well as some experiments to determine a "best practices method" to measure the temperature-history experienced by the sample during a quench operation. Specifically, two different temperature measurement techniques including surface, where the thermocouple is located on the

quench surface, and sub-surface, where the thermocouple is located at an interior position, were analyzed in detail to identify and quantify errors that can be induced in the measured data. The research has highlighted the need to include the thermocouple hole in cases where the thermocouples are instrumented at 90° and a severe water quench occurs at the surface of the sample. Although the work in this study has been conducted on steel alloys, the analysis has been extended to other materials and quench conditions and has identified, in a very simple manner using the Biot number, which quench conditions, material and thermocouple conditions, the effect of the thermocouple insulation needs to be included in the IHC analysis.

Historically, even though many of these experimental measurements have been made to quantify the heat transfer boundary conditions during a quench operation, it appears no one has examined the role the T/C installation can play in creating an error in the measurement of the thermal history and hence calculated heat transfer result using an IHC model.

The optimized IHC model and measurement techniques were then used to assess the influence of material start temperature and sample thickness during a water quench test on samples of AISI 316 stainless steel plate. Start temperature is an important parameter during transient quench conditions as it can influence the overall shape and magnitude of the boiling curve. It was determined that, unlike steady-state boiling conditions, under transient boiling conditions, a unique boiling curve does not exist for different start temperatures. Instead the boiling curve becomes a function of the thermal history experienced by the material during the quench and can vary both in magnitude and shape.

The work has also identified a new region in boiling water heat transfer during transient quench conditions that identifies the initial interaction of the water and the hot surface and has been called the initial cooling region. Regardless of the start temperature, the rate of change in the heat flux as a function of surface temperature appears to be the same in this initial cooling region. In cases where the start temperature of the sample is above the Leidenfrost point, after the initial cooling region is complete, the sample will experience the full boiling curve including, film boiling, transition boiling, nucleate boiling and convective cooling. However if the sample start temperature is much below the Leidenfrost point, after the initial cooling region, the sample will only experience nucleate boiling and convective cooling.

The work has proposed a relatively simple method to incorporate the influence of sample start temperature during transient quench conditions on the boiling curve and involves knowing what the full boiling curve is for the quench condition being studied as well as the change in the heat flux as a function of surface temperature during the initial boiling region.

Specifically during this research, the following work has been completed:

1. Model development

1) A 2-D axisymmetric FE thermal conduction model, which can be used for calculating the thermal field under different boundary conditions, was developed and verified.

2) A 2-D axisymmetric IHC model has been developed and verified, which can be used to estimate the heat transfer boundary conditions during cooling of tube and plate samples. The model was verified and can be used under a variety of cooling conditions ranging from an extreme water quench to much slower air cooling.

3) The sensitivity of the IHC model predictions to material thermal properties, time step, and T/C location under different quench conditions was quantified.

4) Phase transformations for the AISI 52100 steel were incorporated into the IHC model and validated experimentally using an air cool test

2. Temperature measurement technique

1) The effect of using a sub-surface thermocouple to measure the temperature during a quench on the sample thermal field was studied. Influence of installation factors such as T/C diameter, T/C location relative to the quench surface, and material properties have been analysed to quantify their influence on the evolving thermal field in the sample during a quench process and the method of accounting for the T/C hole in the IHC model was verified experimentally.

2) The measurement error associated with using a surface thermocouple to measure the temperature history at the surface of sample during a quench operation has been analysed through analytical calculation and mathematical modelling.

3. Boiling heat transfer

1) The influence of the water spray pattern from a single cone nozzle across a flat plate on the boiling heat transfer in both the water spray zone and water flow zone was quantified.

2) The regions during boiling water heat transfer were identified and a new region related to the initial cooling of the sample was proposed.

3) The effect of initial sample temperature on boiling heat transfer was studied and an innovative method was proposed to predict the boiling curve at different initial temperatures.

4) The effect of sample thickness on boiling heat transfer was studied and modelled.

9.2 Conclusions

From this research the following conclusions can be drawn:

1) The IHC model predictions are sensitive to material thermal properties, time step and assumed T/C location. Carefully choosing or measuring these parameters is important to get accurate results.

2) A surface T/C should not be used for measuring sample surface temperature during a quench process due to the significant error introduced as the T/C wire will act as a cooling fin.

3) A sub-surface T/C can be used to measure sample temperature during a quench process; however, it can be necessary to include the T/C hole into the IHC analysis depending on the material being studied, the size of the T/C hole and the

severity of the quench process. A simple check using the Biot number can be done and if it is greater than 0.1, the T/C hole should be included in the analysis.

4) The initial cooling stage plays an important role during a quench process, especially when the initial sample temperature is lower than the Leidenfrost temperature. The initial cooling stage can cause the quench process to go directly into nucleate boiling, and should be distinguished from the transition-boiling regime.

5) The initial temperature of the sample has a significant effect on boiling heat transfer during a transient water quench. The fully developed boiling curve with the four distinct regions, (i.e film boiling, transition boiling, nucleate boiling, and convective cooling), and the rate of change of the heat flux as a function of sample surface temperature during initial cooling can be used to predict the boiling curves at different starting temperatures.

6) For the conditions studied, the sample thickness appeared to have no effect on boiling heat transfer. This occurred because steel has a relatively low thermal conductivity and the samples used in this study were not thin enough.

9.3 Recommendations for Future Work

Based on the current work and the results, there are still a number of areas that warrant further development including:

1) As shown during this research, the initial cooling region plays an important role during a transient quench process typical of industrial conditions. One important

characteristic of the initial cooling region is that the rate of change in the heat flux as a function of surface temperature appears to be the same regardless of the initial sample temperature. The fundamental theory and mechanisms behind this should be further studied and quantified so that a greater understanding of this region is obtained.

2) An area that has received very little attention in transient boiling water heat transfer is the capacity of the sample to supply heat to its surface and the influence on boiling water heat transfer. Although an attempt was made to quantify this during the present work by examining the role of sample thickness on boiling water heat transfer, the expected effect was not seen. The reason for this was because the minimum thickness of stainless steel sample we could evaluate, without experiencing significant warping due to the severe quench, was not thin enough to demonstrate this effect. This work should be repeated for other materials that have a much higher thermal conductivity such as aluminium or copper so that the influence of thickness or sample capacity to supply heat can be evaluated.

BIBLIOGRAPHY

I. V. Samarasekera, D. Q. Jin and J. K. Brimacombe, "The application of microstructure engineering to the hot rolling of steel", 38th MWSP CONF. PROC., ISS, Vol. XXXIV, 1997, pp 313-327.

2. A. Prasad, S. Jha and N. S. Mishra, "Modeling of microstructural evolution during accelerated cooling of hot strip on the runout table", Steel Research 66, No. 10, 1995, pp 416-423.

3. Ch. Dilg, J. Kirsch, W. Schutz, E. Amoris and A. Streibelberger, "TMCP process including two accelerated cooling stages", La Revue De Metallurgie-CIT, 1995, pp884-892.

4. A. Kumar, C. McCulloch, E. B. Hawbolt, and I. V. Samarasekera, "Modelling thermal and microstructural evolution on runout table of hot strip mill", Materials Science and Technology, April 1991, Vol.7, pp360-368.

5. C. A. Muojekwu, D. Q. Jin, V. H. Hernandez, I. V. Samarasekera and J. K. Brimacombe, "Hot-direct rolling, runout table cooling and mechanical properties of steel strips produced from thin slabs", 38th Mechanical Working and Steel Processing Conference proceedings: volume XXXIV Cleveland, Ohio, October 13-16, 1996, pp351-366.

6. R.V. Kolarik, "Controlled thermo-mechanical processing of tubes and pipes for enhanced manufacturing and performance", Timken internal report.

7. W. J. Lawrence, A. F. MacAlister and P. J. Reeve, "On line modeling and control of strip cooling", Ironmaking and Steelmaking, 1996, Vol. 23, No. 1, pp74-78.

8. J. B. Hernandez-Morales, "Heat transfer and stress generation during forced convective quenching of steel bars", Ph.D. thesis, UBC, 1996.5.

9. M. Lin and S. S. Hansen, "Effects of run-out table cooling profile on the mechanical properities of C-Mn and C-Mn-Nb-V steels", 37th MWSP CONF. PROC., ISS, Vol. XXXIII, 1996, pp79-88.

10. W. B. Morrison, "Microstructure control in practice", Ironmaking and Steelmaking 1995, Vol.22, No.6, pp453-458.

11. Y. Hagasaka, J. K. Brimacombe, E. B. Hawbolt, I. V. Samarasekera, B. Hernandez-Morales and S. E. Chidiac, "Mathematical model of phase transformation and eleastoplastic stress in the water spray quenching of steel bars", Metallurgical Transactions A, Volume 24A, April 1993, pp795-808.

12. L.C. Burmeister, Convectoion Heat Transfer (second edition), John Wiley & Sons Inc., 1993.

13. E. K. Kalinin, I. I. Berlin, and V.V. Kostyuk, "Film-boiling heat transfer", Advances in Heat Transfer, Vol. 11, 1975, pp. 51-197.

14. B. W. Webb and C. F. Ma, "Single-phase liquid jet impingement heat transfer", Advances in Heat Transfer, Vol. 26, pp. 105-217.

15. D. H. Wolf, F.P. Incropera, and R. Viskanta, "Jet impingement boiling", Advances in Heat Transfer, Vol. 23, pp.1-131.

16. J. Filipovic, F. P. Incropera, And R. Viskanta, "Quenching phenomena associated with a water wall jet: II. Comparison of experimental and therotical results for the film boiling region", Experimental Heat Transfer, Vol. 8, 1995, pp. 119-130.

17. Dianfeng Li, The effect of surface roughness on the heat transfer during DC casting process, Master Thesis, University of British Columbia, 1999.

18. D. Li, M. A. Wells and G. Lockhart, "Effect of surface morphology on boiling water heat transfer during secondary cooling of the DC casting process", Light Metals 2001, pp865-871.

19. J. Filipovic, F. P. Incropera, And R. Viskanta, "Quenching phenomena associated with a water wall jet: I. Transient hydrodynamic and thermal conditions", Experimental Heat Transfer, Vol. 8, 1995, pp. 97-117.

20. M. Raudensky, J. Horsky, A. A. Tseng and C. Weng, "Heat transfer evaluation of impingement cooling in hot rolling of shaped steels", The 1994 International Mechanical Engineering Congress and Exposition, Chicago, IL, USA, pp. 683-688

21. S. Chen, J. Kothari and A. A. Tseng, "Cooling of a moving plate with an impinging circular water jet", Experimental Thermal and Field Science 1991, No. 4, pp343-353.

22. M. Raudensky, L. Bending and J. Horsky, "Experimental study of heat transfer in process of rolls cooling in rolling mills by water jets", Steel Research 65 (1994) No. 1, pp29-35.

23. D. A. Zumbrunnen, R. Viskanta and F. P. Incropera, "The effect of surface motion on forced convection film boiling heat transfer", ASME J. Heat Transfer, 111, pp. 760-766, 1989.

24. S. Chen, J. Kothari and A. A. Tseng, "Cooling of a moving plate with an impinging circular water jet", Experimental Thermal and Field Science 1991, No. 4, pp343-353.

25. I. Stewart, J. D. Massingham and J. J. Hagers, "Heat transfer coefficient effects on spray cooling", Iron and Steel Engineer, July, 1996, pp17-23.

26. M. Raudensky and J. Horsky, "Thermal model of rolls and sheets improvement by experimental study of cooling", Journal of Materials Processing Technology, 34 (1992) 247-253

27. U. Reiners, R. Jeschar, R. Scholz, D. Zebrowski and W. Reichlet, "A measuring method for quick determination of local heat transfer coefficients in spray water cooling within the range of stable boiling", Steel Res. 5, 1985, pp226-238.

28. A. Moriyama, K. Araki, M. Yamagami and K. Mase, "Local heat transfer coefficient in spray cooling of hot surface", Trans. ISIJ, 28, 1988, pp104-109.

29. M. A. Ruch and J. P. Holman, "Boiling heat transfer to a freon-113 jet impinging upward onto a flat heat surface", Int. J. Heat Mass Transfer, 18. 1975, pp51-60.

30. M. Monde, and Y. Katto, "Burnout in a high heat-flux boiling system with an impinging jet", Int. J. Heat Mass transfer, 21, 1978, pp295-305.

31. S. Ishigai, S. Nakanishi And T. Ochi, "Boiling heat transfer for a planar jet impinging on a hot surface", Proceedings of the 6th International Heat Transfer Conference, Toronto, Canada, Vo. 1, 1978, pp445-450.

32. D. A. Zumbrunnen, R. Viskanta and F. P. Incropera, "The effect of surface motion on forced convection film boiling heat transfer", ASME J. Heat Transfer, 111, 1989, pp760-766.

33. F. Moreaux and P. Archambault, "Some developments about spray quenching", Materials Australia: The Magazine of Engineering Materials Technology, 24(2), 1992, pp14-16.

34. A. A. Tseng, S. J. Chen and C. R. Westgate, "Determination of local heat transfer coefficients for modeling rolling processes", Symposium on Modeling of Materials Processing, ASME MD- Vol. 3, 1987, pp51-64.

35. A. A. Tseng, F. H. Lin, A. S. Gunderia and D. S. Ni, "roll cooling and its relationship to roll life", Metall. Trans. A, 20A, 1989, pp2305-2320.

36. N. Hatta, and H. Oskabe, "Numerical modeling for cooling process of a moving hot plate by laminar water curtain", ISIJ Int., 29(11), 1989, pp 919-925.

37. S. J. Chen, and J. Kothari, "Temperature distribution and heat transfer of a moving metals strip cooled by a water jet", ASME Paper No. 88-WA/NE-4, 1988.

38. D. E. Hall, F. P. Incropera, and R. Viskanta, "Jet impingement boiling from circular free-surface jets during quenching experiments", HTD-Vol. 333, Proceedings of the ASME Heat Transfer Division, Vol. 2, ASME 1996, pp131-141.

39. S. Kumagai, S. Suzuki, Y. Sano, M. Kawazoe, "Transient cooling of a hot metal slab by an impinging jet with boiling heat transfer", Proceedings, ASME/JSME Thermal Engineering Conference, 1995, pp347-352.

40. V. Olden, A. Smabrekke, and M. Raudensky, "Numerical simulation of transient cooling of hot rolled asymmetrical ship profile (Holland profile), Ironmaking and Steelmaking 1996, vol.23, No. 1, pp88-91.

41. Z. Liu, Experiments and mathematical modelling of controlled runout table cooling in a hot rolling mill, Ph.D. Thesis, University of British Columbia, 2001.

42. N. Hatta, Y. Tanaka, H. Takuda and J. Kokado, "A numerical study on the cooling process of hot steel plates by a water curtain", 1989 ISIJ, pp673-679.

43. J. F. Grandfield, A. Hoadley and S. Instone, "Water cooling in direct chill casting: Part 1, boiling theory and control", Light Metals 1997, pp691-699.

44. J. Langlais, T. Bourgeois, Y. Caron, G. Beland and D. Bernard, "Measuring the heat extraction capacity of DC casting cooling water", Light Metals 1995, pp979-986.

45. Y. Ho, "The effect of cooling water quality on aluminium ingot casting", Light Metals 1985, pp1331-1347.

46. T. Ochi, S. Nakanishi, M. Kaji, and S. Ishigai, "Cooling of a hot plate with an impinging circular water jet", Proceedings, Multiphase Flow and Heat Transfer III, T. N. Veziroglu and A. E. Bergles, eds., Elsevier, 1983, pp671-681.

47. K. Matsuda, S. Nagai, Y. Miyaqta, H. Maehara and I. Tsukuda, "Prevention of cast cracks in Al-Zn-Mg-Cu alloy Casting", 6th International Aluminium Extrusion Technology Seminar, VI, Aluminium Association & Aluminium Extruders Council 1996, pp525-528.

48. M. Raudensky, L. Bending and J. Horsky, "Experimental study of heat transfer in process of rolls cooling in rolling mills by water jets", Steel Research 65 (1994) No. 1, pp29-35.

49. L. Bendig, M. Raudensky, and J. Horsky, "Spray parameters and heat transfer coefficients of spray nozzles for continuous casting", 78th Steelmaking Conference, 1995 Steelmaking Conference Proceedings, Vol. 78, Apr. 1995, pp391-398.

50. D. Hall, F. P. Incropera and R. Viskanta, "Jet impingement boiling", Advances in Heat Transfer, 1993, 23, pp1-132.

51. J. Horsky, M. Raudensky and W. Sauer, "Experimental study of cooling characteristics in hot rolling", Journal of Materials Processing Technology, vol. 45, 1994, pp131-135.

52. P. J. Berenso, "Experiments on pool boiling heat transfer", Int. J. Heat & Mass Transfer, Vol. 5, 1962, pp985-999.

53. T. D. Bui and V.K. Dhir, "Transition boiling heat transfer on a vertical surface", ASME, J. Heat Transfer, Vol. 107, 1985, pp756-763.

54. M. Shoji, et al, "Liquid-solid contact and effects of surface roughness and wetability in film and transition boiling on a horizontal large surface", Pro. 9th Int. Heat Transfer Conf. 1990, Vol.3. pp135-140.

55. J. D. B. and I. M. "An experimental investigation into the relationship between temperature-time history and surface roughness in the spray quenching of aluminium parts", J. of Engineering Materials and Technology, 1996, Vol. 118, pp127-134.

56. M.A. Wells, D. Li and S.L. Cockcroft, "Influence of surface morphology, water flow rate, and sample thermal history on the boiling-water heat transfer during direct-chill casting of commercial aluminum alloys", Metallurgical and Materials Transactions B, Volume 32B, October, 2001, pp929-939.

57. B. Hernandez-Morales and R. Colas, "On the characterization of the heat transfer boundary condition during quenching", The 1st International Automotive Heat Treating Conference, Proceedings of The 1st International Automotive Heat Treating Conference, 13-15 July 1998, Puerto Vallarta, Mexico, pp465-471.

58. M. Bamberger and B. Prinz, "Determination of heat transfer coefficients during water cooling of metals", Materials Science and Technology, 2, 1986, pp410-415.

59. V. K. Dhir, "Nucleate and transition boiling heat transfer under pool and external flow conditions". Int. Heat Transfer 1990, Vol. 1, G. Hetsroni, Ed., Hemisphere Publishing Comp., New York, 1990, pp129-155.

60. H. Auracher, "Transition boiling", Int. Heat Transfer 1990, Vol. 1, , G. Hetsroni, Ed., Hemisphere Publishing Comp., New York, 1990, pp69-90.

61. F. P. Incropera and D. P. De Witt, Fundamentals of Heat and Mass Transfer, 3rd ed., Wesley & Sons, New York, 1990.

62. J. V. Beck, B. Blackwell, "Inverse problems", Handbook of Numerical Heat Transfer, Wiley, New York, 1988 (Chapter 19).

63. O. R. Burggraf, "An exact solution of the inverse problem in heat conduction theory and application", Journal of Heat Transfer 86C, 1964, pp373-382.

64. M. Imber and J. Khan, "Prediction of transient temperature distributions with embedded thermocouples", AIAAJ, Vol. 10, 1972, pp784-789.

65. D. Langford, "New analytic solutions of the one-dimensional heat equation for temperature and heat flow rate both prescribed at the same fixed boundary (with applications to the phase change problem)", Q. Appl. Math, Vol. 24, 1967, pp315-322.

66. V. A. Kover'yanov "Inverse problem of non steady-state thermal conductivity", Teplofizika Vysokikh temperature, Vo. 5(1), 1967, pp141-143.

67. A. N. Tokhonov and V. Y. Arsenin, Solutions of Ill-posed Problems, V. H. Winston, Washington, DC., 1977.

68. O. M. Alifanov, E. A. Artyukhin and S.V. Rumyantsev, "Exterme methods for solving ill-posed problems with applications to inverse heat transfer", Begell House, New York, 1995.

69. M. K. Alam, H. Pasic, L. Anagurthi, and R. Zhong, "Determination of surface heat flux in quenching", HTD-Vol. 364-3, Proceedings of the ASME, Heat Transfer Division, vol. 3, 1999, ASME 1999, pp349-356.

70. J. Taler, "Theory of transient experimental techniques for surface heat transfer", Int. J. Heat Mass Transfer, Vol. 39, No. 17, 1996, pp3733-3748.

71. J. V. Beck, B. Litkouhi, and St. Clair, "Efficient sequential solution of the nonlinear inverse heat conduction problem", Numerical Heat Transfer, Vol. 5, 1982, pp275-286.

72. J. R. Burggraf, "An exact solution of the inverse problem in heat conduction, theory and application", Journal of Heat Transfer, Vol. 86, 1964, pp373-382.

73. J. V. Beck, "Surface heat flux determination using an integral method", Nucl. Eng. Des., Vol. 7, 1968, pp170-178.

74. C. F. Weber, "Analysis and solution of the ill-posed inverse heat conduction problem", Int. J. Heat Mass Transfer, Vol. 24, 1981, pp1783-1792.

75. A. A. Tseng, J. G. Chang, M. Raudensky and J. Horsky, "An inverse finite element evaluation of roll cooling in hot rolling of steels", Journal of Materials Processing &

Manufacturing Science, Vol. 3, No. 4, 1995, pp387-408.

76. D. Lesnic, L. Elliott, and D. B. Ingham, "The solution of an inverse heat conduction problem subject to the specification of energies", Int. J. Heat Mass Transfer, Vol. 41, 1998, pp25-32.

77. C. H. Huang, T. M. Ju and A. A. Tseng, "The estimation of surface thermal behaviour of the working roll in hot rolling process", Int. J. Heat Mass Transfer, Vol. 38, 1995, pp1019-1031.

78. R. G. Keanini, "Inverse estimation of surface heat flux distributions during high speed rolling using remote thermal measurements", Int. J. Heat Mass Transfer, Vol. 41, 1998, pp275-285.

79. M. Raynaud and J. Bransier, "A new finite-difference method for the nonlinear inverse heat conduction problem", Numerical Heat Transfer, Part B, No. 9, 1986, pp27-42.

80. E. Hensel, Inverse Theory and Applications for Engineers, Prentice-Hall, New Jersey, 1986, pp142-164.

81. D. A. Murio, "The mollification and the numerical solution of the inverse heat conduction problem by finite difference", Computer & mathematics with Applications, No. 17, 1989, pp1385-1396.

82. O. M. Alifanov, Inverse Heat Transfer Problem, Springer, New York, 1994, pp227-281.

83. A. A. Tseng, T. C. Chen, F. Z. Zhao, "Direct sensitivity coefficient method for solving two-dimensional inverse heat conduction problems by finite element scheme", Numerical Heat Transfer, Part B, no. 27, 1995, pp291-307.

84. A. A. Tseng, K. Bera, M. Raudensky, J. Horsky, and J. G. Change, "An inverse finite element evolution of roll cooling in hot rolling of steels", Novel Techniques in Synthesis and Processing of Advanced Materials, Edited by J. Singh and S. M. Copley, The Minerals, Metals & Materials Society, 1995, pp345-363.

85. B. Hernandez-Morales, S. M. Gupta, J. K. Birmacombe and E. B. Hawbolt, "Determination of quench heat transfer coefficients using inverse techniques", Proc. Of the 1st Int. Conf. on Quenching and Distortion control, G. E. Totten eds. ASM International, Metals Park, OH, 1992, pp155-164.

86. B. Hernandez-Morales, J. K. Brimacombe and E. B. Hawbolt, " Application of

inverse technique to determine heat-transfer coefficients in heat-treating operations", J. of Materials Engineering and Performance, 1(6), 1992, pp763-771.

87. B. Hernandez-Morales, J. K. Brimacombe and E. B. Hawbolt, "Characterization of the boundary condition in heat treatment operation using an inverse heat conduction algorithm", Proc. of the 1995 International Mechanical Engineering Congress, ASME Heat Transfer Division, Vol. 317-2, San Francisco, California, 1995, pp559-566.

88. S. Chantasiriwan, "Inverse heat conduction problem of determining time-dependent heat transfer coefficient", International Journal of Heat and Mass Transfer, 42(1999), pp4275-4285.

89. A. M. Osman, J. V. Beck, "Investigation of transient heat transfer coefficients in quenching experiments", Journal of Heat Transfer, No. 112, 1990, pp843-848.

90. N. J. Ruperti, J. M. Raynaud and J. F. Sacadura, "A method for the solution of the coupled inverse heat conduction-radiation problem", Journal of Heat Transfer, Transactions of the ASME, Vol. 118, Feb. 1996, pp10-17.

91. K. Hurpisz, "Numerical solution of one case of inverse heat conduction problem", Journal of Heat Transfer, Transaction of the ASME, Vol. 113, May 1991, pp280-286.

92. P. Archambault, S. Denis and A. Azim, "Inverse resolution of the heat-transfer equation with internal heat source: Application to the quenching of steels with phase transformations", Journal of Materials Engineering and Performance, Vol. 6(2), 1997, pp240-246.

93.H. J. Reinhardt, "Towards a stability and error analysis of sequential methods for the inverse heat conduction problem", Proc. 1 Int. Conf. Inverse Problem Eng. Theory Pract. ASME, New York, NY, 1993, pp111-116.

94. J. Taler, "Semi-numerical method for solving inverse heat conduction problems", Heat and Mass Transfer/Waerme-und Stoffuebertragung, Vol. 24, No. 4, pp455-474.

95. A. Maciag and M. J. Al-Khatib, "Stability of solutions of the over determined inverse heat conduction problems when discredited with respect to time", Internal Journal of Numerical Methods for Heat & Fluid Flow, Vol. 10, No. 2, 2000, pp228-244.

96. K. A. Woodbury, "Effect of thermocouple sensor dynamics on surface heat flux predications obtained via inverse heat transfer analysis", Int. J. Heat Mass Transfer, Vol. 33, No. 12, 1990, pp2641-2649.

97. R. Colas and C. M. Sellars, "Computed temperature profiles of hot rolled plate and strip during accelerated aooling", Accelerated Cooling of Rolled Steel, Winnipeg, Canada, 24-25 Aug. 1987, pp121-130.

98. G. Tack, H. Letzke and E. Qaquet: Proc. Symp. On 'Accelerated cooling of steel', Pittsburgh, PA, 19-21 Aug. 1985, The Metallurgical Society of AIME, pp35-54.

99. E. B. Longenberger, "Computer modeling of a hot strip mill runout table", Mechanical Working and Steel Processing. Vol. XXIV. 28th Mechanical Working and Steel Processing Conference Proceedings, Pittsburgh, Pennsylvania, USA, 26-28 Oct. 1986, pp169-172.

100. Y. Miyake, T. Nishide and S. Moriya, "Device and system for controlled cooling for hot strip mill", Trans. Iron Steel Inst. Japan, vol. 20, No. 7, 1980, pp496-503.

101. E. N. Hinrichsen, "Hot strip mill runout table cooling--system view of control, operation and equipment", Iron Steel Eng., Oct. 1976, 53, (10), pp29-34.

102. H. Yada, "Prediction of microstructural changes and mechanical properties in hot strip rolling", Accelerated Cooling of Rolled Steel, Winnipeg, Canada, 24-25 Aug. 1987, pp105-119.

103. M. Morita, K. Hashiguchi, O. Hashimoto, M. Nishida and S. Okano, "On-line transformation detector for property control of hot rolled steel", Accelerated Cooling of Steel, Pittsburgh, Pennsylvania, USA, 19-21 Aug. 1985, The Metallurgical Society/AIME, 1986, pp449-461.

104. A. Hurkmans, G. A. Duit, T. M. Hoogendoorn and F. Hollander, "Accelerated cooling and the transformation of steel", Accelerated Cooling of Steel, Pittsburgh, Pennsylvania, USA, 19-21 Aug. 1985, The Metallurgical Society/AIME, 1986, pp 481-499.

105. L. Henrich, R. Hola and G. Kneppe, "Physically based cooling line model to meet growing demands in temperature and flexibility", Ironmaking and Steelmaking 1996, Vol. 23, No. 1, pp79-81.

106. A. Kumar, C. McCulloch, E. B. Hawbolt and I. V. Samarasekera, "Modelling thermal and microstructural evolution on runout table of hot strip mill", Materials Science and Technology, April 1991, Vol.7, pp360-368.

107. B. Hildenwall and T. Ericsson, "Prediction of residual stresses in case-hardening steels", Hardenability Concepts With Applications to Steel, Chicago, Ill., 24-26 Oct. 1977, Metallurgical Society AIME, 1978, pp579-606.

108. P.C. Campbell, E. B. Hawbolt and J. K. Brimacome, "Microstructural engineering applied to the controlled cooling of steel wire rod: Part II. Microstructural evolution

and mechanical properties correlations", Metallurgical Transactions A, Vol. 22A, Nov., 1991, pp2779-2790.

109. M. Avrami: J. Chem. Phys., 1939, vol. 7, pp1103-1112.

110. M. Umemoto, N. Komatsubara and I. Tamura, "Prediction of hardenability effects from isothermal transformation kinetics", : J. Heat Treating, 1980, Vol. 1, No. 3, pp57-64.

111. J. W. Cahn: Acta Met., 1956, Vol. 4, pp572-275.

112. J. W. Christian: The Theory of Transformations in Metals and Alloys, Pergamon Press, 1965, pp471-495.

113. M. B. Kuban, R. Jayaraman, E.B. Hawbolt and J. K. Brimacombe: Metall. Trans., A, 1986, Vol. 17A, pp1493-1503.

114. M. Avrami: J. Chem. Phys., 1940, 8, pp212-224.

115. M. Avrami: J. Chem. Phys., 1941, 9, pp177-184

116. A. Johnson and R. F. Mehl: Trans. AIME, 1939, vol. 135, pp416-458.

117. E. B. Hawbolt, B. Chau and J. K. Brimacombe, "Kinetics of austenite--ferrite and austenite--pearlite transformations in a 1025 Carbon Steel", Metall. Trans. A. 1985, vol. 16A, pp565-578.

118. E. B. Hawbolt, B. Chau and J. K. Brimacombe: Metall. Trans. A. 1983, vol. 14A, pp1803-1815.

119. D. P. Koistinen and R. E. Marburger: Acta Metall., 1957, vol. 7(1), pp59-60.

120. P. Archambault, S. Denis and A. Azim, "Inverse resolution of the heat-transfer equation with internal heat source: Application to the quenching of steels with phase transformations", Journal of Materials Engineering and Performance, Vol. 6(2), 1997, pp240-246

121. K. W. Andrews, JISI, 1965, 203, (7), July, pp721-727.

122. W. Steven and A.G. Haynes, JISI, 1956, 183, (4), Aug., pp349-359.

123. M. Atkins and B Met, "Atlas of Continuous Cooling Transformation Diagrams for Engineering Steels", British Steel Corporation, 1977.

124. D. Jin, E. Dominik, R. V. Kolarik, J. Ives and E. Damn, "Modeling of controlled thermo-mechanical processing of tubes for enhanced manufacturing and performance", Acta Metallurgica Sinica (English Letters) (China), vol. 13, no. 2, Apr. 2000, pp832-842.

125. William S. J, "Engineering Heat Transfer", PWS Engineering, 1986.

126. Omega Engineering, Inc., "The Temperature Handbook", Vol. 29, 1995.

127. J. V. Beck, et al., "Inverse Heat Conduction — Ill-posed Problem", A Wiley-Interscience Publication, by John Wiley & Sons, Inc., 1985.

APPENDIX A. FINITE ELEMENT METHOD USED IN HEAT CONDUCTION ALGORITHM

1. Basic heat transfer

Referring to Figure A.1, a general 2-D axisymmetric heat conduction model based on the FE method was developed to describe heat transfer in a tube. The model was formulated in a general manner so that it could encompass and be used for the wide variety of geometries used in this study; ranging from industrial tubes, to solid cylinder, to flat circular plates, and to interior thermocouple holes so that the influence of thermocouple installation on the local thermal field in the sample could be assessed. As can be seen in Figure A.1, heat transfer in the tube was assumed to occur in the radial or r-direction to both the outer diameter (OD) as well as the inner diameter (ID) of the tube as well as the axial or z-direction towards the ends of the tube. Heat transfer in the θ-direction was assumed to be equal to zero. Hence, this model is applicable in cases where there is little or no circumferential variation in heat transfer.

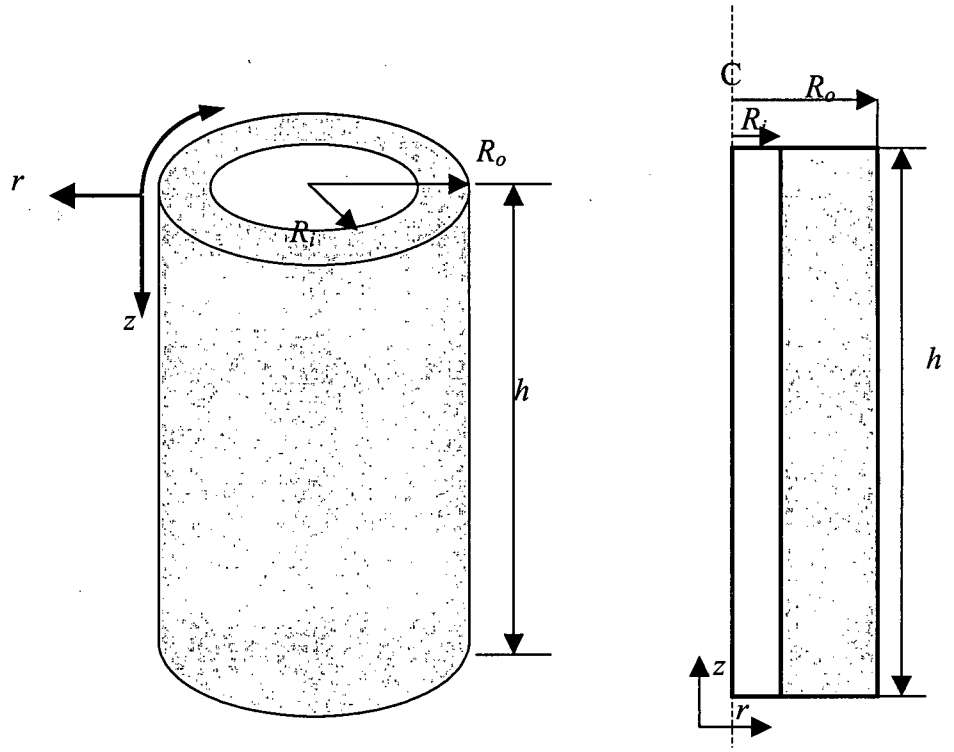

Figure A.1 – Schematic of the geometry used for the 2-D heat conduction model.

In view of the above assumptions, the flow of heat in the sample can be described as follows:

$$\frac{1}{r}\frac{\partial}{\partial r}\left(kr\frac{\partial T}{\partial r}\right)+\frac{\partial}{\partial z}\left(k\frac{\partial T}{\partial z}\right)+\dot{Q}=\rho C_p\frac{\partial T}{\partial t} \qquad \text{(A.1)}$$

where $\dot{Q}$ is the latent heat associated with phase transformations that occur in the steel.

The applicable boundary conditions and initial conditions for the model are defined as follows:

1) At the outside of the tube, $r = R_o$, at times greater than 0 (i.e., $t>0$);

$$-k\left.\frac{\partial T}{\partial r}\right|_{r=R_o} = h_1(T - T_c) = q_1 \tag{A.2}$$

2) At the inner diameter of the tube, $r = R_i$ and times greater than 0 (i.e., t > 0);

$$-k\left.\frac{\partial T}{\partial r}\right|_{r=R_i} = h_2(T - T_c) = q_2 \tag{A.3}$$

3) At the upper end of the tube, $z = h$ and times greater than 0 (i.e., t>0);

$$-k\left.\frac{\partial T}{\partial z}\right|_{z=h} = h_3(T - T_c) = q_3 \tag{A.4}$$

4) At the lower end of the tube, $z = 0$ and times greater than 0 (i.e., t>0);

$$-k\left.\frac{\partial T}{\partial z}\right|_{z=0} = h_4(T - T_c) = q_4 \tag{A.5}$$

5) The initial condition is given by:

$$T(r,z)\big|_{t=0} = T_i(r,z) \tag{A.6}$$

2. FEM algorithm

The finite element solution to the Partial Differential Equation (P.D.E.) is based on the method of weighted residuals. This is a general method for deriving approximate solution to linear and non-linear P.D.E. The technique involves steps:

1) assume the general functional behavior of the temperature, i.e., some approximate solution for the P.D.E.

2) substitute the approximate solution into the P.D.E. and require the error or residual to be minimized.

The function shown in Equation A.7 was chosen to approximately solve the PDE:

$$T \approx \tilde{T} = \sum_{i=1}^{m} N_i(r,z) T_i \tag{A.7}$$

where T is the exact solution.

$\tilde{T}$ is the approximate solution that we have assumed.

T_i is the node temperature.

N_i is the interpolating polynomial or the shape function.

In general, the interpolating or shape functions are polynomials of a degree dependent on the number of nodes per element. The shape function would become very complex and cumbersome for higher order elements.

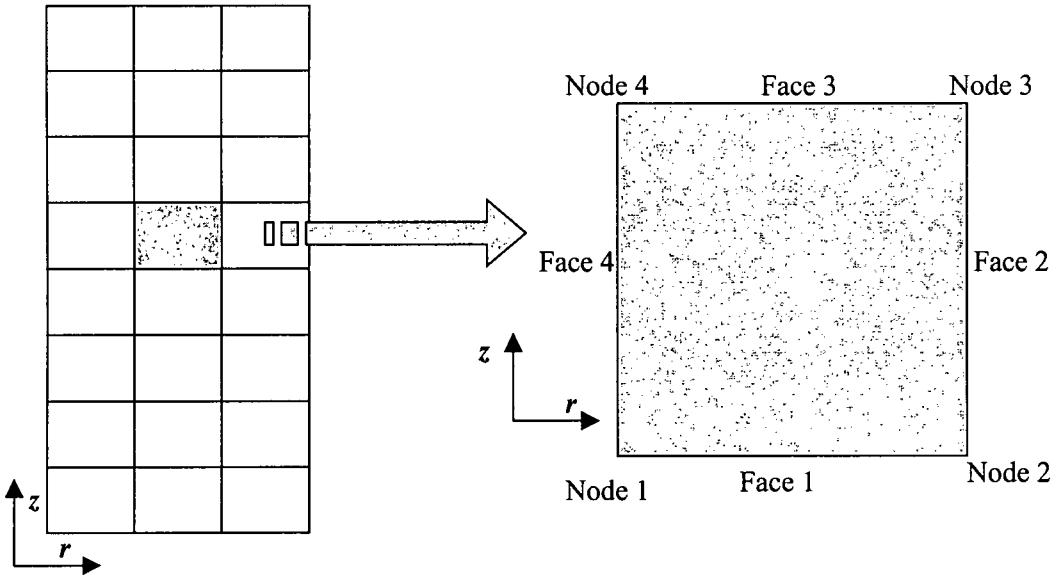

a) geometry with mesh b) a 2-D 4-node element.

Figure A.2. – Schematic of the 2-D axisymmetric FE analysis showing: a) geometry with mesh and b) a 2-D 4-node element

For our FEM model, a 2-D, 4-node, linear temperature element was used as shown in Figure A.2. The coordinate of each element should be (*r*, *z*), but to simplify its definition, the element shape function is usually defined in terms of the local u, v coordinate system (Figure A.3) as shown in Equation A.8:

$$N_i(u,v) = \frac{1}{4}(1+u_0)(1+v_0) \tag{A.8}$$

where $u_0 = uu_i$ $v_0 = vv_i$

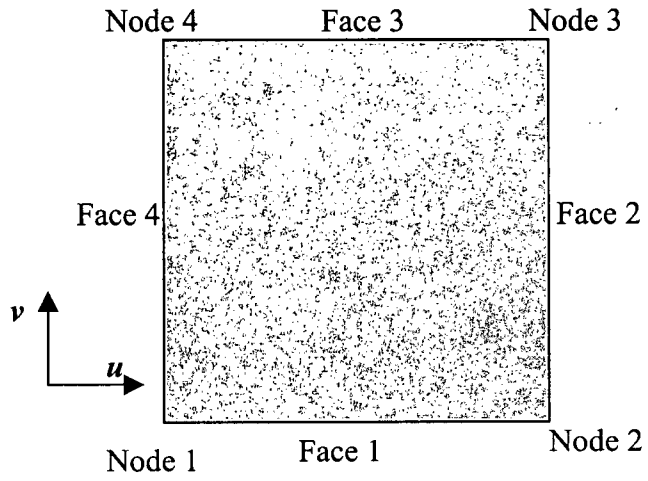

Figure A.3. - 2-D, 4-node linear element used in FE model in local u and v coordinate system

The shape function shown in Equation A.8 can be substituted into Equation A.6, and the expression for the approximate temperature becomes:

$$\tilde{T}(u,v) = \sum_{i=1}^{m} N_i(u,v) T_i^e \tag{A.9}$$

The transformation from the local coordinate to the global coordinate system is done by simply interpolation using the same shape functions shown in Equations A.10 and A.11.

$$r = \sum_{i=1}^{m} N_i(u,v) r_i \tag{A.10}$$

$$z = \sum_{i=1}^{m} N_i(u,v) z_i \tag{A.11}$$

For the case where the interpolating polynomials applied to the coordinate transformation are the same as those adopted for the field variable, the element is referred to as an iso-parametric element.

Substituting the approximation $\tilde{T}$ for T into the P.D.E equation yields:

$$\iint_D w_i \left[\frac{1}{r}\frac{\partial}{\partial r}\left(kr\frac{\partial \tilde{T}}{\partial r}\right) + \frac{1}{r}\frac{\partial}{\partial z}\left(kr\frac{\partial \tilde{T}}{\partial z}\right) + \dot{Q} - \rho C_p \frac{\partial \tilde{T}}{\partial t}\right] dD = \iint_D R w_i dD = 0 \tag{A.12}$$

If $w_i = N_i$ is assumed, the above equation will become:

$$\iint_D N_i \left[\frac{1}{r}\frac{\partial}{\partial r}\left(kr\frac{\partial \tilde{T}}{\partial r}\right) + \frac{1}{r}\frac{\partial}{\partial z}\left(kr\frac{\partial \tilde{T}}{\partial z}\right) + \dot{Q} - \rho C_p \frac{\partial \tilde{T}}{\partial t}\right] dD = \iint_D R N_i dD = 0 \tag{A.13}$$

On an element level:

$$\iint_D N_i \left[\frac{1}{r}\frac{\partial}{\partial r}\left(kr\frac{\partial \tilde{T}^e}{\partial r}\right) + \frac{1}{r}\frac{\partial}{\partial z}\left(kr\frac{\partial \tilde{T}^e}{\partial z}\right) + \dot{Q} - \rho C_p \frac{\partial \tilde{T}^e}{\partial t}\right] dD = 0 \tag{A.14}$$

Because $dD = 2\pi r dr dz$, the above equation becomes:

$$\iint_{A^e} N_i \left[\frac{\partial}{\partial r}\left(kr\frac{\partial \tilde{T}^e}{\partial r}\right) + \frac{\partial}{\partial z}\left(kr\frac{\partial \tilde{T}^e}{\partial z}\right) + \dot{Q} r - \rho C_p r \frac{\partial \tilde{T}^e}{\partial t}\right] dr dz = 0 \tag{A.15}$$

Applying the Green-Gauss theorem to the terms that involve second-order derivatives and after some manipulation:

$$\int_{C^e} N_i kr \frac{\partial \tilde{T}^e}{\partial r} n_r dC - \iint_{A^e} \frac{\partial N_i}{\partial r} kr \frac{\partial \tilde{T}^e}{\partial r} drdz + \int_{C^e} N_i kr \frac{\partial \tilde{T}^e}{\partial z} n_z dC - \iint_{A^e} \frac{\partial N_i}{\partial z} kr \frac{\partial \tilde{T}^e}{\partial z} drdz \tag{A.16}$$

$$+ \iint_{A^e} N_i \dot{Q} rdrdz - \iint_{A^e} N_i \rho C_p r \frac{\partial \tilde{T}^e}{\partial t} drdz = 0$$

Conductivity term

$$\iint_{A^e} k\left(\left[\frac{\partial N}{\partial r}\right]\{T^e\}\frac{\partial N_i}{\partial r} + \left[\frac{\partial N}{\partial z}\right]\{T^e\}\frac{\partial N_i}{\partial z}\right) rdrdz \quad i=1,n \tag{A.17}$$

Because the above equation is true for all the element nodes, we get

$$\iint_{A^e} k\left(\left[\frac{\partial N}{\partial r}\right]\frac{\partial N_i}{\partial r} + \left[\frac{\partial N}{\partial z}\right]\frac{\partial N_i}{\partial z}\right) rdrdz\{T^e\} \tag{A.18}$$

After some manipulation, it turns out to be an expression of the form

$$[K_C]^e\{T^e\} \tag{A.19}$$

$$[K_C]^e = \iint_{A^e} [B]^T [K][B] rdrdz \tag{A.20}$$

$$[B]_{2\times n} = \begin{bmatrix} \frac{\partial N_1}{\partial r} & -- & \frac{\partial N_n}{\partial r} \\ \frac{\partial N_1}{\partial z} & -- & \frac{\partial N_n}{\partial z} \end{bmatrix} \tag{A.21}$$

$$[K]_{2\times 2} = \begin{bmatrix} K_r & 0 \\ 0 & K_z \end{bmatrix} \tag{A.22}$$

For a more general element (iso-parametric element), we need to come up with expressions in terms of *u* and *v*. therefore, we need to express $\frac{\partial N_i}{\partial r}$, $\frac{\partial N_i}{\partial z}$, and *drdz* in terms of *u* and *v*.

$$\frac{\partial N_i}{\partial u} = \frac{\partial N_i}{\partial r}\frac{\partial r}{\partial u} + \frac{\partial N_i}{\partial z}\frac{\partial z}{\partial u} \tag{A.23}$$

$$\frac{\partial N_i}{\partial v} = \frac{\partial N_i}{\partial r}\frac{\partial r}{\partial v} + \frac{\partial N_i}{\partial z}\frac{\partial z}{\partial v} \tag{A.24}$$

In matrix form

$$\begin{Bmatrix} \frac{\partial N_i}{\partial u} \\ \frac{\partial N_i}{\partial v} \end{Bmatrix} = \begin{bmatrix} \frac{\partial r}{\partial u} & \frac{\partial z}{\partial u} \\ \frac{\partial r}{\partial v} & \frac{\partial z}{\partial v} \end{bmatrix} \begin{Bmatrix} \frac{\partial N_i}{\partial r} \\ \frac{\partial N_i}{\partial z} \end{Bmatrix} = [J] \begin{Bmatrix} \frac{\partial N_i}{\partial r} \\ \frac{\partial N_i}{\partial z} \end{Bmatrix} \tag{A.25}$$

We can evaluate the Jacobin matrix using the expression for the coordinate transformation:

$$r = \sum_{i=1}^{n} N_i(u,v) r_i \tag{A.26}$$

$$z = \sum_{i=1}^{n} N_i(u,v) z_i \tag{A.27}$$

$$[J(u,v)] = \begin{vmatrix} \sum_{i}^{n} \frac{\partial N_i}{\partial u} r_i & \sum_{1}^{n} \frac{\partial N_i}{\partial u} z_i \\ \sum_{1}^{n} \frac{\partial N_i}{\partial v} r_i & \sum_{1}^{n} \frac{\partial N_i}{\partial v} z_i \end{vmatrix} \tag{A.28}$$

The desired derivations are evaluated as follows:

$$\begin{Bmatrix} \frac{\partial N_i}{\partial r} \\ \frac{\partial N_i}{\partial z} \end{Bmatrix} = [J]^{-1} \begin{Bmatrix} \frac{\partial N_i}{\partial u} \\ \frac{\partial N_i}{\partial v} \end{Bmatrix} \tag{A.29}$$

To complete the evaluation, *drdz* also need to be evaluated. This is obtained from the following expression.

$$drdz = |J| dudv \tag{A.30}$$

where $|J|$ is defined as the determinant of the Jacobin, *detJ*.

$$\det J = |J| = J(1,1) \times J(2,2) - J(1,2) \times J(2,1) \tag{A.31}$$

$$[J]^{-1} = \begin{vmatrix} \frac{J(2,2)}{\det J} & -\frac{J(1,2)}{\det J} \\ -\frac{J(2,1)}{\det J} & \frac{J(1,1)}{\det J} \end{vmatrix} \tag{A.32}$$

Then, we can rewrite the expression for [K_c].

$$[K_C]^e = \int_{-1}^{1} \int_{-1}^{1} [B]^T [K][B] \sum_{i=1}^{n} N_i(u,v) r_i \det J du dv \tag{A.33}$$

The nice thing about this expression is that it leads itself easily to numerical integration. In particular, the Gauss Quadratic method can be used for this purpose.

The general method for numerical integration, for example, the two-point form is as follows.

$$T \approx w_0 f(x_0) + w_1 f(x_1) \tag{A.34}$$

where w_0 and w_1 are referred to as the weighting functions and x_0, x_1 are referred to as the integration points. The error tends to vanish by choosing suitable values of x_0, x_1, w_0, w_1.

For 2 points Gauss quadratic, when we choose

$$w_0 = w_1 = 1 \quad \text{and } x_0 = -\frac{1}{\sqrt{3}} \qquad x_1 = \frac{1}{\sqrt{3}}$$

It yields exact solution up to a cubic function. The general form is

$$\int_{-1}^{1} f(x)dx = \sum_{j=1}^{n} w_j f(x_j) \tag{A.35}$$

Where n= number of integration points.

$$[K_C]^e = \int_{-1}^{1}\int_{-1}^{1}[B]^T[K][B]\sum_{i=1}^{n} N_i(u,v)r_i \det J dudv \tag{A.36}$$
$$= \int_{-1}^{1}\int_{-1}^{1} f(u,v)dudv$$
$$= \sum_{i=1}^{n}\sum_{j=1}^{n} w_i w_j f(u_i, v_j)$$

For 2-points or *2x2* integration

$$[K_c]^e = \sum_{i=1}^{2}\sum_{j=1}^{2} w_i w_j [B]^T[K][B]\det J \sum_{k=1}^{4} N_k(u_i, v_j) r_k \tag{A.37}$$

Heat capacitance term

$$\iint_{A^e} N_i \rho C_p r[N]\left\{\frac{\partial T^e}{\partial t}\right\}drdz \qquad i=1,n \tag{A.38}$$

In matrix form

$$[C]^e \frac{\partial T^e}{\partial t} = \iint_{A^e}\{N\}\rho C_p r[N]drdz\left\{\frac{\partial T^e}{\partial t}\right\} \tag{A.39}$$

In numerical notation, using Gauss quadratic method, we have

$$[C]^e = \sum_{i=1}^{2}\sum_{j=1}^{2} w_i w_j \{N\}\rho C_p[N]\det J \sum_{k=1}^{4} N_k r_k \tag{A.40}$$

The boundary term

For the terms associated with the various boundary conditions, the boundary quadrature must be evaluated first. So we need to derive an expression that will allow us to calculate the arc length of a boundary or arbitrary length in *r, z* space.

$$ds = \sqrt{dr^2 + dz^2} = \text{arc length} \tag{A.41}$$

In the local coordinate system *u, v*, the quadrature on face (1) turns out to be:

$$\int_{C^e} q_s r N_i dC = \int_{-1}^{1} f(u) du \tag{A.42}$$

$$dr = \frac{dr}{du} du \qquad dz = \frac{dz}{du} du \tag{A.43}$$

And we have

$$\frac{dr}{du} = J_{11} = \sum_{i=1}^{4} \frac{\partial N_i}{\partial u}(u,v) r_i \qquad \frac{dz}{du} = J_{12} = \sum_{i=1}^{4} \frac{\partial N_i}{\partial u}(u,v) z_i \tag{A.44}$$

So we can get

$$ds = du\sqrt{J_{11}^2 + J_{12}^2} \tag{A.45}$$

Thus

$$\int_{C^e} q_s r N_i dC = \int_{-1}^{1} q r N_i \sqrt{J_{11}^2 + J_{12}^2} du \tag{A.46}$$

In vector form

$$\{f_q\} = \int_{C^e} qr\{N\} dC \tag{A.47}$$

And in numerical form, we have

$$\{f_q\} = \sum_{i=1}^{2} (w_i q \{N\} \sqrt{J_{11}^2 + J_{12}^2} \sum_{j=1}^{4} N_j r_j) \tag{A.48}$$

Because the quadrature of N_3, N_4 on face 1 is zero,

For face 1:

$$\{f_q\} = \sum_{i=1}^{2} (w_i q \{N\} \sqrt{J_{11}^2 + J_{12}^2} \sum_{j=1}^{4} N_j r_j) = \begin{Bmatrix} f_1 \\ f_2 \\ 0 \\ 0 \end{Bmatrix} \quad (v=-1,\ u=\pm 0.577) \tag{A.49}$$

Similar expressions can be derived for face 2, 3, 4.

Distributed volume heat source

$$\{f_Q\} = \iint_{A^e} \{N\} \dot{Q}\, r dr dz \tag{A.50}$$

In numerical form:

$$\{f_Q\} = \sum_{i=1}^{2} \sum_{j=1}^{2} (w_i w_j \{N\} \dot{Q} (\sum_{k=1}^{4} N_k r_k)) \det J \tag{A.51}$$

Now, reassemble all the terms to comprise one FE equation

$$[C_p]^e \left\{\frac{dT}{dt}\right\}^e + \left|[K_c]^e + [K_h]^e\right| \{T\}^e = \{f_Q\}^e + \{f_q\}^e + \{f_h\}^e \tag{A.52}$$

$$\left\{\dot{T}\right\}_\theta = \frac{\{T_{n+1}\} - \{T_n\}}{\Delta t} \tag{A.53}$$

$$\{T\}_\theta = (1-\theta)\{T_n\} + \theta\{T_{n+1}\} \tag{A.54}$$

$$\left[\frac{[C]^e}{\Delta t} + \theta[K]^e\right] \{T_{n+1}\}^e = \frac{[C]}{\Delta t} \{T_n\}^e - [K]^e (1-\theta)\{T_n\}^e + \{f\}^e \tag{A.55}$$

Now, the FE equation can be expressed as:

$$[A]^e\{T_{n+1}\}^e = \{B\}^e \tag{A.56}$$

$$[A] = \left[\frac{[C]^e}{\Delta t} + \theta[K]^e\right] \tag{A.57}$$

$$\{B\}^e = \frac{[C]^e}{\Delta t}\{T_n\}^e - (1-\theta)[K]^e\{T_n\}^e + \{f\} \tag{A.58}$$

$$[K]^e = [K_c]^e + [K_h]^e \tag{A.59}$$

$$\{f\}^e = \{f_Q\}^e + \{f_q\}^e + \{f_h\}^h \tag{A.60}$$

3. FEM code

The flowchart shown in Figure A.4 shows the procedure used for the FE method.

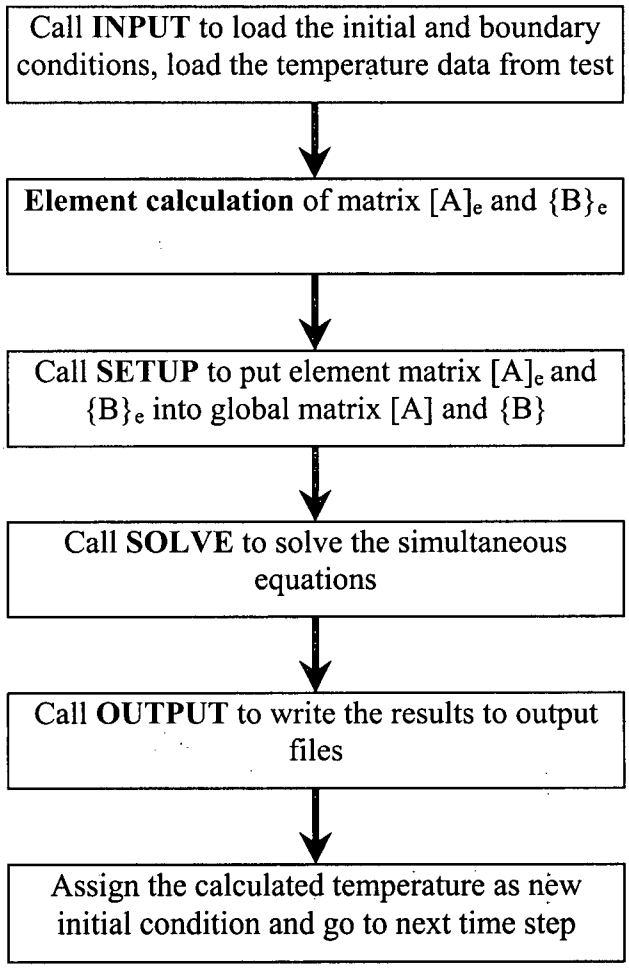

Figure A.4. - Calculation procedure used for FE code.

APPENDIX B. EQUATIONS USED TO QUANTIFY THE HEAT LOSS DUE TO RADIATION AND NATURAL CONVECTION DURING AIR COOLING OF A TUBE

1. Radiation

For radiation, the Stefan-Boltzmaan law can be used to calculate the heat flux as shown in Equation B.1 [125]

$$q_r = \varepsilon_{tube}\sigma T_w^4 \tag{B.1}$$

where q_r is the heat flux due to radiation (W/m^2), T_w is the surface temperature of the tube in °K, ε_{tube} is the emmisivity of the tube and σ is the Stephan Boltzman constant (5.676 x 10^{-8} W/(m^{2}K^4)). After choosing an emmisivity value, $\varepsilon_{tube} = 0.43$, the heat transfer due to radiation from the tube to the surroundings can be expressed using Equation B.2:

$$q_r = \varepsilon_{tube}\sigma T_w^4 = 0.43 \times 5.676 \times 10^{-8} T_w^{\ 4} = 2.44068 \times 10^{-8} T_w^{\ 4} \tag{B.2}$$

2. Natural Convection

For natural convection, the following equations can to used to quantify the heat transfer coefficient [125]:

$$Nu = \frac{hD}{k_f} = \left\{ 0.60 + \frac{0.387 Ra_D^{1/6}}{\left[1 + \left(\frac{0.559}{\mathrm{Pr}}\right)^{9/16}\right]^{8/27}} \right\}^2 \tag{B.3}$$

where, Nu is the Nusselt number, h is the convection heat transfer coefficient (W/m^2/K), D is the cylinder diameter (m), k_f is the fluid thermal conductivity (W/m/K), Ra is Rayleigh number and Pr is Prandtl number.

The Rayleigh number (Ra_D) must be in the following range:

$$10^{-5} < Ra_D = \frac{g_x \beta (T_w - T_\infty) D^3}{\nu \alpha} = \frac{9.81(1/298)(T_w - 298)(0.08)^3}{(15.68\times10^{-6})(0.2216\times10^{-4})} \qquad \text{(B.4)}$$
$$= (4.8508\times10^4)(T_w - 298) < 10^{12}$$

where, g_x is gravitational acceleration (m/s^2), β is coefficient of thermal expansion (1/K), T_w is tube surface temperature (K), T_∞ is the air temperature (K), ν is the kinematic viscosity (m^2/s) and α is thermal diffusivity (m^2/s).

Prandtl number (Pr) is in the following range:

$$0 < \mathrm{Pr} = \nu / \alpha = 15.68\times10^{-6} / (0.22160\times10^{-4}) = 0.708 < \infty \qquad \text{(B.5)}$$

For an ideal gas, the coefficient of thermal expansion (β) can be calculated by:

$$\beta = 1/T_\infty = 1/298 \qquad \text{(B.6)}$$

$$h = \frac{0.02624}{0.08}\left\{0.6 + \frac{0.387\times\left[(4.8508\times10^4)(T_w - 298)\right]^{1/6}}{\left[1+\left(\frac{0.559}{0.708}\right)^{9/16}\right]^{8/27}}\right\}^2 \qquad \text{(B.7)}$$
$$= 0.328\{0.6 + 1.94(T_w - 298)^{0.1667}\}^2$$

3. Total air cooling heat flux

The heat flux due to natural convection can now be estimated using Equation B.8 as shown below:

$$q_c = h \times (T_w - 298) = 0.328\{0.6 + 1.94(T_w - 298)^{0.1667}\}^2 \times (T_w - 298) \quad \text{(B.8)}$$

So, the total heat flux transferred from the tube surface to the surroundings can be calculated by using Equation B.9 as shown below:

$$q = q_r + q_c = 2.44068 \times 10^{-8} T_w^4 + 0.328\{0.6 + 1.94(T_w - 298)^{0.1667}\}^2 \times (T_w - 298) \quad \text{(B.9)}$$

APPENDIX C. ERROR OF THE HEAT FLUX SENSOR UNDER HIGH HEAT FLUX BOUNDARY CONDITIONS

Although heat flux sensors have been used extensively to measure the value of the heat flux in a number of situations, they are rarely used to measure the heat flux under quenching conditions. The reason for this will be discussed in the following sections.

C.1. Theory of the heat flux sensor

For a heat flux sensor, two thermocouples are installed into the test sample as shown in Figure C.1 to obtain the heat flux. Under steady state conditions, the heat flux can then be determined using:

$$q = \frac{Q}{At} = k\frac{T_2 - T_1}{d} \tag{C.1}$$

When the distance (***d***) between the two thermocouples is small enough, and the assumption is made that steady state is maintained between these two thermocouples, then the above equation can be used to approximate the heat flux under unsteady-state conditions. In this case, the accuracy of the heat flux sensor will depend on factors such as the distance between the two thermocouples, the distance of the thermocouple from the surface of the sample and the magnitude of the heat flux at the surface. However, no matter how close the thermocouples are, steady state cannot be maintained between the thermocouples and the calculated heat flux will have an associated error under unsteady-state conditions.

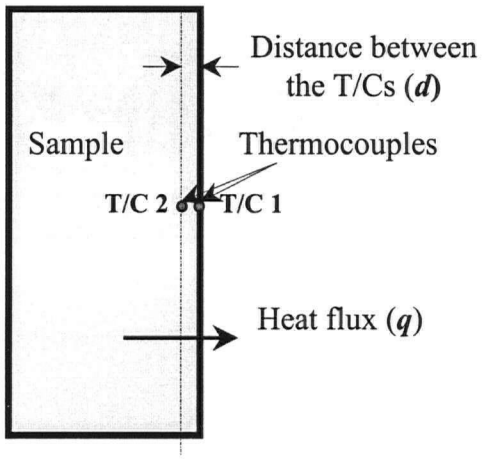

Figure C.1. Schematic of a quench test sample with a heat flux sensor.

C.2. Comparison of the calculated results with applied ones

In order to determine the accuracy of this method, a theoretical analysis was conducted by assuming different thermocouple positions relative to the surface of the sample, different distances (d) between the two thermocouples used for the heat flux sensor. This analysis was done under a variety of quench conditions ranging from boiling curves with high peak heat fluxes to boiling curves with low peak heat fluxes. The 2-D FE model outlined in Chapter 5 was then used to generate the temperature histories at the assumed thermocouple positions. The calculated temperature data was then put into Equation C.1 to calculate the resulting heat fluxes. The results are shown in Figure C.2.

For the calculation, the distance (d) between the two thermocouples for the heat flux sensor were assumed to vary from 1 mm to 2 mm, and the distance of the heat flux sensor from the quenched surface, i.e., the distance of T/C 1 from the quenched surface, was assumed to vary from 0 mm to 3 mm.

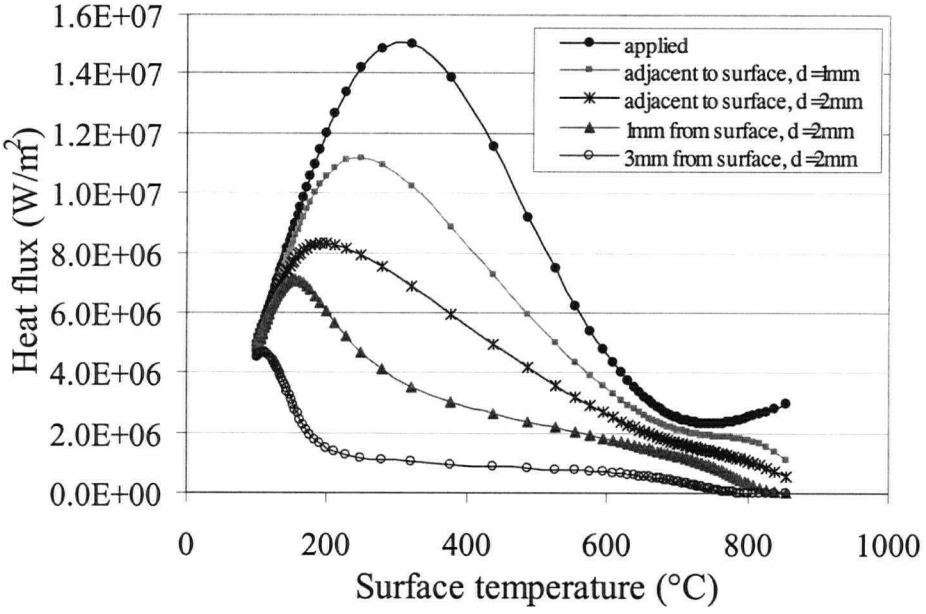

a) high heat flux conditions.

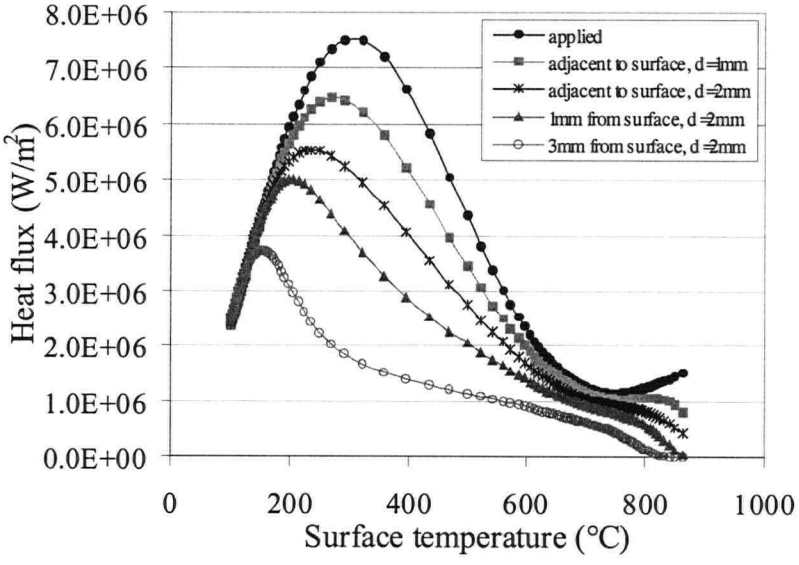

b) medium heat flux conditions.

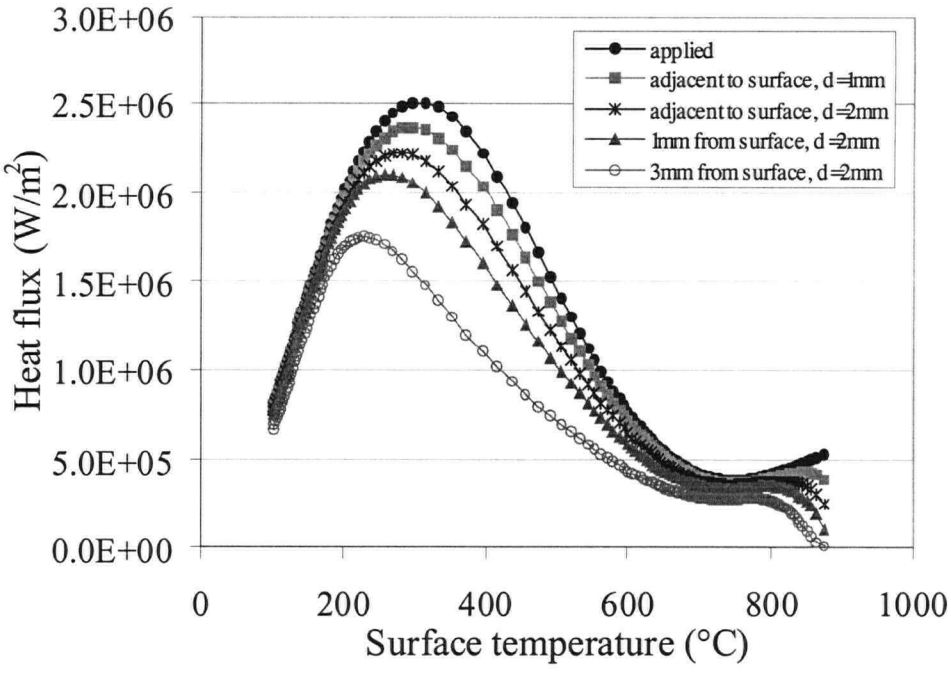

c) low heat flux conditions

Figure C.2. Comparison of the calculated and applied heat fluxes under: a) high heat flux conditions, b) medium heat flux conditions can c) low heat flux conditions.

From Figure C.2, it can be seen that, under high heat flux conditions, using a heat flux sensor would produce a large error in the calculated heat flux. Even when the distance of the heat flux sensor is 0 mm from the sample surface and the distance between the two thermocouples of the heat flux sensor is 1mm, the error on the generated heat flux is still very striking.

Figure C.2b and C.2c shows the even under medium and low heat flux conditions, the error in the calculated boiling curve using a heat flux sensor is still significant.

From these calculations, the following conclusions can be made:

1. Under quench conditions when the heat flux is high, a heat flux sensor should not be used to determine the boiling curve as the error in the calculated boiling curve will be too large. As the severity of the quench increases the resulting error in using a heat flux sensor will also increase.

2. The heat flux calculated using a heat flux sensor can be affected by the heat flux sensor position, sensor thickness (the distance between two thermocouples), and severity of the quench at the surface of the sample.

APPENDIX D. DIFFICULTIES OF THE INVERSE HEAT CONDUCTION (IHC) PROBLEM

First, let us have a look at the following example: a semi-infinite body heated by a sinusoidal surface heat flux of frequency ω,

$$q = q_{\max} \cos(\omega t) \tag{D.1}$$

where, q_{max} is the maximum value of the surface heat flux (W/m^2), t is the time (s). After a sufficiently long time, the temperature solution also becomes periodic and is given by: [127]

$$T = T_0 + \frac{q_{\max}}{k}\left(\frac{\alpha}{\omega}\right)^{1/2} \exp\left[-x\left(\frac{\omega}{2\alpha}\right)^{1/2}\right]\cos\left[\omega t - x\left(\frac{\omega}{2\alpha}\right)^{1/2} - \frac{\pi}{4}\right] \tag{D.2}$$

where, α is the thermal diffusivity (m^2/s), k is thermal conductivity (W/m/K), T_0 , a constant, is the initial temperature distribution (K), x is the distance from the surface where the heat flux is being applied. Rearranging the above equation gives:

$$\begin{aligned} T - T_0 &= \frac{q_{\max}}{k}\left(\frac{\alpha}{\omega}\right)^{1/2} \exp\left[-x\left(\frac{\omega}{2\alpha}\right)^{1/2}\right]\cos\left[\omega t - x\left(\frac{\omega}{2\alpha}\right)^{1/2} - \frac{\pi}{4}\right] \\ &= (T - T_0)_{\max} \cos\left[\omega t - x\left(\frac{\omega}{2\alpha}\right)^{1/2} - \frac{\pi}{4}\right] \end{aligned} \tag{D.3}$$

$$(T-T_0)_{max} = q_{max} k^{-1} \left(\frac{\alpha}{\omega}\right)^{1/2} \exp\left[-x\left(\frac{\omega}{2\varepsilon}\right)^{1/2}\right] \tag{D.4}$$

where $(T\text{-}T_0)_{max}$ is the maximum temperature change inside the sample from x=0 $\rightarrow \infty$. As the frequency ω increases, the value of $(T\text{-}T_0)_{max}$ decreases. The maximum temperature rise occurs at x=0 and is proportional to $\omega^{-1/2}$. For an interior location:

$$\frac{(T-T_0)_{max}}{(T-T_0)_{max,x=0}} = \exp\left[-x\left(\frac{\omega}{2\alpha}\right)^{1/2}\right] \tag{D.5}$$

which shows that the maximum temperature change of interior temperatures sharply decreases for increased x-values. The exponential in the above equation also indicates a large effect as ω is increased. To obtain some insight from this equation, the case is considered wherein the right-hand side is less than 0.01 or

$$x\left(\frac{\omega}{2\alpha}\right)^{1/2} > 4.6 \tag{D.6}$$

For steel with $\alpha=10^{-5}$ m^2/s and $\omega=2\pi$ rad/s =1 Hz, there is negligible response for $x > 0.82$ cm. This is a large damping. But if ω were further increased, say by a factor of 100, there would be negligible response for x > 0.08 cm.

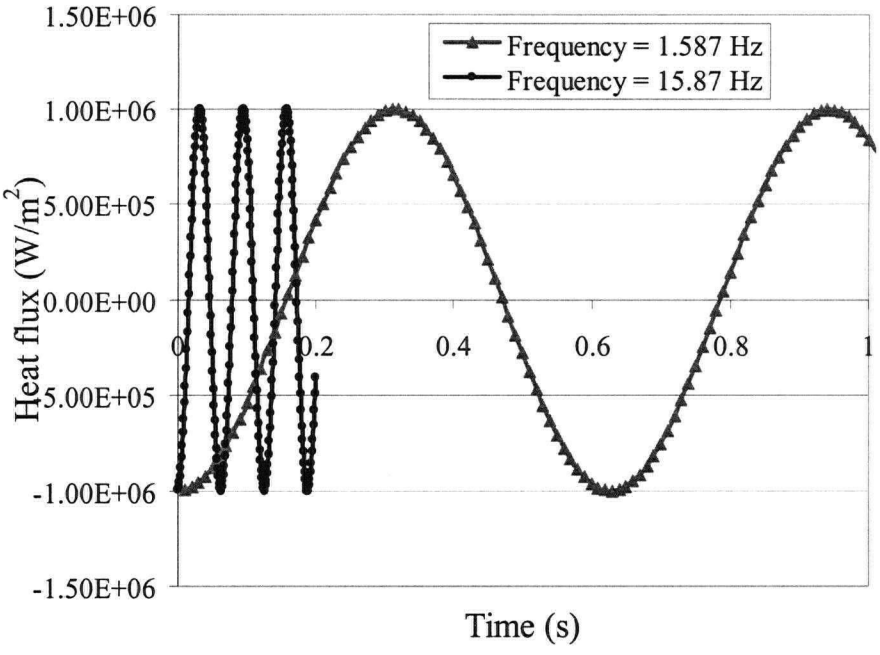

Figure D.1. Applied sinusoidal surface heat flux of frequency 1.587Hz and 15.87Hz.

Figure D.1 shows the applied sinusoidal surface heat flux of frequency 1.587 and 15.87 Hz. Under such surface heat flux conditions, the calculated temperature profiles in the sample are shown in Figure D.2 and Figure D.3. It can be seen that the temperature response to the surface heat flux in the sample decreases with increased distance from the surface. When the distance from the surface is 5 mm, the temperature is influenced only slightly by the sinusoidal surface heat flux of 1.587 Hz. When the distance is increased to 10 mm, the temperature is not influenced at all by the surface heat flux. With the increase of heat flux frequency to 15.87 Hz, the temperature at a distance x = 1mm from the surface just has a very tiny response to the surface heat flux, and the temperature at a position x = 5 mm is not influenced at all by the surface heat flux. As a result, three difficulties of inverse heat conduction problem can be identified:

1) Damping of temperature data at interior locations in the sample. As discussed above, the temperature at an inner location in the sample is always a damped response. Hence if a thermocouple is not properly placed in the sample as close as possible to the surface, it may lose completely the ability to measure the change in the surface heat flux accurately.

2) Sensitivity to errors in the measured temperature. Because the measured temperature is damped, a very high heat flux on the surface may produce only a very small change in the measured inner temperature. It is therefore critical that the noise in the measured temperature is small and is not of the same order of magnitude as the temperature change which occurs in response to a change in the surface heat flux. For example, there is 2 °C noise in the measured temperature, the measured temperature change in response to the surface heat flux at x = 1 mm in Figure D.2 should be around 20 °C. In this case a 2 °C noise would not produce a large error when the measured temperature is used to calculate the surface heat flux. However, if the thermocouple is located at x = 5 mm, the measured temperature change in response to the surface heat is about 2 °C, so a 2 °C noise in the measured temperature will make it impossible to distinguish the change in temperature due to noise versus the change in temperature due to the change in the surface heat flux.

3) Non-uniqueness of the solution. Since the measured temperature at an inner location is damped, and used to calculate the surface heat flux, the solution will not be unique. Figure D.4 shows the temperature profiles at x = 1 mm in the sample under different heat flux frequencies of 6.4 –159 Hz. The sample generates almost the same temperature profiles at x = 1 mm when surface flux frequency is 80 Hz and 159

Hz. This means that, if such temperature data is used to calculate the surface heat flux, it can produce a heat flux that can have any frequency larger than 80 Hz.

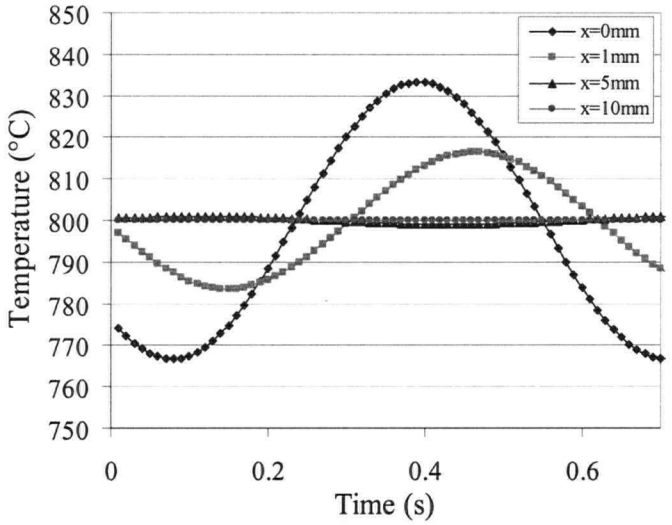

Figure D.2. Temperature profiles at different locations in a sample under a sinusoidal surface heat flux of frequency 1.587 Hz.

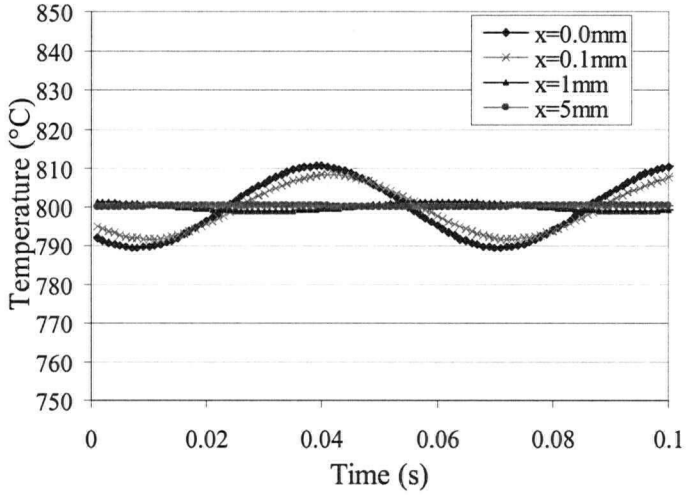

Figure D.3. Temperature profiles at different locations in a sample under a sinusoidal surface heat flux of frequency 15.87 Hz

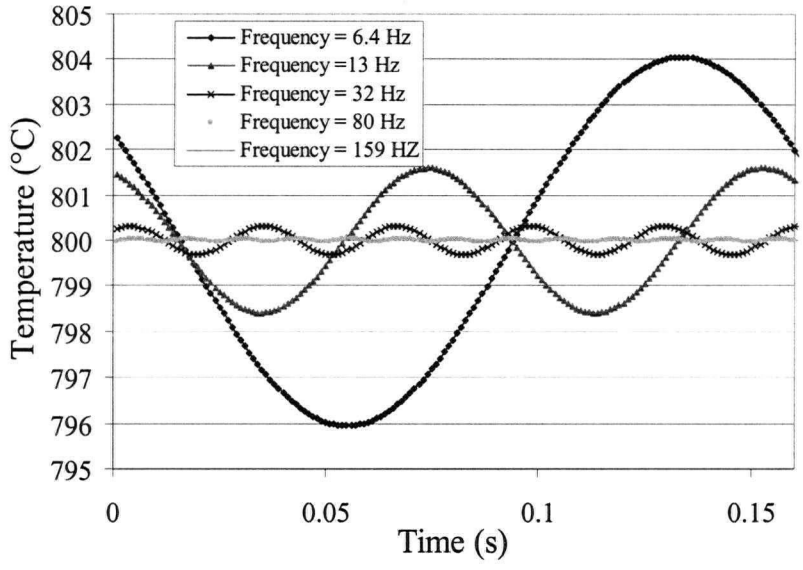

Figure D.4. Temperature profiles at x=1mm in a sample under sinusoidal surface heat flux of different frequency

One should pay great attention to these difficulties when solving an IHC problem. In order to minimize these difficulties, thermocouple should be put as close as possible to surface so that damping is minimized, temperature data frequency should as high as possible to capture the detailed temperature change.